DEVELOPMENT OF PEAK GROUND ACCELERATION (PGA) BASED PRE-CODE REINFORCED CONCRETE FRAME BUILDING FRAGILITIES FOR ISTANBUL

by

İpek Dolağan

B.S., Civil Engineering, Yıldız Technical University, 2015

Submitted to the Kandilli Observatory and Earthquake Research Institute
in partial fulfillment of the requirements for the degree of
Master of Science

Graduate Program in Earthquake Engineering

Boğaziçi University

2019

ACKNOWLEDGEMENTS

I would like to take this opportunity and deeply thank my supervisor, Prof. Dr. Sinan Akkar, whose constant guidance and understanding proved to be of great aid to my endeavour. It has been a great privilege to work with him.

I would also like to thank to my colleague Halil İbrahim Duran, for his friendship and contribution to this thesis.

Finally, I would like to express my special gratitude to my parents Sema Dolağan, Tayfun Dolağan and my brother Kerim Dolağan, for their love and support throughout my whole life.

ABSTRACT

DEVELOPMENT OF PEAK GROUND ACCELERATION (PGA) BASED PRE-CODE REINFORCED CONCERETE FRAME BUILDING FRAGILITIES FOR ISTANBUL

An important portion of pre-code building stock in Istanbul runs significant earthquake risk. Given a building class, the uncontrolled construction of pre-code buildings in the past leads to a considerable model variability and complicates the prediction of losses for future earthquakes in Istanbul. However, the social and economic loss estimations are necessary for Istanbul to have planned actions to improve the earthquake resilience in the city. At this point, fragility curves; which represent the exceedance probability of a particular damage state are one of the most important components of resilience-based building inventory studies for large building stocks at large metropolitan areas. This study aims to provide fragility curves for pre-code reinforced concrete frame residential buildings in Istanbul. For this purpose, 800 mid-rise frame buildings located in the Zeytinburnu district in Istanbul are compiled and 16 representative building models are developed to account for the model variability of the same building class. The examined buildings do not comply with the code requirements of any period after 1975 and they can be considered as low code. The fragilities are based on Peak Ground Acceleration because such practical ground-motion intensity measures are being popularly used in the loss assessment of large building stocks. Nonlinear building responses are derived from three-dimensional nonlinear response history analysis that are carried out by using OpenSees Software (Open System for Earthquake Simulation). Incremental Dynamic Analysis is performed to determine the statistical distribution of the response parameters. A set of real ground motions, which are consistent with the disaggregation results of a probabilistic seismic hazard assessment for Istanbul are considered in the development of fragilities for each building model. Therefore, the variability in building models of the same building class as well as the record-to-record variabilities are considered in the developed fragilities. The fragility model is a backbone cure with upper and lower bounds covering the model and ground-motion variabilities for mid-rise low-code reinforced concrete frame buildings in the investigated building stock.

ÖZET

DEPREM YÖNETMELİKLERİNE UYGUN TASARLANMAMIŞ ORTA KATLI BETONARME ÇERÇEVE BİNALARIN EN BÜYÜK YER İVMESİNE BAĞLI KIRILGANLIK İLİŞKİLERİNİN ELDE EDİLMESİ

İstanbul'da özellikle geçmiş yıllardaki kontrolsüz yapılaşma ve yetersiz denetimler, deprem performansı bilinmeyen yapı stoku ile sonuçlanmıştır. Muhtemel bir depremin bu yapı stokuna vereceği zararın önceden tahmin edilmesi, deprem öncesinde yenileme çalışmalarının planlanmasında ve deprem sonrasında acil müdahale edilecek bölgelerin belirlenmesinde önemlidir. Deprem risk analizi çalışmalarının unsurlarından olan kırılganlık eğrileri, farklı deprem seviyeleri için bir hasar düzeyinin ulaşılması ve aşılması olasılığını vermektedir. Kırılganlık eğrileri, büyükşehirlerin yapı stoklarının deprem performansı incelenmesine hızlı çözüm getirmektedir. Bu çalışma kapsamında İstanbul ilinde bulunan ve güncel deprem şartnamelerine göre tasarlanmamış betonarme konut tipi yapıların kırılganlık eğrileri sunulmaktadır. Bu amaçla, Zeytinburnu ilçesinden 800 adet orta katlı, konut tipi binanın betonarme detayları incelenmiştir. İncelenen yapılar 1975'den sonra yayınlanan hiçbir deprem yönetmeliğine uygun değildir. Mevcut yapıların deprem performanslarını etkileyebilecek parametreler üzerine yapılan istatistiksel bir çalışmanın sonucunda, temsili 16 adet model türetilmiştir. Çalışma kapsamındaki bina envanterinde, yapıların taşıyıcı sistemi ağırlıklı olarak çerçevelerden oluştuğundan sadece bu tip binalar değerlendirilmiştir. Yapı modellerinin tepki parametreleri, OpenSees (Open System for Earthquake Simulation) yazılımda gerçekleştirilen üç boyutlu doğrusal olmayan zaman tanım analizleriyle belirlenmiştir. Muhtemel yer hareketi düzeylerinin dikkate alınabilmesi ve kırılganlık eğrilerine gerekli istatistiksel verinin sağlanabilmesi için çok kayıtlı Artımsal Dinamik Analiz yöntemi uygulanmıştır. Yapısal analizlerde, İstanbul İli için gerçekleştirilen olasılıksal sismik tehlike analizinin deprem ayrıklaştırma sonuçlarına uygun olarak seçilen, gerçek deprem kayıtları kullanılmıştır. Bu bağlamda elde edilen kırılganlık ilişkilerinde yapısal değişkenlik ve yer hareketi kayıtlarındaki değişkenlik dikkate alınmıştır.

TABLE OF CONTENTS

LIST OF FIGURES

LIST OF TABLES

LIST OF SYMBOLS

b	Section force interpolation matrix
e	Section deformation vector
I	Geometric vector relating section deformations to fiber strains
M_w	Moment magnitude
N	Shape functions for displacements
N_p	Number of integration points
q	Element basic force vector
R_{JB}	Joyner-Boore distance
s	Section force vector
u_a	Transverse displacement
u_t	Axial displacement
V_{S30}	Average shear wave velocity in top 30 meters of soil
w	Element integration weight
β	Standart deviation
ε	Material strain
κ	Curvature
μ	Mean value
ν	Nodal displacement vector
σ	Material stress
$\Phi(\cdot)$	Normal cumulative distribution function

LIST OF ACRONYMS/ABBREVIATIONS

2D	Two Dimensional
3D	Three Dimensional
ATC	Applied Technology Council
CP	Collapse Prevention
Dof	Degree of Freedom
EDP	Engineering Demand Parameter
EMS	European Macroseismic Scale
FEMA	Federal Emergency Management Agency
IDA	Incremental Dynamic Analysis
IM	Intensity Measure
IO	Immediate Occupancy
KOERI	Kandilli Observatory and Earthquake Research Institute
LS	Life Safety
MIDR	Maximum Interstory Drift Ratio
MMI	Modified Mercalli Intensity
MRF	Moment Resisting Frame
MSK	Medvedev – Sponheuer – Karnik Scale
NEHRP	National Earthquake Hazard Reduction Program
NRHA	Nonlinear Response History Analysis
PBBE	Performance-Based Earthquake Engineering
PDF	Probability Density Function
PEER	Pacific Earthquake Engineering Research Center
PGA	Peak Ground Acceleration
PGV	Peak Ground Velocity
Psa	Pseudo-Spectral Acceleration
PSHA	Probabilistic Seismic Hazard Assessment
RC	Reinforced Concrete
SA(T1)	Spectral Acceleration at the Fundamental Period of the Building
Sd	Spectral Displacement
SDOF	Single Degree of Freedom

Tcl	Tool Command Language
TEC	Turkish Earthquake Code

1. INTRODUCTION

The rapid urbanization in 1970's and 1980's resulted in large residential building stocks with low quality in the metropolitan cities in Turkey. A large portion of these buildings are poorly engineered against seismic action since the first national earthquake code is enforced in Turkey in 1975. This is because the design engineers were not fully aware of the fundamentals of earthquake resistant design. Besides the lack of control during the construction period further increased the vulnerability of these buildings against earthquakes. This led to enormous economic losses and casualties in 1999, the Marmara Earthquakes, the first urban earthquakes in Turkey. The lessons learned from the Marmara earthquakes motivated the Turkish state to replace the poor quality building stock in metropolitan areas, in particular large earthquake prone cities such as İstanbul, Bursa and İzmir. This national policy triggered many earthquake engineering studies both in academia and professional environment having objectives of rapid seismic performance assessment (e.g., Erdik et al., 2003). The first seismic performance assessment studies are generally based on a deterministic methodologies such as those reported in FEMA-356 (Federal Emergency Management Agency, 2000) and ATC-40 (Applied Technology Council, 1996).

Currently, seismic performance assessment is risk-oriented and follow probabilistic approaches due to inherent uncertainties in ground motions, building models and building response due to complicated interaction between earthquakes and buildings. Probabilistic methods in risk-oriented seismic performance assessment make use of occurrence probability of ground motion amplitudes given a specific time interval and occurrence probability of different damage states under this excitation (Moehle and Deierlein, 2004). Besides, the monetary loss due to temporal stop in business and loss of market for a specific business branch are now also considered in probabilistic risk-based performance assessment (e.g., FEMA P-58-1, 2012). These parameters are essentially used as the components of decision metrics for the performance assessment of buildings.

Regardless of the complications in probabilistic risk-oriented performance assessment methods, one of the corner stones in these approaches is fragility functions that are used to estimate the exceedance probabilities of damage states given a ground motion demand. The

fragilities can be component- or building-based. The latter assess the damage state probabilities of the entire structure by considering relevant engineering demand parameters such as interstory drift, roof drift or plastic rotation. Development of building-based fragility functions for no code buildings in Istanbul is the main topic of investigation in this thesis that can be used in probabilistic risk-oriented performance assessment. The following sections in this chapter first define the fragility functions and then summarize the relevant studies in Turkey. The chapter concludes with the overall scope of the thesis.

1.1. Evaluation of Fragility Functions

Fragility curves represent the probability of reaching or exceeding a specific damage state for a given Engineering Demand Parameter (EDP) of the structure. Components of the fragility curves are the intensity measure and the damage state definition. Intensity measure correlates the earthquake parameter to the building damage. Most common intensity measures are the ground motions parameters such as Peak Ground Acceleration (PGA), Peak Ground Velocity (PGV), Pseudo-Spectral Acceleration (PSa), Spectral Displacement (Sd) or seismic intensity parameters such as Modified Mercalli Intensity Scale (MMI) (Wood and Neumann, 1931) and MSK scale (Medvedev and Sponheuer, 1969). The damage state definitions are related to the evaluated performance metrics. There are various damage state definitions such as Immediate Occupancy, Life safety, and Collapse Prevention in the guidelines and in the literature. These definitions indicate the likely damage state of the structure due to an earthquake. Traditionally, fragility curves are expressed by lognormal distribution. The lognormal distribution defines the conditional probability of the damage state of interest at various intensity levels. For a regional earthquake risk assessment, fragility curves are derived for a class of building group such as mid-rise reinforced concrete moment resisting frame buildings are used.

There are mainly three approaches to develop fragility curves: empirical, analytical, and hybrid methods. Empirical methods rely on the post-earthquake reports and expert judgment. The empirical methods depend on observed damage in the building inventory. Empirical fragility curves are subjective since they are the interpretations of different experts. Nevertheless, empirical fragility curves are valuable since they represent information from real (observed) data and reflect overall building inventory characteristics.

The use of empirical fragility functions in building inventories having similar features or their calibration for building inventories that have similar characteristics to those used in the development of fragilities are common practice. Essentially, fragilities provide information about the structural deficiencies of buildings about the implementation of earthquake resistant design. The analytical fragility functions are derived from computer simulations. The representative building models or sample buildings are evaluated either by simplified procedures or response history analysis. The analytical methods for deriving fragility curves provide flexibility for assessing the earthquake risk of structures when there is lack of field (observed) data. On the other hand, many assumptions are done in analytical methods such as analytical description of representative building models, selection of ground motion intensity measure or the damage state definitions. In order to develop meaningful fragility curves by analytical methods; assumptions should be confined to the characteristics of the target buildings and the seismicity of the region. Whenever the field data are available, empirical methods can be used to calibrate or verify the analytical procedures. The last approach in fragility development is hybrid method that considers both empirical and analytical solutions together by determining the building capacity through field observations and by following analytical solutions to calculate the demand statistics at various intensity levels.

The damage state definitions and selection of intensity measures mostly depend on the methodology used in the fragility development as well as the characteristics of the target building stock. In the empirical methods, the seismic intensity parameters such as MSK are the commonly used intensity measures. In contrast, a variety of ground motion parameters can be used in analytical methods. It should be noted that the correlation between the structural damage and the selected ground motion parameter depends on the characteristics of the building. For example, PGA may correlate well with the damage for low rise and short period structures whereas for a medium rise building, pseudo-spectral acceleration at the fundamental period of the structure may correlate with damage better than PGA. This is because the first mode dominant structures are sensitive to the frequency content of the ground motion in the vicinity of fundamental period. For tall buildings, which are sensitive to the higher mode effects, the correlation of damage with the fundamental mode spectral acceleration would be weak.

Damage state definitions in empirical fragility curves are set by some well recognized standards that depend on the building type. One of these standards is European Macroseismic Scale 1998 (EMS; Grünthal,1998) and it defines the damage states as negligible to slight damage, moderate damage, substantial to heavy damage, very heavy damage and destruction from the field observations of damaged buildings after an earthquake. In EMS-98 Scale, the failure of a single upper floor is considered as very heavy damage in reinforced concrete structures whereas failure of the walls and partial failure of the roofs and floors are defined as heavy damage for masonry buildings. For analytical methods, damage states are related to the threshold values of the EDPs computed from response history analysis. The EDPs are either global parameters such as interstory drift ratio, global (roof) drift ratio, base shear or local responses of structural elements such as strain, plastic rotation and chord rotation. Selection of these parameters depends on the behavior and type of the structure under consideration. If the structure is not regular in elevation, the global drift may not be representative for the performance metric of interest (e.g., life safety, immediate occupancy, etc.). Similarly, base shear would not be a good damage estimator for flexible structures. Moreover, if the interested performance metric includes the damage state of the non-structural components, a more specific response parameter such as floor acceleration is preferred as the damage indicator. Another aspect of the analytical method is the determination of the threshold values for the damage states. Seismic guidelines and regulations provide some damage state limits depending on the response parameters and the structure class. Given a performance metric it is also possible to define the damage state limits from analytical models: conducting pushover analysis and associating the damage limit states with the yield and collapse points on the pushover curve. Note that the yield and collapse points on pushover curves can be used for light damage and collapse damage prevention damage states. However, it is difficult and debatable to define threshold values for moderate damage state by analytical methods. The threshold values based on analytical solutions should be verified or calibrated by using real earthquake damage data or laboratory test results.

In analytical fragility curve development for a building inventory, there are many sources of uncertainties like seismic hazard, structural variability, damage state definitions, and analytical modeling. To treat these uncertainties, a suite of scenarios that can be formulated from computer simulations are used (FEMA P-58-1, 2012). Sampling techniques

such as Latin Hypercube Sampling, Monte Carlo Simulation, Incremental Dynamic Analysis, and Multiple Stripe Analysis are commonly used simulation (analysis) techniques to incorporate a probabilistic sense and provide a statistical basis for fragility curve development. It should be noted that the fragility curves are also affected by the chosen simulation techniques.

As summarized in this section, there is no single approach for the derivation of fragility curves. Main components of analytical fragility functions are seismic hazard, ground motion intensity measure, engineering demand parameter, damage limit state, analysis and simulation techniques as well as the uncertainties.

1.2. Literature Survey

There is a rich literature about the derivation and the use of fragility curves for building inventories. The present study mainly deals with the derivation of analytical fragility curves. In this context, the available literature on the derivation of analytical fragility curves is investigated and mostly studies targeting the Turkish building stock are included in this chapter.

Erberik and Ay (2008) conducted a vulnerability assessment for low-rise and mid-rise Reinforced Concrete (RC) Moment Resisting Frame (MRF) buildings by considering the Turkish construction practice. Buildings are evaluated in three classes (superior, typical and poor) by this study. While the superior class models represent buildings having good construction practice, poor class models represent buildings, which do not meet seismic code requirements. The typical class models typify most of the RC building stock, which constitute engineered-structures but do not meet all the fundamental code requirements. Each class consists of 3 to 9 story generic frame models. The generic models can represent the uncertainties arising from material and structural variability by making use of Latin Hypercube Sampling method. The threshold values for the immediate occupancy, life safety, and collapse prevention limit states are in terms of maximum interstory drift ratios that are obtained by monitoring the local performance of the structural members and by using the softening index which depends on the stiffness change. Since the threshold values derived from different methods present an apparent scatter, they are defined as random variables in

a probabilistic manner with lower and upper bonds. Erberik and Ay (2008) provide fragilities in a probabilistic sense for the Turkish building stock and demonstrate the importance of probabilistic limit state definitions instead of a single value.

Akkar et al. (2005) derived fragility curves of low-code RC MRF buildings in Turkey by using a hybrid approach. The methodology comprises of determining the lateral stiffness, strength, and deformation capacities of the target buildings from the field data and developing fragility curves by employing Nonlinear Response History Analysis (NRHA). Field data contains 32 sample buildings selected from Düzce, which have stories ranging from two to five. Pushover analyses are utilized to find the structural capacities of the sample buildings and the threshold value for limit states. Limit states of immediate occupancy, life safety and collapse prevention were associated with the median yield and median ultimate global drift ratios. The computed limit state threshold values are found to be smaller than the ones proposed in the standards of the United States or Japan. Thus, the authors emphasize the importance of country-specific vulnerability assessments. The statistics of the modal parameters and base shear coefficients were used to find the ranges that represent the characteristics of the buildings in the building inventory. Then, each range is divided into different subgroups to generate Single Degree of Freedom (SDOF) systems with specific properties. The authors perform NRHA of SDOF systems to develop the fragility curves. An important aspect of this study is the work done to understand the correlation of EDP with PGV and PGA. It is found that PGV correlates better with the EDP and therefore, with the structural damage of the investigated structures.

An extensive study about the correlation between EDP and ground motion intensity measure is conducted by Hancılar and Çaktı (2015). The correlations of interstory drift ratios, beam plastic end rotations and floor accelerations with various ground motion features (including time domain parameters, spectral values at the fundamental building period and energy-related parameters) are evaluated. The authors used unscaled real ground motion records to perform NRHA of code-conforming generic frames that have various strength capacities and fundamental periods. Then, they run regression analysis to compute the correlations between the ground motion intensity measures (IMs) and EDPs of interest. Hancılar and Çaktı (2015) show that the correlation between IM and EDP may vary significantly depending on the characteristics of the buildings. For instance, for low- and

mid-rise buildings, the first mode spectral acceleration correlates well both with the interstory drift ratio and the plastic end rotations however, for high-rise buildings, the correlation of PGV is better with the EDPs. For stiff structures, the authors indicate a relatively good correlation between beam plastic end rotations and PSa or PGV. The fragility curves of code-complying RC MRF buildings are given by Hancılar and Çaktı (2015) by utilizing the best correlated IM-EDP pairs.

Kırçıl and Polat (2006) derived fragility curves for mid-rise RC MRF buildings which are designed according to the 1975 national earthquake code (TEC, 1975). They evaluate the sample frames analytically with a set of artificial records. In contrast with many other studies, the damage states chosen by these authors are yielding and collapse. The fragility curves, which are functions of interstory drift ratio are developed to identify the immediate occupancy and collapse prevention limit states. The immediate occupancy limit state is considered as the stiffness of the structure remaining almost the same as the initial stiffness. Its threshold value is assigned as the value corresponding to 5% probability of exceedance from the yield probability curve. Similarly, the value of the 5% probability of exceedance of the collapse probability curve is defined as the threshold value for the collapse prevention limit state, which implies an extensive nonlinear behavior without collapses.

Tüzün and Aydınoğlu (2007) used Park and Ang damage index (Park and Ang, 1985) as the damage indicator for developing fragilities for existing 2 to 7 story RC MRF structures. The selected damage levels are none to slight, moderate, extensive and complete. The threshold values of these damage levels are associated directly with the threshold values of the Park and Ang damage index. The procedure determines a local damage index for each element based on ductility ratio and corresponding total hysteretic energy. Then it defines a global damage index by calculating a weighted average of the local damage indices where the weighting function is proportional to the dissipated energy within that element. Tüzün and Aydınoğlu (2007) provide fragility curves as functions of spectral acceleration at different fundamental periods for buildings having different number of stories.

Erberik (2007a) developed fragility curves for mid-rise and low-rise RC MRF buildings. The building inventory consists of existing structures in Düzce. This study also includes a parametric work for investigating the influences of limit state definition, post-

yield to initial stiffness ratio, sampling technique, sample size and degrading hysteretic behavior on the resulting fragility curves. Building models include 2 to 6 story bare frames and infill frames with masonry infill walls. The analytical solution includes pushover analysis to determine the SDOF representations of the sample buildings that is followed by performing NRHA of the SDOF systems to generate fragility curves where the structural input parameters considered as random variables. Threshold values for serviceability, damage control and collapse prevention limit states are obtained from the analytical models in terms of spectral displacement. Serviceability limit state is related to the softening index while the damage control and collapse prevention limit states are related to the ultimate deformation capacity and the level of strength drop in the capacity curve, respectively. The parametric study also shows that while the post-yield to initial stiffness ratio, sampling techniques and sample size do not affect the final fragility curves, changes in fragilities can be significant if the limit states are defined in a probabilistic manner or if different degradation characteristics are employed in the structural model.

Uçar and Düzgün (2013), investigated the vulnerability of the structures designed according to the 1975 national earthquake code (TEC, 1975). Models are constructed based on the selected 30 sample buildings from Izmir. Three- to eight-story buildings are focused in this study. While the buildings with three- to six-story are RC MRF systems, buildings with seven and eight-story are RC MRF-Wall systems. Both limit states and EDPs are based on pushover analyses of the three-dimensional (3D) building models. Demand parameters are obtained for three hazard levels and for two soil conditions by considering the earthquake hazard that is defined in the 2007 national earthquake code (TEC, 2007). Authors stated that even though these buildings have appropriate strength capacities, their ductility capacities are low, which indicate that the deformations would be the main reason for structural damage.

Ozmen et al. (2010) derived fragility curves for two-, four-, and seven-story RC-MRF buildings, which comply with the requirements of either the 1975 or 1998 national earthquake codes (TEC, 1975; 1998). Before developing the fragilities, an inventory study is conducted for 475 existing residential buildings. The representative building models are established based on the inventory study and previously mentioned codes. The representative building models are grouped according to their number of stories, building-code as being

pre-code (TEC-1975) or modern-code (TEC-1998), amount of the transverse reinforcement and material quality. The fragility curves are derived separately for each building group. The pushover analysis of the 3D models is utilized to obtain the building capacities and their SDOF representations. Damage state threshold values as being Immediate Occupancy, Life Safety and Collapse Prevention depend on the capacity curves. Then fragility curves are constructed by using the NRHA results of the SDOF systems. This study also includes discussions on the parameters that are more effective on the fragilities at different code periods (i.e., 1975 and 1998 national earthquake codes). For instance, the material and the detailing quality effects are more significant on the fragility curves of buildings designed under the 1998 national earthquake code.

There are other fragility studies available in the literature, which involve different categories of building stock in Turkey. Bilgin (2016) investigated the RC hospital buildings, which hold the formal template design for the hospital buildings. This study utilizes the global response statistics of simplified analytical models. Hancılar et al. (2014) developed fragility curves for school buildings in Istanbul based on typical projects. The methodology adopts NRHA of the building models, in which material properties, geometrical characteristics, section dimensions as well as the ground motion input are randomly selected via Monte Carlo simulations in each analysis. Erberik (2007b) examined the vulnerability of masonry structures. The models rely on the observed characteristics of existing masonry buildings. The author investigated 120 subgroups of masonry buildings differing in the number of stories, load-bearing wall material, regularity in plan, and the 1998 national earthquake code conformity. Generated fragility curves are functions of base shear since the force-based demand is sufficient for indicating the damage for low-rise and mid-rise masonry structures with brittle structural walls. The limit state definitions of Erberik (2007b) rely on the pushover analysis, while the EDPs are calculated via NRHA. Odabaşı (2016) focused on the 10 to 30 story high-rise RC core wall-frame building stock in Turkey and developed fragility curves in a probabilistic sense through NRHA analysis. The models of Odabaşı (2016) rest on an inventory study which constitute various tall building structures located in the metropolitan cities of Turkey.

The summarized literature survey indicates that the fragility functions should be compatible with the local construction practice and adopting the fragilities specifically

derived for other countries may lead to erroneous structural performance estimations. The general application in specifying representative building models to develop fragilities is either by selecting some sample buildings from existing inventories or by designing fictitious models based on some assumptions and code regulations which were valid during the time of construction of the target building. It is believed that there is a lack of study involving a comprehensive building inventory investigation.

For limit state definitions, most of the studies utilize pushover analysis and relate the threshold limit state values with the significant points on the capacity curve. The most important component of bias in pushover analysis is the monotonic loading of the structure depending on the modal shape. Structural response to real ground motions is complex, and limit states defined from capacity curves should be evaluated with some reservation by considering the simplifications within this procedure. Also, pushover analysis should be used in caution, especially for the definition of the moderate damage states.

Mostly the damage state criteria rely on the global response parameters such as global drifts, maximum interstory drift and excludes the performance of the local elements. On the other hand, it is a fact that the overall performance is strictly related to the performance of the individual members. Especially recent guidelines define the performance by considering the percentage of structural elements failures given the target performance level. Few studies include local responses by using damage indices such as the one in Park and Ang (Park and Ang, 1985). The literature review also suggests that the number of damage states is variable from one study to the other.

The studies which conducted NRHA mostly utilize SDOF systems that are representative of buildings or simplified two-dimensional (2D) frames since three-dimensional (3D) frame analysis requires much time. In building models many geometrical characteristics are neglected, which may be important in earthquake-induced damage upon their use in the models. Some of these characteristics can be stated as the structural element locations on the plan, the elevation and frame configuration. The low-engineered buildings in Turkish construction practice exhibits poor geometrical characteristics and should be accounted for in the fragility curves. It is believed that studies conducted with 3D models

would contribute to the development of more realistic and advanced fragility functions in comparison to those developed from simplified models.

1.3. Scope of the Thesis

According to Turkish Statistical Institute (2011), 21.7% of households in Istanbul are in buildings constructed before 1980, 42.8% of households are in buildings constructed before 1990, and 10.2% of households are in buildings with unknown construction year. Until today nine national earthquake codes are published. The earthquake loads are first considered in the 1949 code by a simple expression. However, the 1975 code provides the first more detailed provisions in terms of earthquake resistant design. The earthquake performance of buildings in Istanbul after the 1999 Marmara earthquakes suggest that many residential buildings constructed before 1975 (or even before 1980) are vulnerable to seismic actions because they do not comply with the fundamental of earthquake resistant design and they are poorly constructed due to lack of a strict control mechanisms. This short discussion suggests the importance of risk assessment and risk planning in İstanbul (e.g., KOERI, 2003), in particular for residential buildings constructed before 1980 (These buildings are generally referred to as no code buildings in the literature).

The present study aims to provide fragility curves for no code residential buildings in Istanbul for different damage states. The technical drawings (blue prints) of approximately 800 pre-1980 buildings located in Zeytinburnu District are examined to capture the most common construction features in İstanbul for the pertaining period. Since the inventory generally consists of moment resisting mid-rise frame buildings, this study covers only residential buildings of this type. Many parameters including geometrical characteristics, section dimensions and material properties are evaluated statistically to define the dominant features of the inventory. These statistics provided the necessary data for establishing the 3D building models. Main observations from the inventory study are unsymmetrical plan configuration, poor frame configurations (discontinuity in columns and beams along a frame axis), existence of soft-stories and closed cantilevers in the upper stories. The observed deficiencies can trigger more structural damage for the type of residential buildings considered here and their effect can be best reflected by performing 3D NRHA. Currently,

fragilities developed for Turkey for the building group of concern bear on simplified SDOF or 2D frame NRHA.

Incremental Dynamic Analysis (IDA) (Vamvatsikos and Cornell, 2002) is performed to determine the statistical distribution of the EDPs (interstory drift ratio, plastic chord rotation and strain). IDA is applied by incrementally scaling a ground motion intensity measure (PGA in this study) and by performing NRHA at each incremental step. A set of real ground motions, which are consistent with the disaggregation results of a probabilistic seismic hazard assessment for Istanbul are compiled from the Pacific Earthquake Engineering Research Center (PEER) strong motion database (https://ngawest2.berkeley.edu/) and are used in the analysis. OpenSees v3.0 Software (Open System for Earthquake Simulation; UC Berkeley, 2019) is utilized to perform NRHA. In order to shorten the computation time, a script which lets the OpenSees execute in multi-core computers was generated, and the analyses were performed with cloud computing. The overall NRHA as well as the 3D building models result in assessing the effects of record-to-record variability, structural variability, ground motion model uncertainty and limit state definition uncertainty on the fragility functions of the subject building class.

2. BUILDING INVENTORY

The blueprints of 800 residential buildings in Zeytinburnu District that are built before 1980 (pre-1980 buildings) are examined to develop subject fragility functions. The construction practice of the residential buildings compiled from Zetyinburnu is similar to most of the existing pre-1980 residential buildings in Istanbul. Thus, it is believed that the compiled building inventory is representative of pre-1980 residentail buildings in Istanbul.

Given a building in the inventory, more than 50 parameters that characterize material properties and geometrical characteristics (e.g., plan dimensions, element cross-sections, story height, etc.) are extracted from the blueprints. The statistics of these parameters are combined to establish representative building models for nonlinear response history analysis. This chapter first summarizes the building inventory information and then presents the representative building models.

2.1. General Inventory Information

The building inventory includes (a) Reinforced Concrete Moment Resisting Frames (RC-MRF), (b) Reinforced Concrete Wall Frames (RC-Wall-Frame), (c) Reinforced Concrete Frames having flat slabs (RC-Frame-Flat-Slab), and (d) Reinforced Concrete Wall frames having flat slabs (RC-Wall-Frame-Flat-Slab. Since 95% of these buildings are RC-MRF, only this building typology is included within the scope of this study. However, it should be noted that most of the RC-Wall-Frame buildings have similar geometrical configurations, material properties and section dimensions with the RC-MRF buildings. Therefore, the geometrical, material and section dimension parameters of the wall-frame systems are also included in the survey, although the generated models do not have wall elements. Since flat slab structures, which constitute a small portion of the building inventory are eliminated from the inventory a total of 754 buildings are investigated to establish the overall characteristics of RC-MRF buildings. The collected data from the building inventory consist of the following parameters:

- Material properties
- Geometrical shape of the plan view

- Plan dimensions
- Projection dimensions beyond the re-entrant corners in the plan
- Total area of the openings in the floor area
- Number of bays
- Span dimensions
- Number of stories
- Number of basement stories
- Ground floor height
- Average normal story height
- Existence of added floor and mezzanine floors
- Number of columns
- Unit area (normalized area) of total columns per total plan area
- Average column sections within the floor and its standard deviation
- Changes in the column dimensions along the elevation
- Discontinuities of the columns along the elevation
- Discontinuity in columns and beams along a frame axis
- Typical beam section
- Slab System
- Slab dimensions

Given a building, the longer plan dimension is always considered as x-axis while specifying the dimension related parameters and column dimensions.

The literature survey reveals that the number of stories has a significant effect on the vulnerability of the building, especially for no-code buildings (Akkar et al., 2005). Increase in the story number results in higher vulnerability against earthquakes for no-code buildings in Turkey. For this reason, most of the researchers group the fragility functions by considering story numbers or building height (e.g., low-rise, mid-rise, etc.). The compiled building inventory is limited in terms of story numbers to consider modeling of different height-based building classes. Hence, the models established from the database is representative of mid-rise RC-MRF pre-1980 buildings in Turkish building construction. This is discussed further in the following paragraph.

The investigated buildings are four- to six-story and 69% of the buildings are five-story excluding basement stories (Figure 2.1). The member sections and geometrical characteristics in the subject database are not sensitive to the number of stories. For this reason, only five-story building models are constructed as the representative of mid-rise pre-1980 RC-MRF buildings. Since the blueprints do not have any information regarding the basement floor, the basement floors are disregarded in the models.

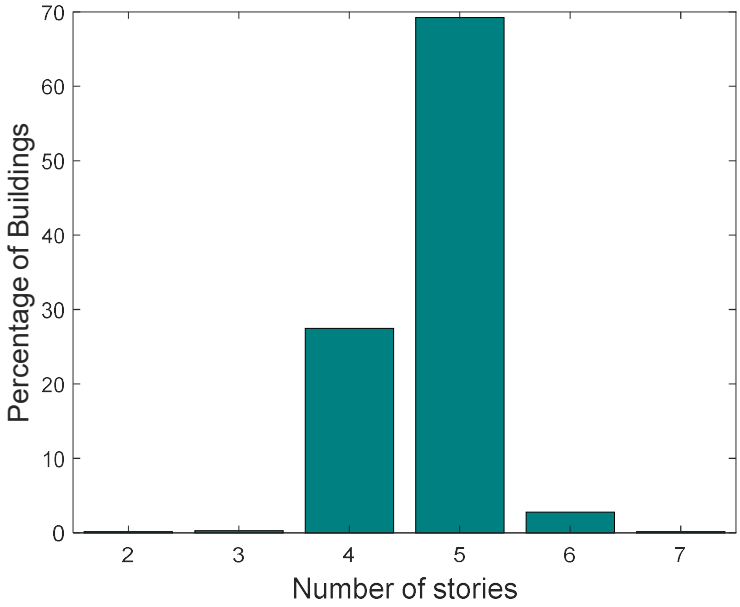

Figure 2.1. Distribution of building inventory in terms of the total number of stories.

One of the crucial matters in the subject building stock is the low material quality. While the Turkish Seismic Code of 2019 (Disaster and Emergency Management Authority, 2018) does not allow concrete class less than C25, most of the investigated no-code residential buildings have concrete strength much lower than this. The buildings in the present study have concrete strengths that are representatives of C10 and C14. The distribution of concrete strength in the building database is presented in Figure 2.2. Since there are only two concrete-classes in the considered building inventory and since most of the buildings belong to C10 concrete-class, the model buildings are assumed to have C10 concrete strength and uncertainty in concrete strength is disregarded. Using the mean of the probability density function (PDF) fitted on the concrete class distribution, the concrete strength is assumed as 11 MPa (C11) in all building models. All buildings in the database

are in S220 reinforcement class and reinforcement yield strength is directly taken as 220 MPa in the building models.

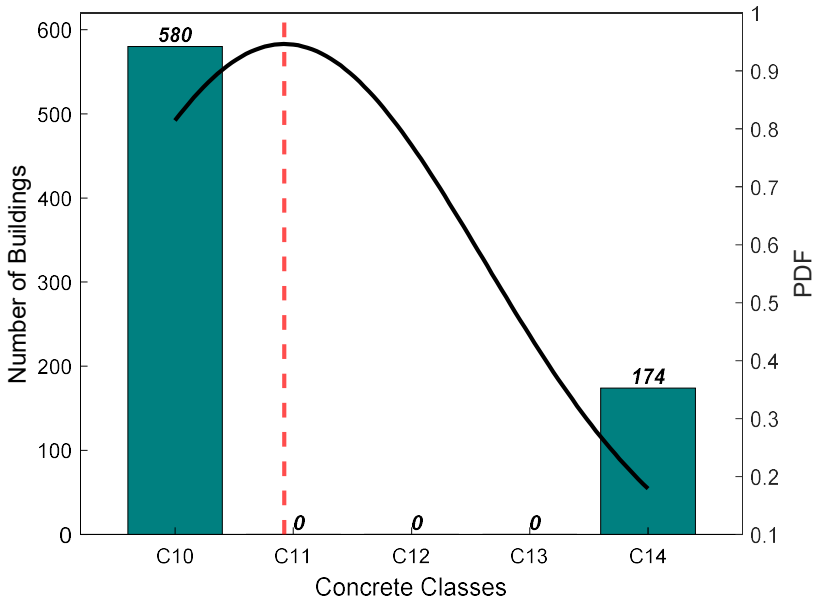

Figure 2.2. Distribution of building concrete class in the inventory

More than half of the buildings have an added floor, a mezzanine floor in the ground story or both as presented in Figure 2.3. However, the existence of the added floor and mezzanine floor is only apparent in the cross section views, and there is no information in the blueprints regarding their geometry and the material properties. However, since added floor and mezzanine floors may have a significant effect on the seismic behavior of buildings they are included in the models.

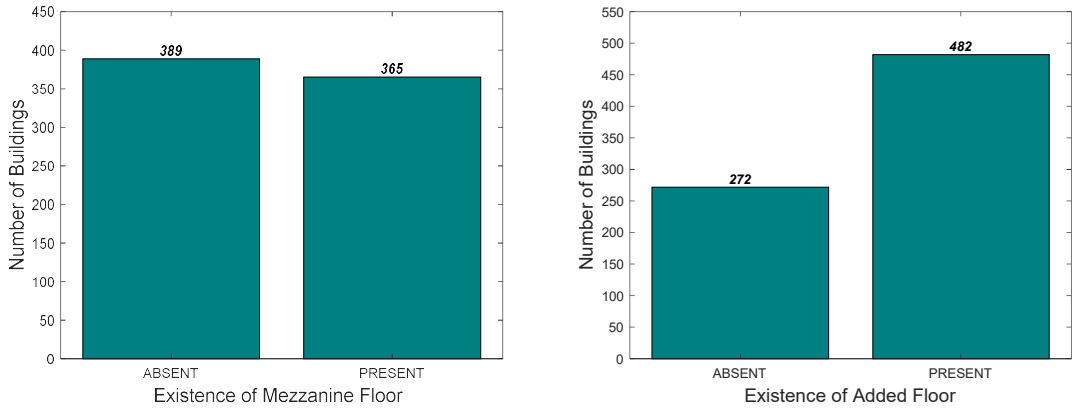

(a) (b)

Figure 2.3. Distribution of Mezzanine Floor (a) and Added Floor (b) in the building database.

The buildings with mezzanine floors have taller ground stories in height without changing the column dimensions throughout the entire building height. Besides, the mezzanine floors have large floor openings. These characteristics may lead to soft story and torsional irregularity. Therefore, mezzanine floor effect is considered in the model. The height of the ground floor is available in the cross-section views of the blueprints. It is assumed that there is an RC-mezzanine floor at the half of the ground story level. The floor plan of mezzanine is set randomly from a portion of the ground floor and is modeled as part of the structure. Additional masses are used at the roof to represent the added floor for building models that mimic added floor effect. Since it is expected that the first story of these buildings will reach their capacities before their top stories do, increasing the mass at the roof level is believed to be sufficient to capture the added floor effect against earthquake action.

One of the observed deficiencies in the building stock is the discontinuity in columns and beams along a frame axis. For instance, Figure 2.4 presents the ground floor plan and the typical upper story floor plan of a building in the inventory. Most of the perimeter beams at the ground level do not continue in the upper story floors. This feature is frequently observed for most of the buildings in the inventory.

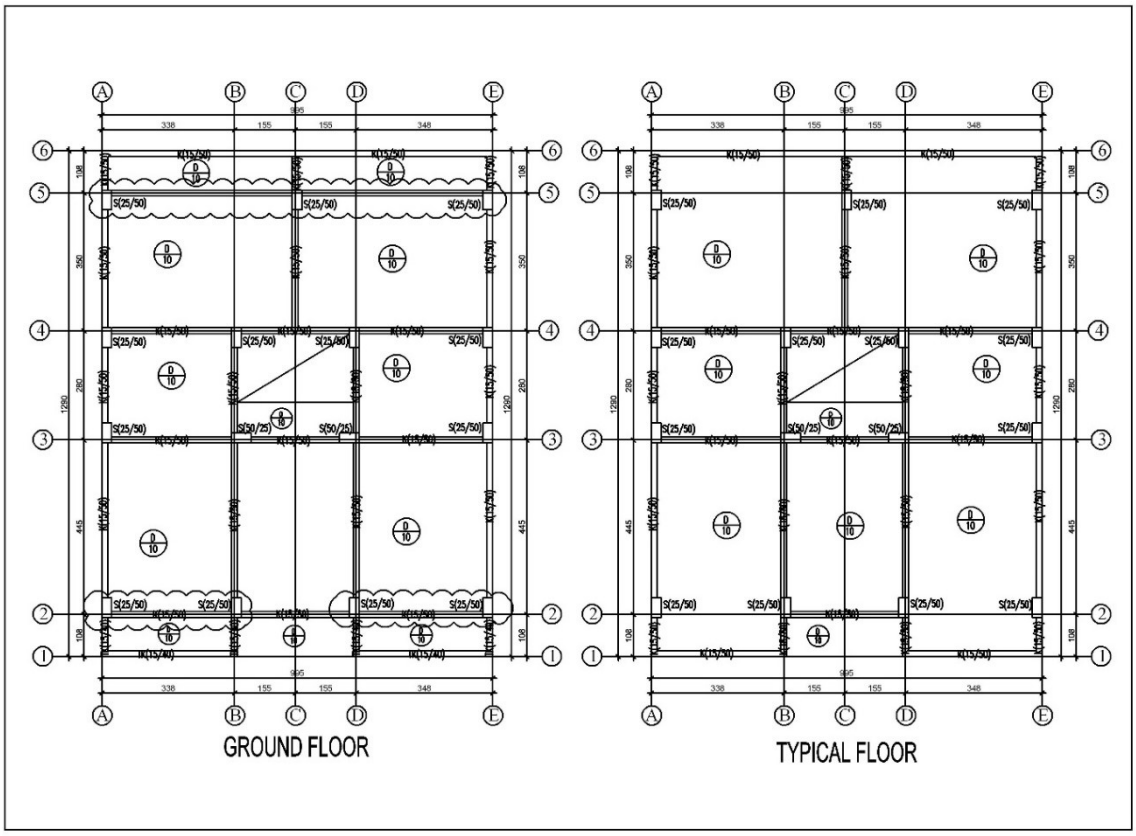

Figure 2.4. Example blueprint from the building database (Periphery beams at ground level do not continue in the upper story floors).

The number of unrestrained columns along the lateral directions (x- and y- axes) is included in the statistical survey. Figure 2.5 presents the percentages of unrestrained columns by beams along x- and y- axes in the building inventory. These statistics are given for a single story and applies to all typical stories. In most cases, the columns at the edges and corners of the buildings are unrestrained in the perpendicular direction to the cantilevers. Figure 2.6 presents the number of buildings having unrestrained columns along x- and y-axes. In general, the number of unrestrained columns along y-direction is higher than those along x-direction. Since the framing configuration is one of the critical components in earthquake induced damage the representative models account for 0-10% and 0-30% of unrestrained columns along x- (long) and y- (short) axes, respectively under the light of statistics given in Figure 2.6.

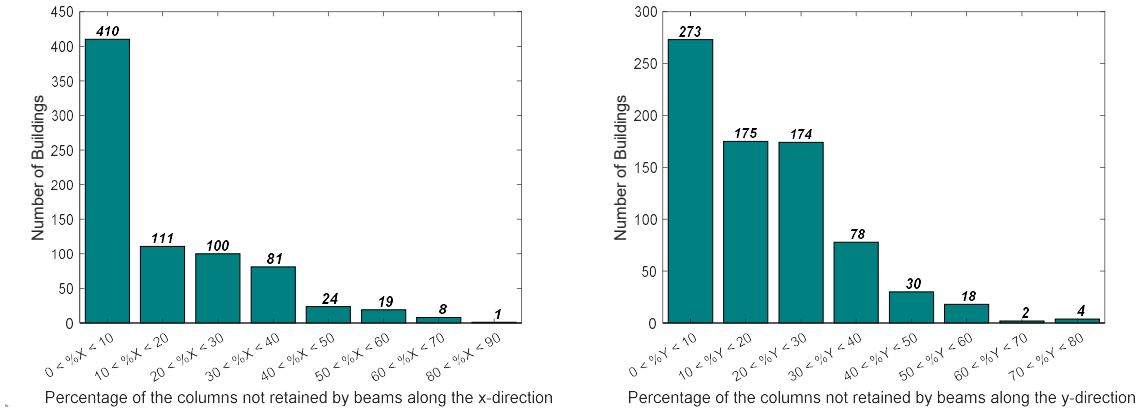

(a) (b)

Figure 2.5. Distribution in the building inventory in terms of column percentages that are not restrained by beams in a story along (a) x-axis and (b) y-axis.

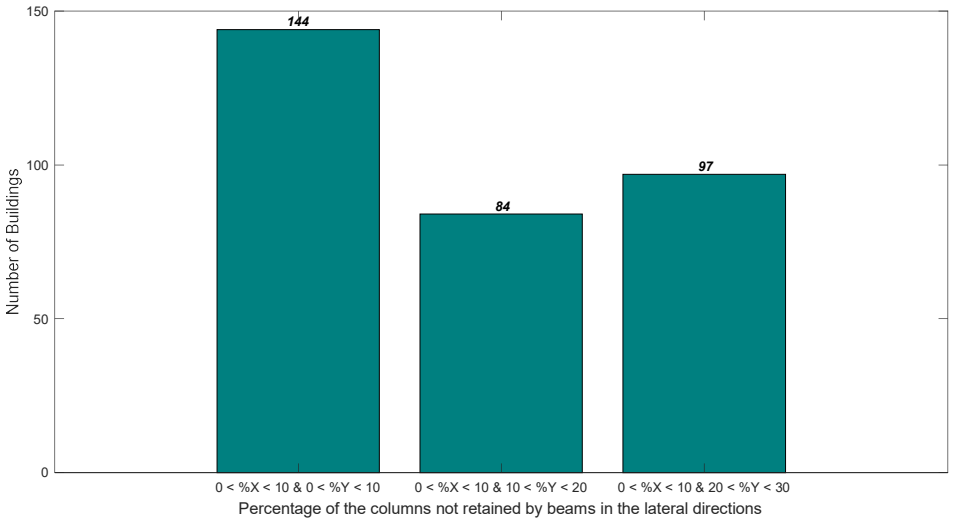

Figure 2.6. Distribution in the building inventory in terms of building numbers that have unrestrained columns (by percentage) in a story along x- and y-axes

The buildings in the inventory do not exhibit significant percentages of discontinuous columns along the vertical axis that may happen to occur by removing a column resting on the column or on the beam in the upper story (Figure 2.7). Thus, such irregularities are disregarded in the representative building models.

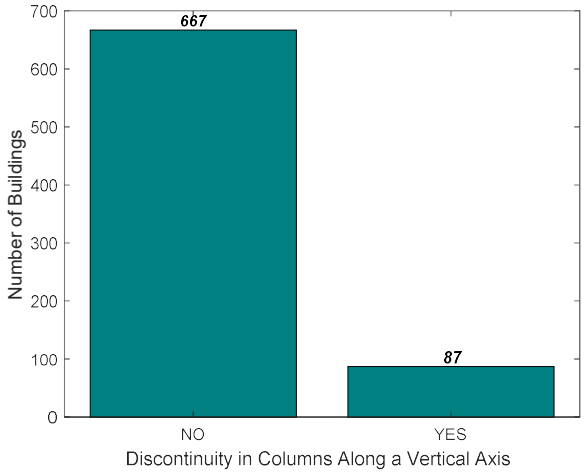

Figure 2.7. Distribution of discontinuous columns along the vertical axis in the building inventory.

There is no information regarding the reinforcement detailing and the construction year of the buildings in the inventory. Since the buildings are considered to be constructed before 1980, the 1968 and 1975 national earthquake design codes (TEC, 1968; TEC, 1975) are assumed as the reference design codes while evaluating the missing reinforcement detailing information. There is quite limited information about the detailing requirements of RC structures in TEC (1968); the topics in TEC (1968) are mostly about the section dimensions. Thus, it is assumed that the beams and columns meet the minimum longitudinal reinforcement requirements of TEC (1975). Evidently most of the buildings in the database do not fully comply with all the provisional requirements of TEC (1975). For example, there are beam sections with 15 cm width, which is not allowed in TEC (1975) but applicable in TEC (1968) (Figure 2.20 in the referred code). However, for the longitudinal reinforcements, the minimum requirements by TEC (1975) is considered as sufficient for the overall structural damage estimation of the entire building stock. The confinement in RC sections is another critical feature in the damage assessment. While the confinement details are fully given in TEC (1975), TEC (1968) only requires the use of half spacing of the mid-column transverse reinforcement in the column-beam joints. There is no information about the hook angles of the transverse reinforcement. Since the distribution of ductile detailing in the inventory is unknown, with and without confinement conditions are accounted for in the model buildings. The minimum confinement requirements by TEC (1975) are taken into account in the confinement detailing of model buildings that are representatives of confined building case studies in the fragility functions.

The structural features discussed in this section are essential for proper structural analysis as well as structural damage estimation of the building inventory. As such, Figure 2.8 shows the breakdown of model buildings that represent one or more distinctive effects of the structural parameters on the building inventory of interest.

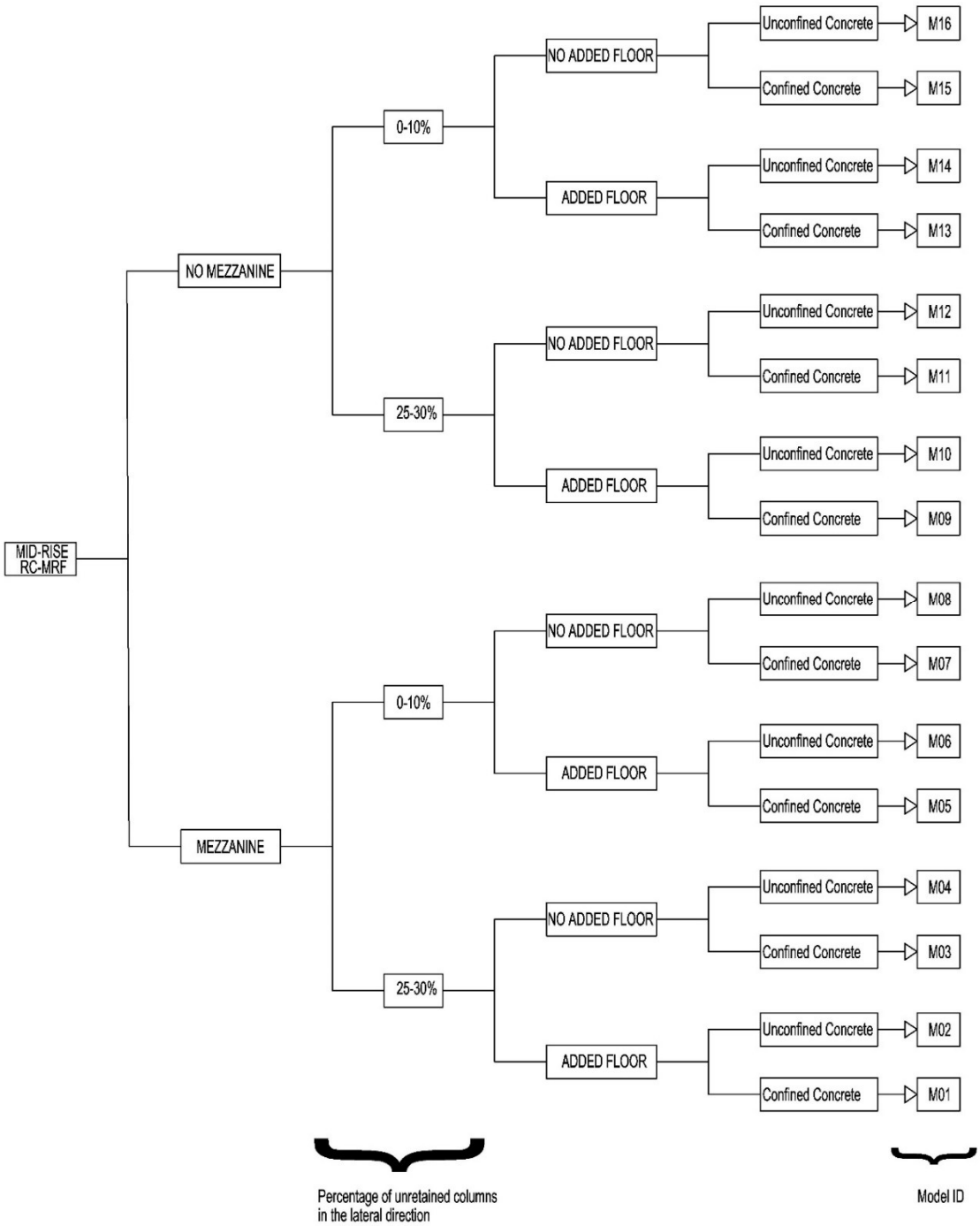

Figure 2.8. Building models reflecting the overall structural behavioral characteristics of the building inventory.

2.2. Definitions of the Building Characteristics

The statistics of plan geometry and section dimensions are presented in this section. Since there are no significant variations within these features in the subject inventory, their most observed values are assigned to the model buildings either randomly or in a deterministic manner.

Figure 2.9 presents the distribution of building floor plans in terms of their geometrical shapes. 75% of the buildings have a rectangular shape in floor plan while the rest has trapezoidal shape or has unique floor plan geometries which are not statistically meaningful to establish a distribution. Besides 95% of the buildings do not have any bulges in the floor plan or have bulges less than 20% of the total length in the related direction. Therefore, only buildings having regular rectangular plan geometries are considered in the models.

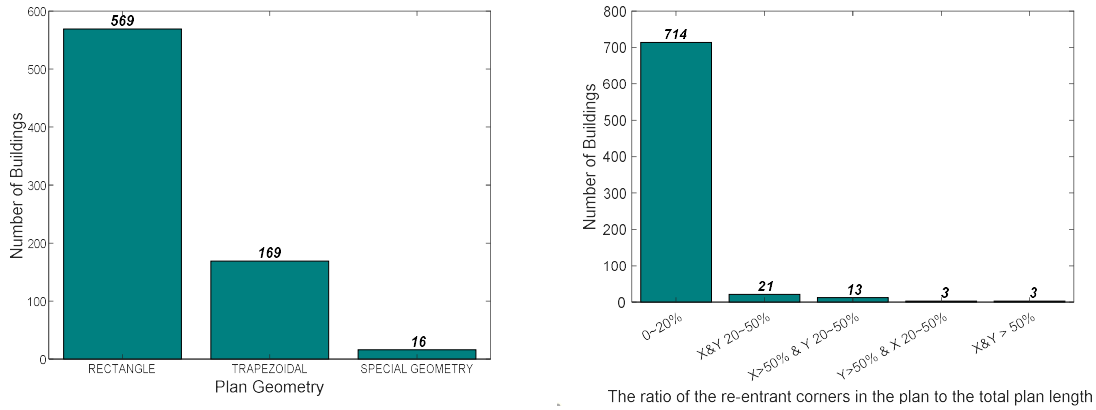

Figure 2.9. Distribution of building inventory in terms of floor plan geometry (a) and the ratio of the re-entrant corners in the plan to the total plan length (b).

Regular placement of columns on the floor plan is not applicable in the buildings even if they exhibit rectangular floor plan. As it is seen in the sample blueprint in Figure 2.4, the location of columns is not symmetrical in the long direction. Asymmetrical configuration of structural elements in the building inventory is one of the main observations in the majority of the buildings. In essence, the asymmetrical placement of structural components is significantly influenced by architectural reasons such as locations of the stairwells or configuration of the apartments in the buildings having different floor plans and dimensions.

In the modeling phase, buildings having similar architectural configurations are grouped together and a common floor plan is generated from their structural member layouts for the pertaining model buildings. For each building group, the general floor plans also consider the statistics of bay numbers, span dimensions, relative span dimensions within the floor plan, the offsets in abnormal column locations and vertical irregularities such as discontinuous column axis. Figure 2.10 and Figure 2.11 present the distributions of span numbers in both principal axes and the dependent number of spans, respectively. Most buildings in the inventory have three spans in the long direction and three or two spans in the short direction. Therefore, 3x3 and 3x2 frame grid systems are used in the models.

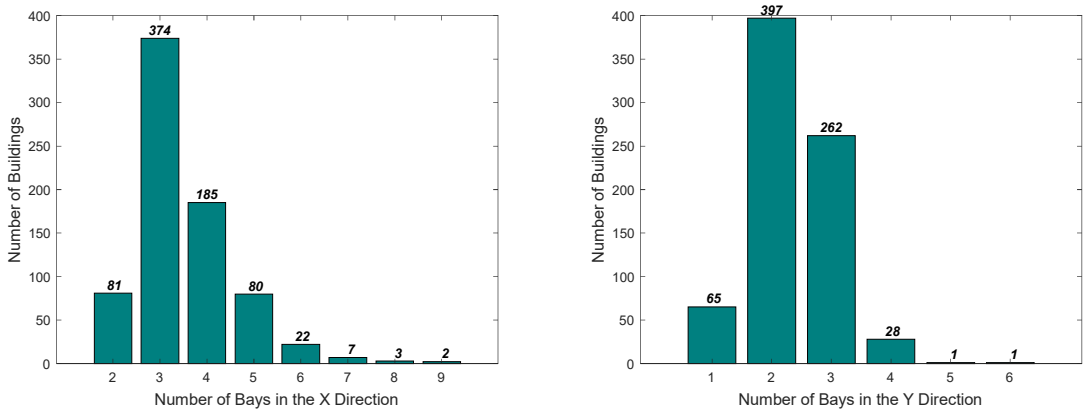

(a) (b)

Figure 2.10. Distribution of span number in the building inventory: (a) x-direction and (b) y-direction.

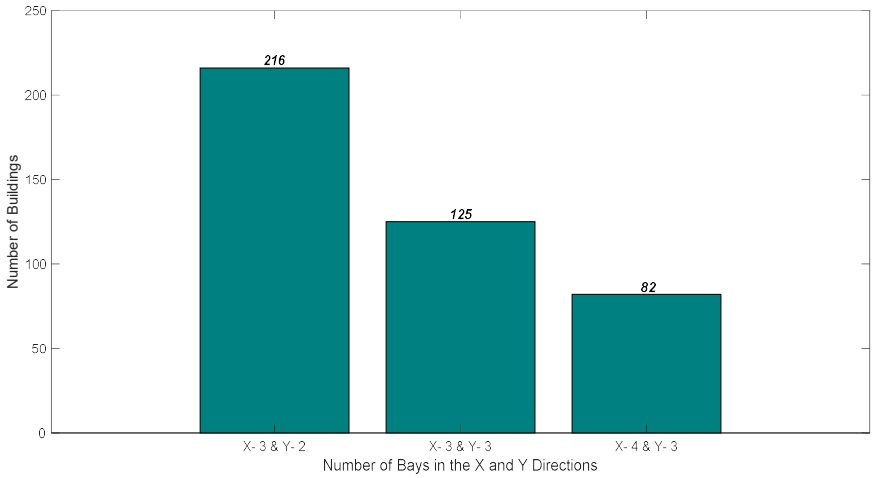

Figure 2.11. Distribution of dependent number of spans in the building inventory.

Span dimensions are computed from the probability density functions given in Figure 2.12. The relative span dimensions in both principal directions (i.e., x- and y-axes) are also considered during these computations. Figure 2.12 shows the probability distributions of maximum and minimum span dimensions in both directions. The hatched area presents the plus/minus one standard deviation. The probability distributions suggest that the building inventory does not show significant differences in span dimensions along the principal directions. The span dimensions of the building models are assigned randomly in both principal directions by using these probability distributions and the architectural floor layouts that are discussed in the previous paragraphs.

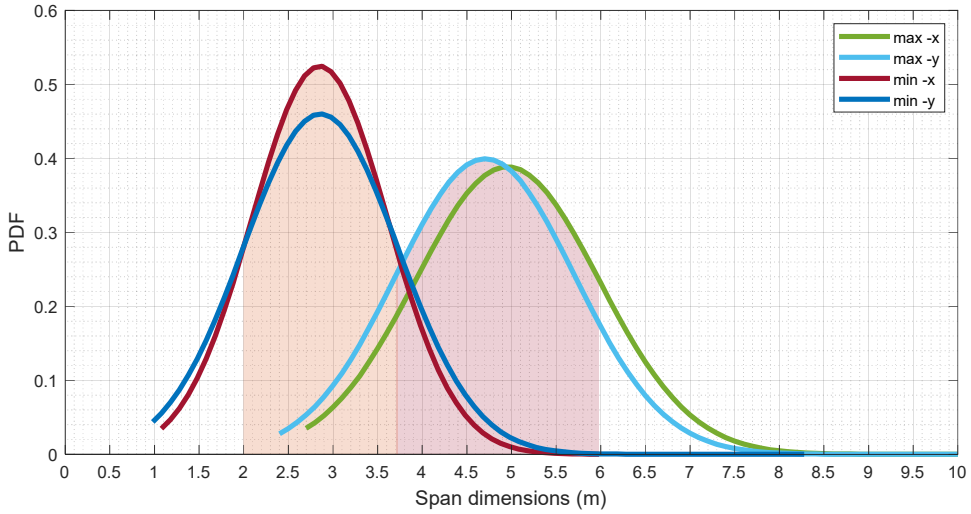

Figure 2.12. Probability density functions of span dimensions along principal directions.

Another dominant feature of the building stock is the cantilever beam system (to increase the floor area) that starts from the second floor and continues in all upper stories. This architectural system is common in almost all pre-1980 residential buildings in Turkey. The distribution of the cantilever beam lengths is given in Figure 2.13. As it is depicted from this figure, the cantilever beam length mostly varies between 1.0 m and 1.5 m, and the model buildings consider this length as 1.5 m. Their architectural layout is perpendicular to the columns that are not constrained by the beams and this configuration is considered in the model buildings. (See discussions in Section 2.1 for constrained and unconstrained columns in the building inventory).

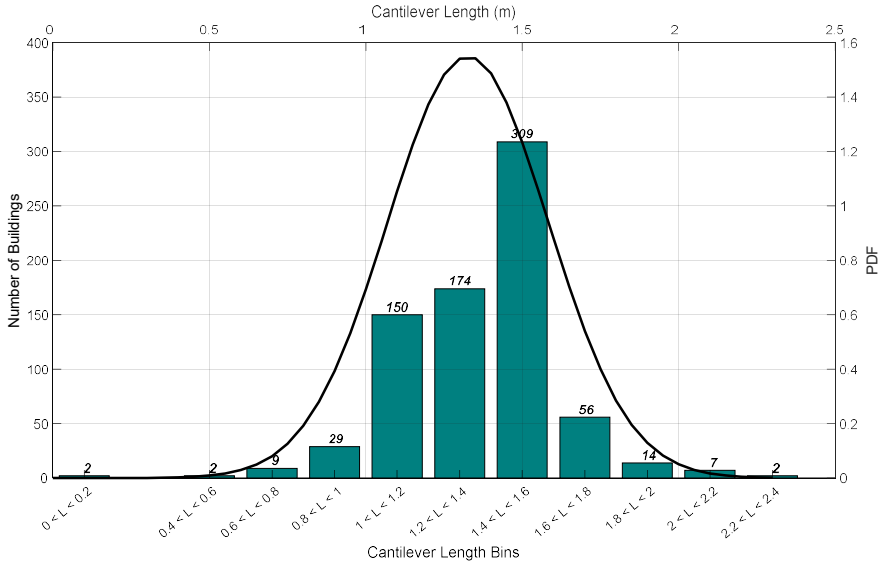

Figure 2.13. Distribution of cantilever bean length in the building inventory.

The distributions of a typical floor and ground floor story heights are given in Figure 2.14 and Figure 2.15, respectively. (Side note: typical floor refers to stories above the ground story). There is no significant variation in the typical floor height in the building inventory. As such, the story height of a typical floor is considered as 2.75 m in the building models. The story height of the ground floor is higher than the typical floor height as this floor is generally utilized for commercial purposes. The distributions given in Figure 2.15 indicate that the ground floor story height changes with the existence of mezzanine floor. For the sake of simplicity, the story height of the ground floor having a mezzanine floor is taken as 5.5 m in the building models. This height is 3.25 m for the models that disregard the mezzanine floor at the ground level.

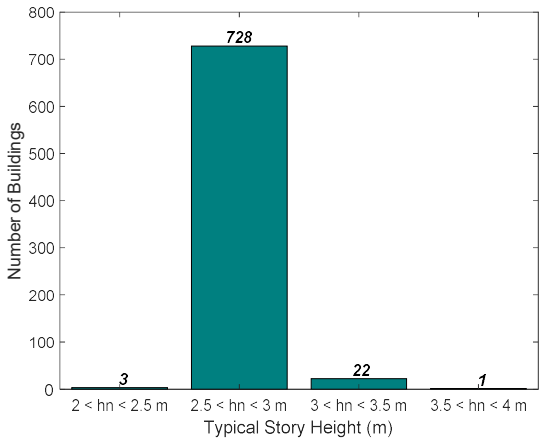

Figure 2.14. Distribution of building inventory in terms of typical floor story height.

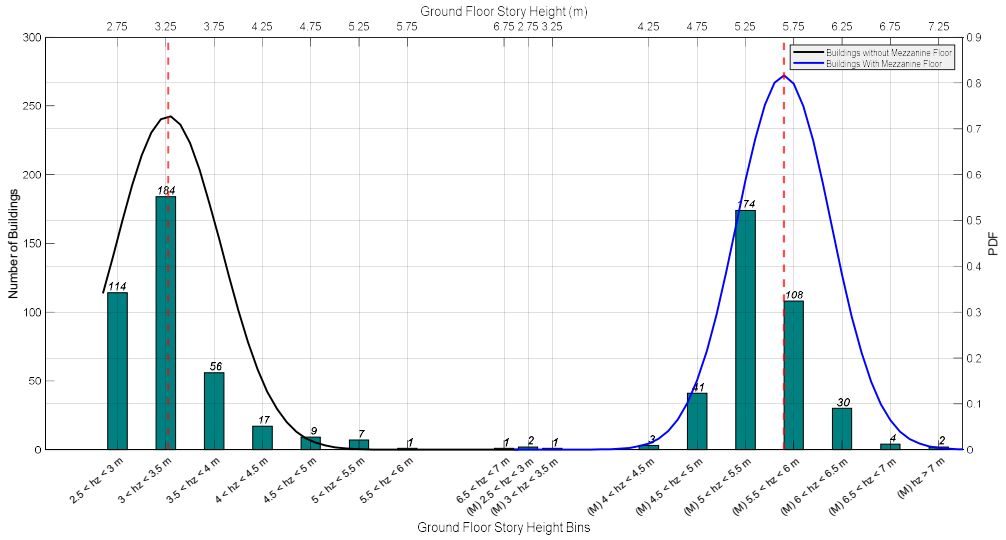

Figure 2.15. Distribution of ground floor story height (with and without mezzanine floor) in the building inventory.

The distributions of mean column dimensions along the principal directions (i.e., x- and y-axes) are given in Figure 2.16. The mean column dimensions mostly vary between 30 to 50 cm along the long- and short- directions in the buildings. While establishing the 3D building models, the mean column dimension distributions are evaluated together with the statistics depicted in Figure 2.17 and Figure 2.18. Figure 2.17 shows the mean column dimension distribution in y-direction by considering the most observed mean column dimensions in x-direction. Figure 2.18 shows the same mean column distribution for x-direction with the consideration of most observed mean column dimensions in y-direction. No correlation is detected between the column dimensions and the other features of the buildings (e.g., span dimensions or story heights) in the inventory. Thus, column dimensions are not assessed separately for the building groups presented in Figure 2.8. Figure 2.16, Figure 2.17, and Figure 2.18 indicate that the choice of mean 45/35 cm column section is sufficient enough to achieve the representative column density since it is the most observed dimension.

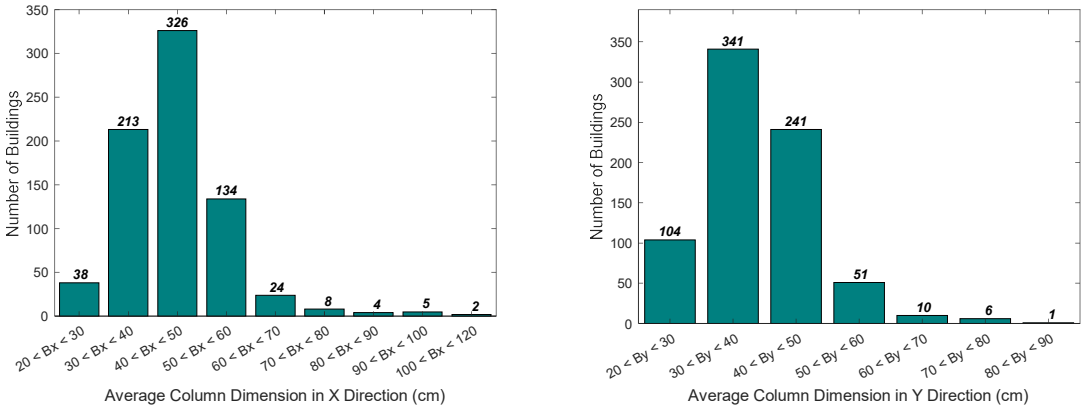

Figure 2.16. Distribution of mean column dimensions in the building inventory (a) x-direction and (b) y-direction.

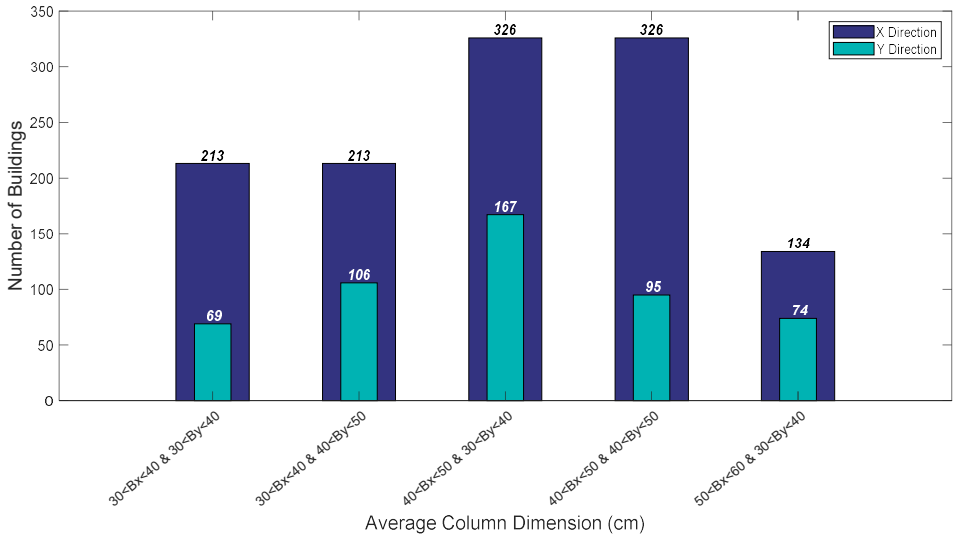

Figure 2.17. Distribution of mean column dimensions in y-direction by considering the most observed mean column dimensions in x-direction.

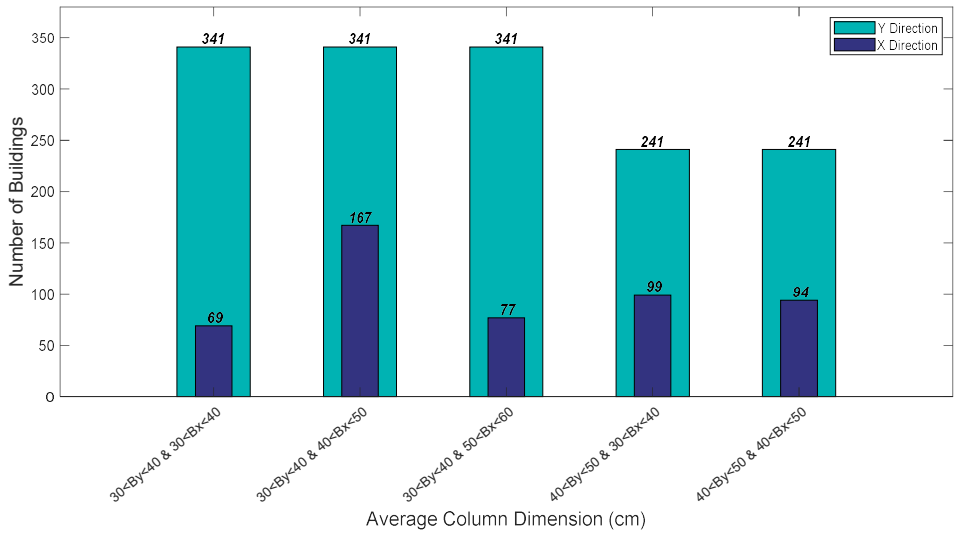

Figure 2.18. Distribution of mean column dimension in x-direction by considering the most observed mean column dimensions in y-direction.

Figure 2.19 shows the building statistics that have variant and invariant column dimensions along the building height. The statistics indicate that buildings having invariant column dimensions along the building height constitute the majority in the inventory. This is the major reason for disregarding the change in column dimensions towards upper stories in the model buildings.

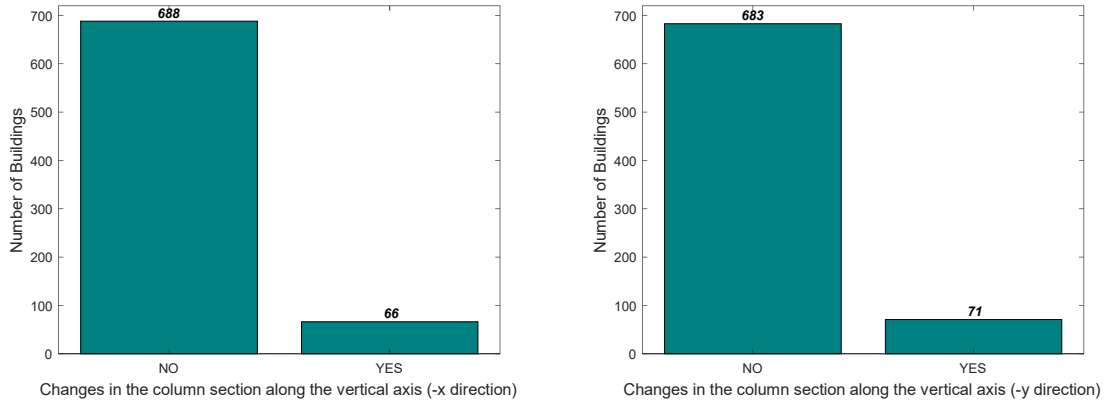

(a) (b)

Figure 2.19. Changes in the column section in the (a) x-direction and (b) y-direction along the building height.

Figure 2.20 shows the variations in beams dimensions in the building inventory. The majority of buildings have 20 cm by 50 cm beam dimensions and they are used in the model buildings.

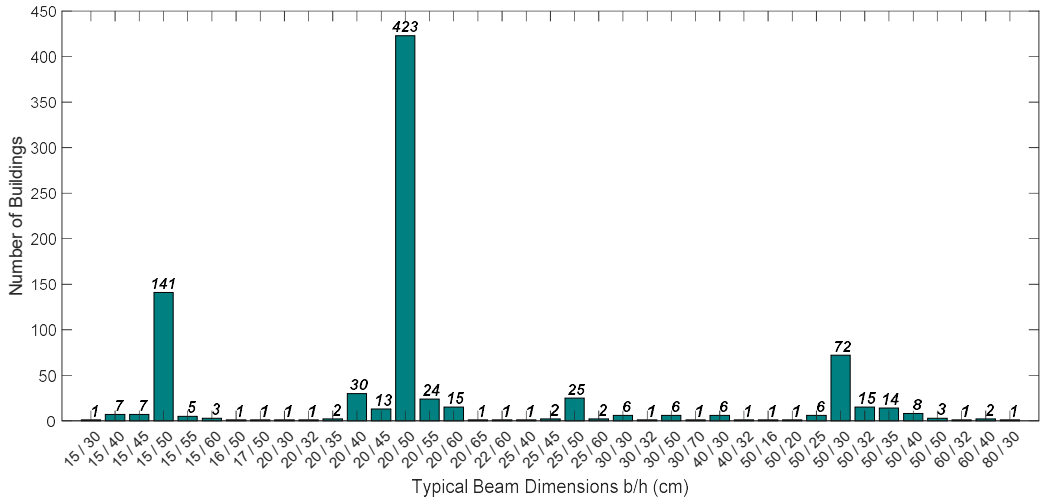

Figure 2.20. Distribution of beam sizes in the building inventory.

2.3. Representative Building Models of The Investigated Building Inventory

The floor plans of representative building models as well as other statistics (histograms) collected from the building inventory regarding the total plan area, total plan dimensions, number of columns, and unit column area are given as an appendix (Appendices A and B) at the end of the thesis. Although these statistics are not directly used while establishing the representative models, the model buildings do reflect the major features given by these distributions.

The resulting building models carrying the essential characteristics of the investigated building inventory. They represent the no code (or low code) construction and design practice in pre-1980 residential buildings in Istanbul, which can also be valid for the entire country. The model buildings also reflect the architectural layout (floor plans, mezzanine floors, added floors, structural member configurations, etc.) in residential buildings at that time. As the models reflect geometrical uncertainties (to a certain extent) by making use of distributions that are presented in the previous sections, they would show the sensitivity of structural damage patterns against earthquake action that will be discussed in the next chapters.

3. ANALYTICAL MODELING

3.1. Introduction

Computer aided response analyses are the most efficient way to determine the response of the structure against seismic action. Although there are empirical methods such as testing of individual structural components under cyclic loading and shake table tests of the scaled structures; their implementation is not practical to describe the complete structural behavior considering the complicated relationship between the earthquake, structure, and soil. In general, such tests are used for calibration and verification of component hysteretic models or for verification of the mathematical formulations, which are used to estimate dynamic parameters of the structures. The calibrated hysteretic models or verified mathematical formulations are latter used in computer aided response analysis of structures. There are numerous proposed techniques to be used in computer aided dynamic response analyses of structures. The modeling techniques and appropriateness of accompanying assumptions for the considered case study are the critical points while running these techniques for understanding the dynamic structural behavior.

Structures usually exhibit nonlinear behavior when they are exposed to severe earthquake ground motions. Thus, to determine the ductility demands and their ultimate capacity, nonlinear modeling is a must. Unlike linear analysis, nonlinear modeling is not straightforward and is considerably sensitive to modeling assumptions. Also, solution algorithms used in nonlinear response analysis are not unconditionally stable and require special treatment to approximate the structural response within an acceptable tolerance level. Thus, a more significant challenge underlies regarding the interpretation of nonlinear structural response computed from an analytical model.

OpenSees Software (Open System for Earthquake Simulation; UC Berkeley, 2019) is used to generate the 3D numerical models of the model buildings. OpenSees Software is based on Tool Command Language (Tcl). Although the model description is time consuming in OpenSees compared to other software with graphics interface; the possibility of using loops in the scripts enables the users to carry out many simulations within a lesser software

execution time. For example, the present study conducts Incremental Dynamic Analysis (IDA) with different scaling increments for each ground-motion record. A total of 25 ground-motion records having two horizontal components are implemented to 16 model buildings. Since the directional uncertainty in ground motion is also considered in the analysis, for each incremental scaling of the ground motion record, two structural analysis is performed in each principal building axis. Each model building is considered as a separate case and the scaled records that are applied in principal building directions are looped for every case. This type of batch processing is relatively easy with the looping feature of OpenSees software.

The adopted modeling strategy that is utilized in OpenSees software is presented in the following sections. OpenSees includes many solution algorithms (e.g., Newton Line Search, Modified Newton, etc.) because convergence is a crucial issue in Nonlinear Response History Analysis (NRHA). The availability of different solution algorithms in OpenSees and being able to change the solution algorithm, or the solution algorithm parameters at the non-converged time step in the analysis substantially facilitates the convergence issues. The parallel processing algorithm is utilized for each execution, and all the analyses are completed in 5 days by using the computer resources provided by the National Center for High Performance Computing of Turkey (UHeM).

The following sections first briefly summarize the available nonlinear modeling strategies and then present the modeling and solution techniques used in the present study. The chapter ends by introducing the considered earthquake hazard as well as the ground motion records that are used in the nonlinear response history analyses.

3.2. Modeling Strategies

There are mainly three modeling approaches for structural systems; global models, discrete finite element models, and microscopic finite element models (Taucer, 1991). Global models are based on the representation of the structural system with concentrated degrees of freedom. SDOF systems or multi-degree of freedom systems having one lateral degree of freedom (dof) at each floor are examples of this modeling approach. Nonlinear behavior is represented by the hysteretic characteristic of the global response parameter (e.g.,

global drift response) simulated by the dofs. Since global models disregard the response of individual members, their use for design or performance assessment of a single structure is not practical. On the other hand, the use of global models in regional risk assessment is widespread due to its simplicity and computational speed. In contrast, microscopic finite element models are detailed and sophisticated models, in which the members and joints have meshed into a vast number of finite elements. It is possible to define the cracks, bond-slippage deteriorations and other complex structural behavior at the component level by microscopic finite element models (Taucer, 1991). The modeling and the computer solution is time-consuming and not efficient in microscopic finite element models while modeling, for example, RC structures whose material and behavior are very well known. Microscopic finite element models are generally useful in the analysis of single components and the historical structures.

The third modeling approach, discrete finite element model, consists of idealized elements, which reflect the characteristics of structural components (e.g., section dimensions, inertia, force-deformation relations, etc.) (Neuenhofer,1997). The elements are connected to the nodes to establish a similar configuration with the actual system. Since discrete finite element models establishes an optimized balance between modelling simplicity and response accuracy, and since they can reflect the geometrical characteristics of the structure, this modeling approach is adopted in the present study.

There are two ways to define nonlinearity in the structural elements. The first one is the lumped plasticity model, which concentrates the plasticity at the critical sections of the element (Giberson, 1967). It is usually applied by modeling an elastic member having nonlinear springs at its two ends. There are various constitutive models to define hysteretic characteristic of the springs such as stiffness degrading, stiffness degrading with shear deterioration and bilinear with axial interaction. Lumped plasticity approach should be used with some caution because nonlinear element behavior is dependent of loading and deformation histories, and some lumped constitutive models have deficiencies to represent this behavior (Taucer, 1991). The other approach to define nonlinearity is the distributed plasticity, in which the nonlinear element behavior is represented at the section level through stress-strain resultants or material constitutive relations that are controlled at the fibers (Spacone, 1996). Distributed plasticity models are conceptually more accurate than the

lumped plasticity models since the nonlinearity may be defined at any section in the element. Hence, the actual nonlinearity spreads to a zone within the element (Taucer, 1991).

There are various distributed models available in the literature. The common assumption in these models is that the plane sections remain plane where the strains are linearly distributed over the cross-section (Neuenhofer,1997). The element behavior is obtained from the weighted integration of the section responses where the yielding is permitted. The yielding zone may be defined within a hinge length or along the element length (Scott, 2011).

The model buildings of the present study represent no-code (do not comply with seismic design codes) or low-code (fail to comply with seismic design codes) and it would be inconvenient to restrict the yielding zones with the element ends. Thus, distributed models along the entire member length are utilized, even though this preference results in additional computer time and numeric stability problems.

The element deformations and forces are the unknowns in the distributed plasticity models; therefore, assumptions related to one of these unknowns would affect the solution of the other. There are mainly two types of solution algorithms: (1) displacement-based (stiffness-based) method and (2) force-based (flexibility-based) method (Spacone, 1996). The former methodology specifies an approximate displacement field along the element while the latter one interpolates internal forces (Correia,2008). Both algorithms are investigated in a detailed manner in terms of accuracy at high nonlinear levels and computational time since the adopted IDA algorithm requires a significant computational effort and building models have to mimic high levels of nonlinearity.

The displacement-based elements that are used in distributed plasticity modeling are also called as stiffness-based elements. This methodology is based on assuming a displacement field along the element by considering Hermitian polynomials (Spacone, 1996). For instance, Eq. 3.1 presents cubic interpolation function and linear interpolation function for the transverse displacement and the axial displacement, respectively for the uniaxial bending case.

$$N(x)=\begin{bmatrix}\psi_1(x) & 0 & 0 & \psi_2(x) & 0 & 0\\ 0 & \phi_1(x) & \phi_2(x) & 0 & \phi_3(x) & \varphi_4(x)\end{bmatrix}$$

$$\psi_1(x)=1-\frac{x}{L} \qquad \psi_2(x)=\frac{x}{L} \tag{3.1}$$

$$\phi_1(x)=2\frac{x^3}{L^3}-3\frac{x^2}{L^2}+1 \qquad \phi_2(x)=\frac{x^3}{L^2}-2\frac{x^2}{L}+x$$

$$\phi_3(x)=-2\frac{x^3}{L^3}+3\frac{x^2}{L^2} \qquad \phi_4(x)=\frac{x^3}{L^2}-\frac{x^2}{L}$$

Multiplication of the nodal displacement vector, ν, that is given in Eq. 3.2 with the interpolation function leads to transverse displacement (u_a) and axial displacement (u_t) along the longitudinal axis of the element (Eq. 3.3). The torsional degrees of freedom are assumed linear elastic and uncoupled from the axial and flexural degrees of freedom for this case. Regarding small displacement assumption and the plane sections remain plane assumption, section deformations are computed (Eq. 3.4) where ε and κ denote the axial strain and the curvature, respectively.

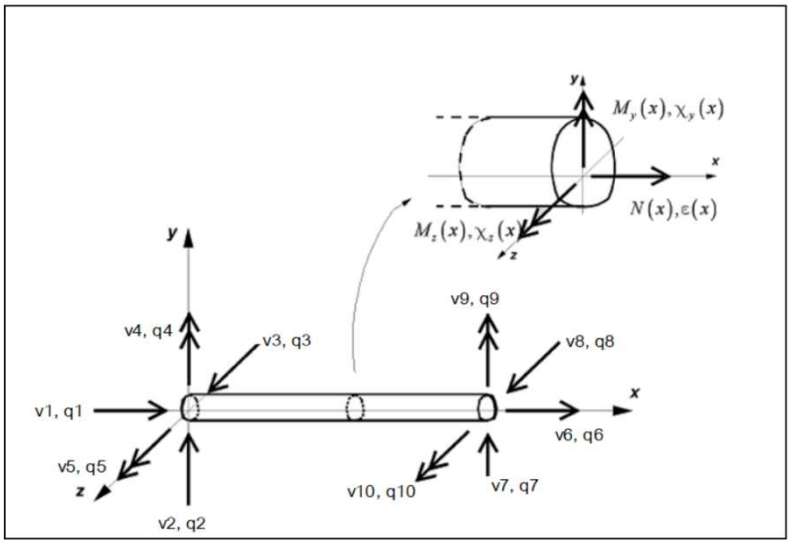

Figure 3.1. Beam element with rigid body modes in the local coordinate system.

$$v=\{v_1 \quad v_2 \quad v_5 \quad v_6 \quad v_7 \quad v_{10}\}^T \tag{3.2}$$

$$\begin{bmatrix} u_a(x) \\ u_t(x) \end{bmatrix} = N(x) \cdot v \tag{3.3}$$

$$\varepsilon_a(x) = u_a'(x), \qquad \kappa(x) = u_t''(x) \tag{3.4}$$

This way, section deformations are obtained from Eq. 3.6 where B(x) (given in Eq. 3.5) is derived from the interpolation function, N(x). Eq. (3.5) describes constant axial strain and linear curvature, which is only valid for the prismatic linear elastic elements.

$$B(x) = \begin{bmatrix} \psi_1'(x) & 0 & 0 & \psi_2'(x) & 0 & 0 \\ 0 & \phi_1''(x) & \phi_2''(x) & 0 & \phi_3''(x) & \varphi_4''(x) \end{bmatrix} \tag{3.5}$$

$$e(x) = \begin{bmatrix} \varepsilon_a(x) \\ \kappa(x) \end{bmatrix} = B(x) \cdot v \tag{3.6}$$

Once the section deformations are obtained, section forces can be derived from constitutive material laws (in the fiber section case) or stress-strain relations. For fiber sections, the procedure is as follows: (1) obtain fiber strain from section deformations (e) and the geometric vector (I) (given in Eq. 3.7) for the fiber of interest, (2) then for a given material model determine the stress at the fiber (Eq. 3.8), and (3) obtain section forces from the integration of fibers (Eq. 3.9).

$$I_i(y) = \begin{bmatrix} 1 & -y \end{bmatrix} \tag{3.7}$$

$$\varepsilon_i(x, y) = I_i(y) \cdot e(x), \qquad \sigma_i = \sigma(\varepsilon_i) \tag{3.8}$$

$$s(x) = \begin{bmatrix} N(x_i) \\ M(x_i) \end{bmatrix} = \sum_{i=1}^{N_{fibers}} I_i^T \cdot \sigma_i \cdot A_i \tag{3.9}$$

Principle of virtual displacements is utilized to obtain the element forces (q) from section forces (Eq. 3.10). For the distributed models (including the force-based elements), the integration of the element forces is applied numerically on the selected sections. N_p and w terms in Eq. 3.10 denote the considered number of integration points and section weight

for integration, respectively (Taucer, 1991). In this method, internal element forces are not in equilibrium with the basic element forces.

$$q = \int_0^L B^T(x) \cdot s(x)\, dx \approx \sum_{j=1}^{N_p} B^T(x_j) . s(x_j) . w_j \tag{3.10}$$

Force-based elements utilize force interpolation functions for the solution of element forces and satisfy exact equilibrium equations within the section level and within the element level (Neuenhofer,1997). On the other hand, since internal deformations and forces are the unknowns in the system, the procedure requires iterative solutions. There are different iterative procedures at different levels of complexity for force-based elements (Correia,2008). The following example algorithm is presented here to describe the underlying theory of the force-based elements and to compare it with the displacement-based elements.

The first equilibrium, which requires iteration is on the element level between the external (ν) and the internal (ν_R) element deformations as given in Eq. 3.11. Internal deformations (ν_R) are related to the section deformations (e) and force interpolation functions (bx) (shown in Eq. 3.12) through Eq. 3.13. Note that Eq. 3.13 utilizes the principle of virtual force and it is also called as compatibility function. For this example, the force interpolation function gives constant axial force and linear bending moment along the element (Eq. 3.12).

$$\nu - \nu_R = 0 \tag{3.11}$$

$$b(x) = \begin{bmatrix} 1 & 0 & 0 \\ 0 & \frac{x}{L} - 1 & \frac{x}{L} \end{bmatrix} \tag{3.12}$$

$$v_R = \int_0^L b(x)^T \cdot e(x)\, dx = \sum_{i=1}^{N_P} b(x_i)^T \cdot e(x_i)\, . w_i \tag{3.13}$$

The procedure starts with an initial estimation of basic element force (q). The section deformation (s) derived from Eq. 3.14 must be in equilibrium with the resisting section forces (s_R) as presented in Eq. 3.15. To satisfy the equilibrium condition given in Eq. 3.15,

an iterative procedure at the section level that starts with an initial estimation of the section deformation (e) is used. The estimated section deformation (e) is used to calculate the resisting sectional forces from fiber integration procedure, as given in Eqs. 3.7, 3.8 and 3.9.

$$s(x) = b(x) \cdot q \tag{3.14}$$

$$s - s_R = 0 \tag{3.15}$$

Once section deformations (e) that satisfy the equilibrium in Eq. 3.15 are computed, internal deformations (v_R) are obtained from the compatibility equation (Eq. 3.13). Note that if the equilibrium in Eq. 3.11 is not satisfied, then the initial estimate of the basic force (q) is calibrated, and the procedure is repeated.

The solution algorithm for the nonlinear systems either with displacement-based and force-based elements are given in Figure 3.2 (Scott et al., 2008).

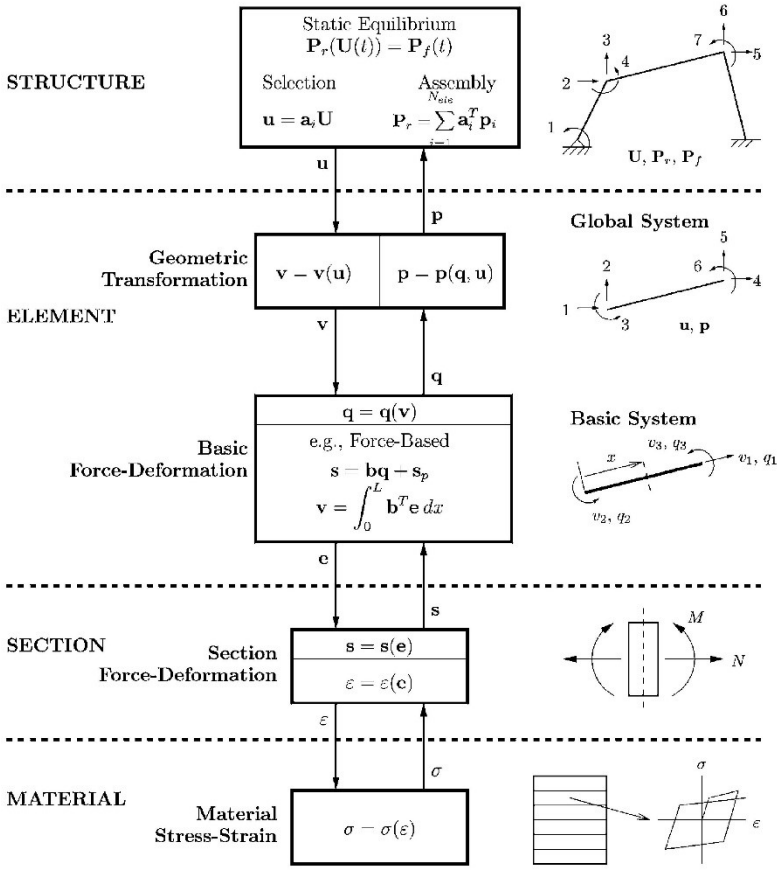

Figure 3.2. Modelling hierarchy for nonlinear structural analysis (Scott et al., 2008).

The solution algorithm of the force-based elements is not straightforward like displacement-based elements and requires iterative procedures in structural, element, and section level while the displacement-based elements require iteration only at the structural level (Neuenhofer,1997). Hence, nonlinear response history analyses by using force-based elements are more time consuming. On the other hand, as previously indicated, the linear curvature assumption in the displacement-based elements is only valid for prismatic linear elastic elements (Correia,2008). Thus, to converge a realistic solution to the nonlinear problem in hand, the analysis requires meshing of the elements (Feng, 2016, Neuenhofer,1997). The use of higher order shape functions is another alternative (the discussions in the above paragraphs are for cubic Hermitian interpolation function and they are already complicated); however, the nonlinear solution always will be dependent of the assumed displacement field along the element length and might lead to erroneous results (especially in local responses) (Scott,2004). Since the present study conducts IDA analysis to capture the response of structures at high levels of nonlinearity (e.g., collapse), displacement-based elements might lose their computational efficiency even their solution accuracy due to the need for fine element meshing.

Force-based elements, however, satisfy equilibrium conditions both at the section and element levels; independent of the extent in nonlinearity (Spacone, 1996). Besides, fine element meshing is not required for the force-based elements (Scott, 2008).

Although force-based element modeling is more suitable for NRHA of the building models in the present study, for the sake of proving the properness of this model, building model called as Model 09 (Figure 3.3) is evaluated in terms of response comparisons for both displacement-based and force-based elements. The implementation of displacement-based elements with more than two segments would require significant computational time. This would lead to losing its computational advantage against force-based elements. Therefore, structural members modeled by displacement-based elements are only divided into two segments for the given building model in the following comparisons. Figures 3.4 to 3.9 compare the nonlinear responses of the chosen structural members in Model 09 when the building is modeled by using force-based and displacement-based elements as two separate cases.

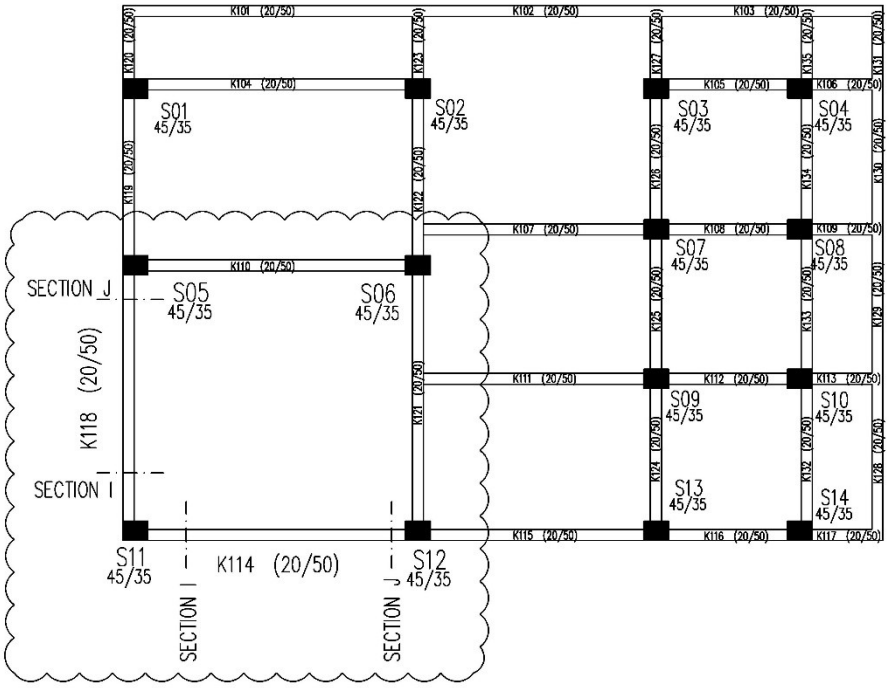

Figure 3.3. Ground floor plan of Model09 and the structural members whose responses are stored (recorded) for comparison of displacement-based and force-based element modeling.

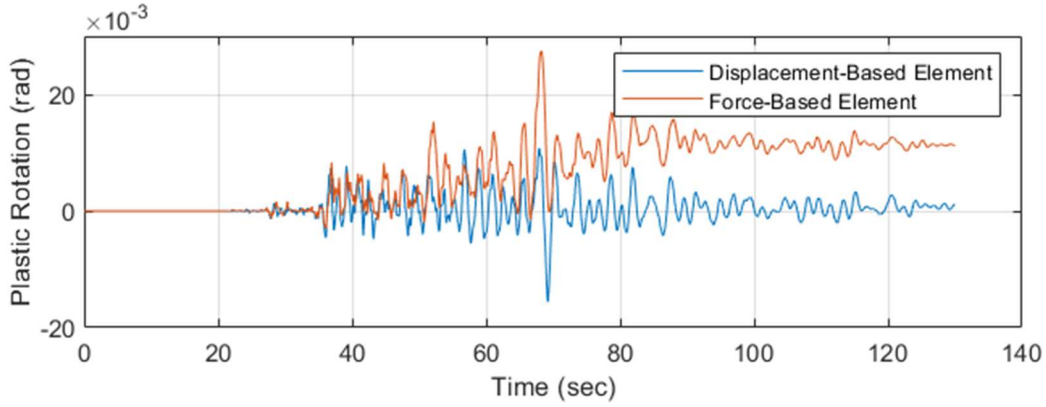

Figure 3.4. Plastic rotation response of the bottom of the S11 column.

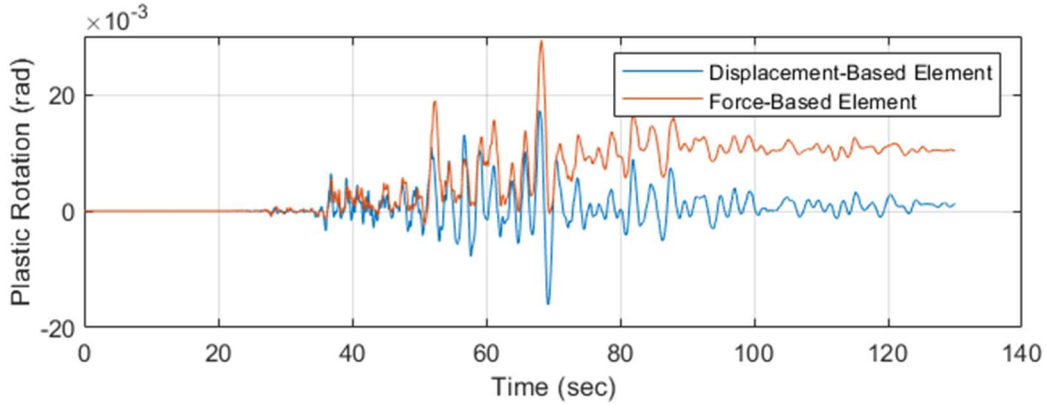

Figure 3.5. Plastic rotation response of the bottom of the S12 column.

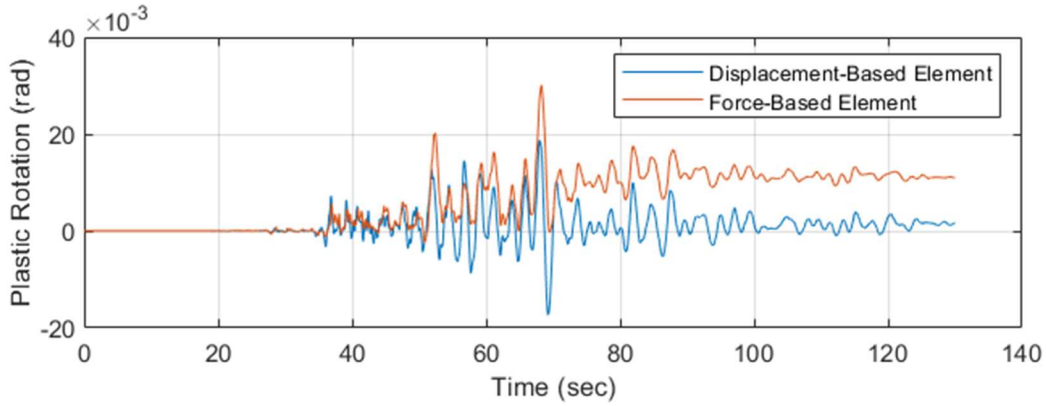

Figure 3.6. Plastic rotation response of the bottom of the S06 column.

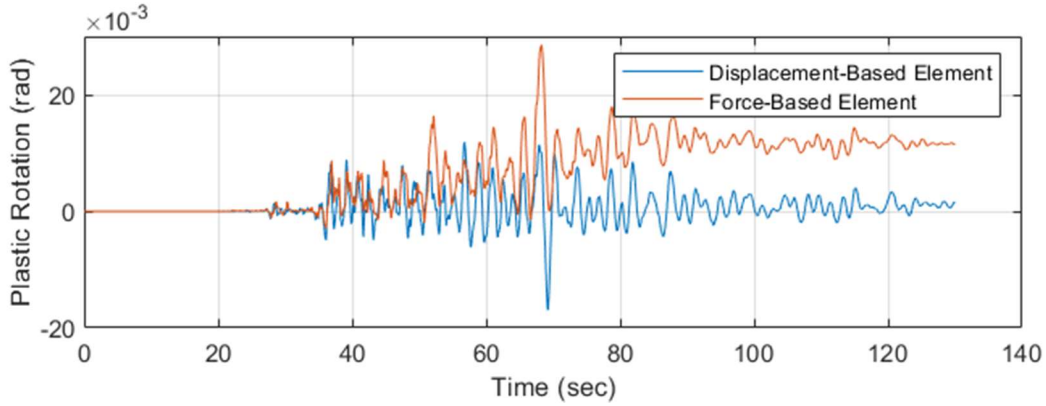

Figure 3.7. Plastic rotation response of the bottom of the S05 column.

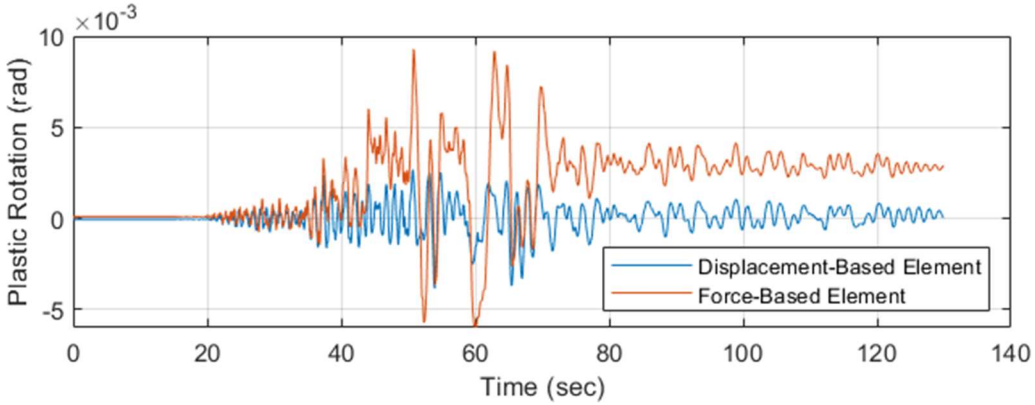

Figure 3.8. Plastic rotation response of the J section of the K114 beam.

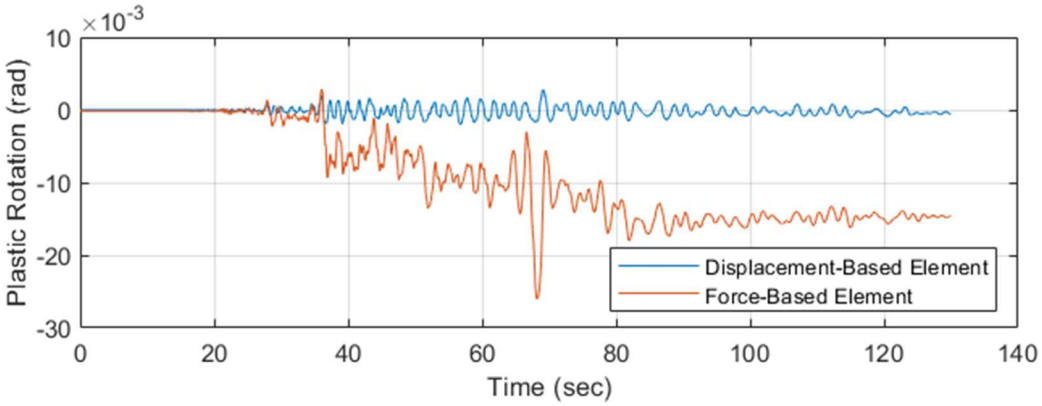

Figure 3.9. Plastic rotation response of the I section of the K118 beam.

Sample analyses are conducted for Model09 with an unscaled record of El Mayor-Cucapah Mexico Earthquake (M_w 7.2). The building (Model09) modeled by displacement-based and force-based elements simultaneously have the same modeling details that are presented in the following sections. The plastic rotation responses of the selected structural members (see, Figure 3.3) indicate that the use of displacement-based elements with elements meshed into two segments is not enough to capture the actual nonlinear behavior of the structure. Thus force-based elements are utilized for the building models.

As mentioned before, section level nonlinearity in distributed plasticity models is defined either through stress-strain resultants or by discretizing the section into fibers that have material stress-strain relation. Fiber section has various advantages over the resultant sections. No prior moment-curvature analysis is needed for fiber sections and the hysteretic behavior is directly defined through uniaxial material properties. The coupled behavior of axial force and moment is automatically included in the model (Du, 2012). The interaction

between the flexural strength in orthogonal directions for biaxial loading case is also directly considered. Besides, the strength reduction within the element is calculated from the strain softening feature of the material. Therefore, fiber section modeling is straightforward and more complete in terms of material nonlinearity definition. The present study adopts fiber sections both for beam and column section modeling.

Fiber section of a reinforced concrete element consists of reinforcement steels and core and cover concrete segments (Figure 3.10). The inputs for fibers are their locations in the local reference system, their areas, and the material model (Spacone, 1996). Then the force-deformation relation of the section is obtained by integrating the response of the fibers as presented in Eq. 3.9.

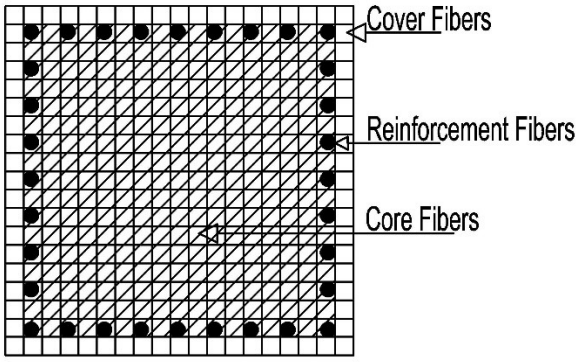

Figure 3.10. Section modelling with fibers.

3.3. Modelling Details

Beam and column elements are modeled with force-based ‘nonlinearBeamColumn’ command in OpenSees, which considers the spread plasticity along the element. Gauss-Lobatto Integration (Neuenhofer and Filippou, 1997) is utilized by using five integration points within the element. P-Δ effects are considered along the columns in all buildings. The columns are fixed at the base floor.

The elements are modeled with fiber sections, in which the cover and the core concrete are divided into 10 x 10 and 20 x 20 subsections, respectively and the reinforcing bars are defined by straight layers. Both for the unconfined and confined concrete, ‘Concrete04’

material of OpenSees is utilized. Confined concrete model is implemented in accordance with the model proposed by Mander et al. (1984). Tensile strength of concrete is neglected.

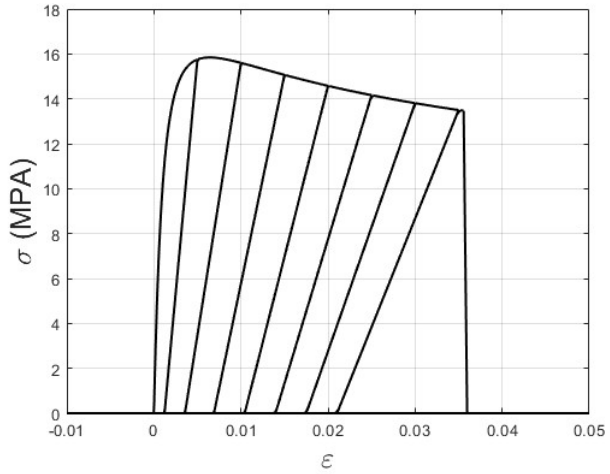

Figure 3.11. Confined concrete model for column sections.

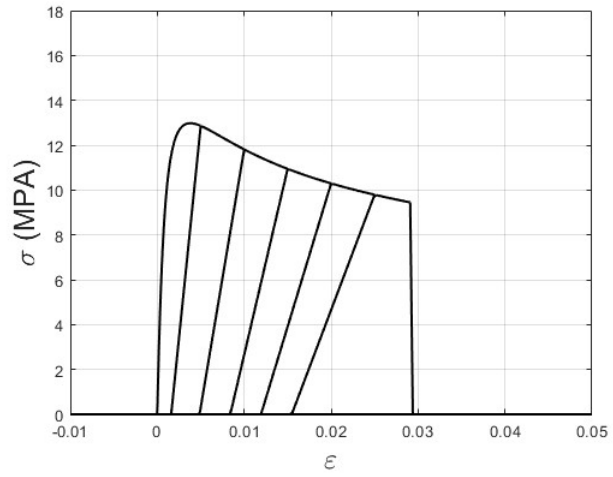

Figure 3.12. Confined concrete model for beam sections.

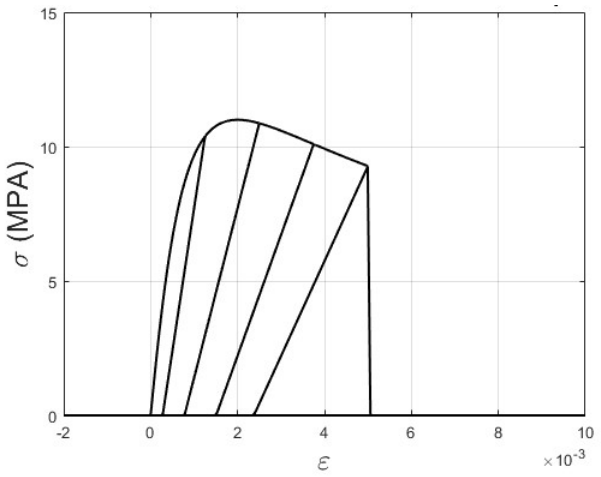

Figure 3.13. Unconfined concrete model.

The hysteretic behavior of steel is defined according to Menegotto and Pinto (1973) with a yield strength of 220 MPa and 0.0025 isotroping strain hardening ratio. The steel reinforcing material is implemented using the Steel02 command in OpenSees.

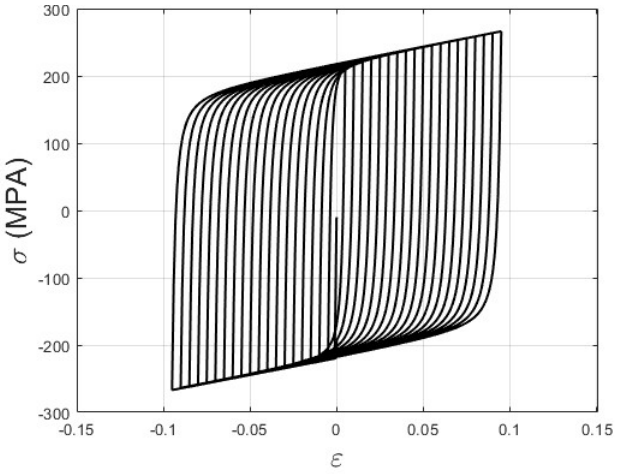

Figure 3.14. Reinforcing steel model.

The coupled axial and biaxial-bending behavior is directly modeled in fiber sections. Shear behavior is introduced linearly (uncoupled axial/flexural-shear behavior) to the models. For columns, brittle shear failure is taken into account (i.e., analysis stops when the column experiences shear failure) by considering the member shear capacity formulation defined in Turkish Standards for Design and Construction of RC Structures, TS-500 (Turkish Standards Institute, 2000). Shear failure is not explicitly included in the analytic models for beams because it is not desired to stop the analysis due to brittle failure of one (or few) beams. However, the occurrence of shear failure in beams is post-processed. No other

deterioration modes such as bond-slip, local buckling, and fracture of reinforcing steel are considered because the utilized fiber model is not capable of capturing such effects. Consideration of such nonlinear failure modes increases the complexity in the analytical models and may lead to convergence problems. It should be noted that neglecting these failure modes would affect the response of no-code (or low-code) building models that are of interest in this study. Therefore, resulting fragility functions that are presented in the following chapters should be evaluated within this limitation imposed to the analytical models.

Slabs are not modeled as structural members in the analytical models. Since slabs have significant in-plane stiffness, rigid diaphragm behavior (rigid body motion at the floor level) is assumed and is implemented to the models by using rigid constraints (two translation dofs in x-and y-axis and rotational dof around z-axis) at the floor nodes. Therefore, all the nodes on the floor are forced to have the same lateral displacements, which should result in zero axial strain on the beam members. However, this expected behavior does not occur in the analytical models if additional measures are not taken as described in the next lines.

The consequential effect of rigid floor assumption is the resulting axial strains at the nonlinear fiber sections that leads to the shift in neutral axis, which means increased bending capacity of the beams. Development of axial strains at the beam sections would mask their actual bending moment capacity and would lead to incorrect shear forces in the columns. Because the rigid diaphragm assumption is found to be practical for the present study to ensure the lateral load transfer from floors to the columns, the above consequential effect of rigid diaphragm modeling is surmounted by introducing axial springs with low axial stiffness at one end of each beam.

The gravity loads are calculated using the superimposed 0.15 ton-force and the self-weight of the slab with 12 cm thickness. Live loads are assumed as 0.2 ton-force. The story masses are obtained according to the dead and 30% of the live loads and are assigned to the beam-column joints. Modal damping of 2.5% is assumed for the building models.

3.4. Evaluation and Verification of the Models

To verify the sanity of OpenSees analytical models, eigenvalue analysis is conducted by using the models of OpenSees and ETABS (Computers and Structures Inc., 2011). It should be noted that the cracked section stiffness is disregarded because the cracked section stiffness in the OpenSees models is computed from the fiber sections. Table 3.1 shows the modal period comparisons of the model buildings from eigenvalue analysis of OpenSees and ETABS. The eigenvalue analysis results suggest that the considered (and modeled) buildings are flexible against lateral dynamic behavior due to inadequate section dimensions and excessive mass.

Table 3.1 Eigenvalue analysis results of the building models.

MODEL ID	MODE NUMBER	OpenSees	ETABS
MODEL01	1	1.70	1.70
	2	1.42	1.43
MODEL02	1	1.44	1.46
	2	1.38	1.40
MODEL03	1	1.48	1.48
	2	1.18	1.19
MODEL04	1	1.28	1.29
	2	1.12	1.14
MODEL05	1	1.39	1.41
	2	1.20	1.22
MODEL06	1	1.59	1.59
	2	1.29	1.31
MODEL07	1	1.58	1.59
	2	1.22	1.24
MODEL08	1	1.31	1.32
	2	1.22	1.23
MODEL09	1	1.28	1.30
	2	1.14	1.16
MODEL10	1	1.23	1.24
	2	1.03	1.05
MODEL11	1	1.23	1.24
	2	0.96	0.97
MODEL12	1	1.13	1.14
	2	0.97	0.98
MODEL13	1	1.24	1.25
	2	1.07	1.09
MODEL14	1	1.32	1.33
	2	1.24	1.26
MODEL15	1	1.05	1.06
	2	0.97	0.98
MODEL16	1	1.24	1.25
	2	1.08	1.09

Figure 3.15 and Figure 3.16 show sample response histories for the hysteretic behavior of moment rotation for one of the ground floor columns (S05) and beams (K114),

respectively (see Figure 3.3 for the chosen structural members in Model 09). The column member shows significant stiffness degradation and pinching (Figure 3.15) although the nonlinear models disregard bond-slippage. The beam member (Figure 3.16) does not show any indication of axial deformation, which should be the case after the considered modeling measures taken in the analytical modeling.

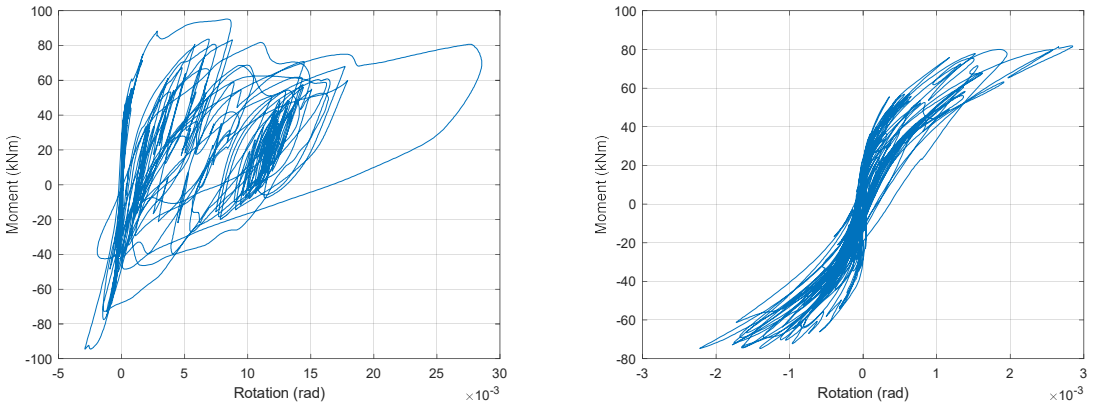

(a) (b)

Figure 3.15. Moment-rotation hysteresis (a) at the bottom, (b) at the top of the Model09, S05 column under a ground motion recorded from the El Mayor-Cucapah Mexico Earthquake (Mw 7.2).

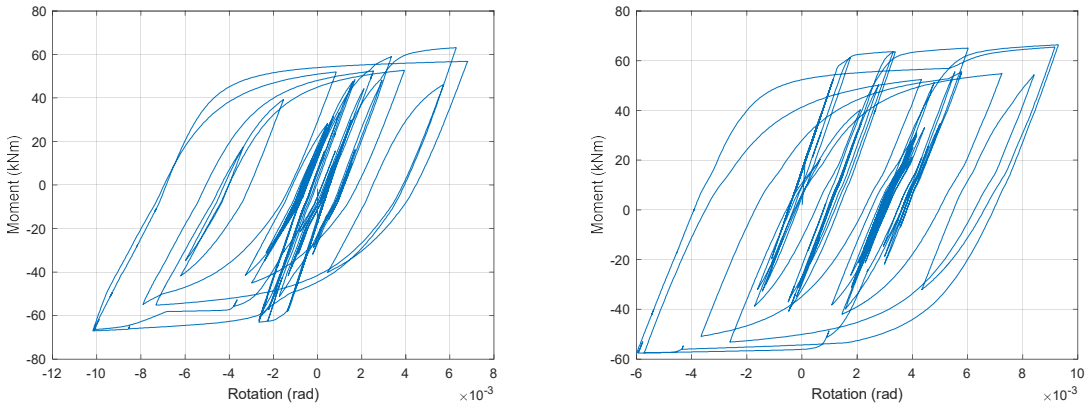

(a) (b)

Figure 3.16. Moment-rotation hysteresis a) at the I section, b) at the J section of the Model09, K114 beam under a ground motion recorded from the El Mayor-Cucapah Mexico Earthquake (Mw 7.2).

3.5. Ground Motion Data and Target Hazard

The record dataset is compiled from the Pacific Earthquake Engineering Research (PEER) Center Strong Motion database (https://ngawest2.berkeley.edu/) and represents the site-specific Probabilistic Seismic Hazard Assessment (PSHA) at a site in Istanbul. The selected ground motions are consistent with the deaggregation results as presented in Figure 3.17, Figure 3.18 and Figure 3.19. The site-specific hazard curves that are computed for three different ground-motion predictive models (Kale et al., 2015, -KAAH15-, Akkar et al., 2014 -ASB14- and Chiou and Youngs, 2014 -CY14-) that are presented in Figure 3.17. They are used for guidance in the incremental scaling of IDA analysis. The site-specific hazard curves and their deaggregation for PGA are provided by Professor Özkan Kale from the Civil Engineering Department of TED University. The ground-motion predictive models and the ground-motion records are representative of regional hazard for Istanbul.

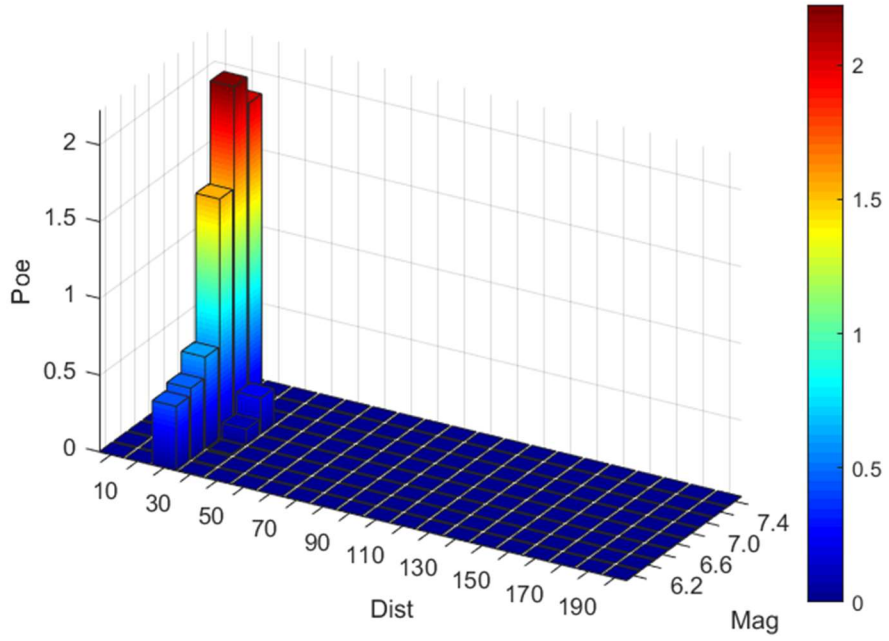

Figure 3.17. Most likely event according to KAAH15

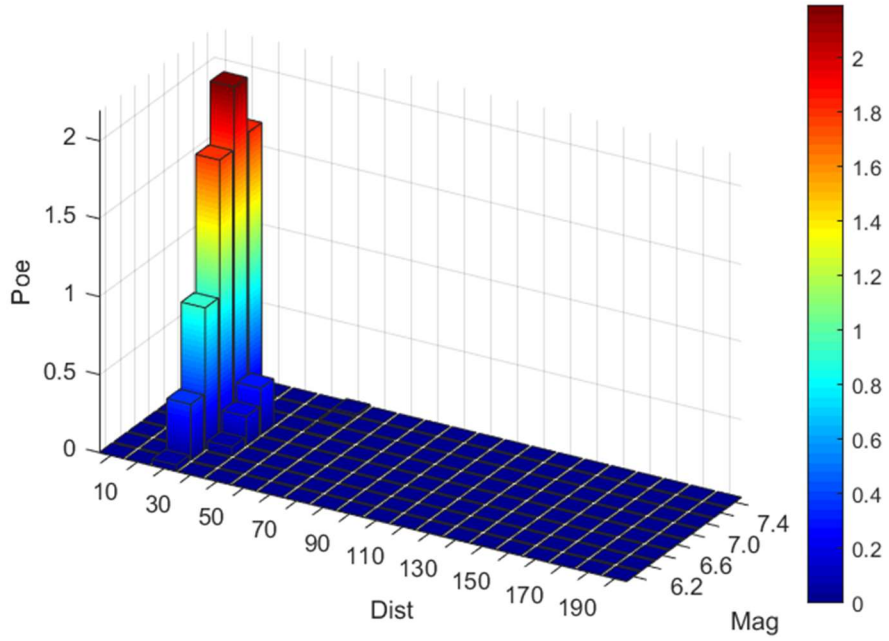

Figure 3.18. Most likely event according to ASB14

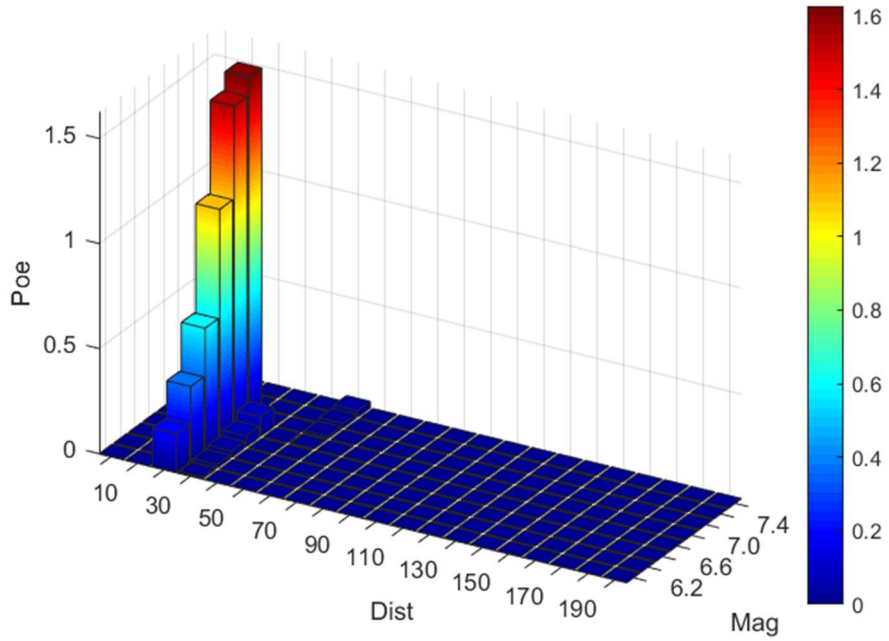

Figure 3.19. Most likely event according to CY14

In essence, the compiled ground-motion dataset consists of 25 ground-motion records of strike-slip faulting, within a moment magnitude range of $6.0 \leq M_w \leq 7.6$ and Joyner-Boore

distance of 15 km ≤ R_{JB} ≤ 35 km. The records are from sites pertaining to site classes ZC and ZD (TEC-2019) having average shear wave velocities at the top 30 m soil layer 360 m/s ≤ V_{S30} ≤ 760 m/s and 180 m/s ≤ V_{S30} ≤ 360 m/s, respectively. The site classes of the selected ground-motion records are representatives of site-specific hazard study. Pulse-dominant waveforms are not included in the ground motion record set. Table 3.2 lists the important seismological features of the compiled ground-motion dataset.

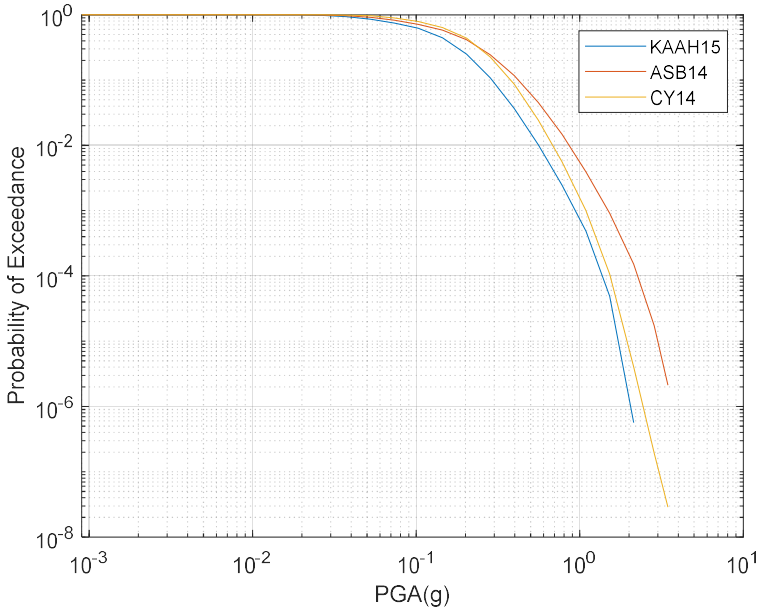

Figure 3.20. Target hazard curves.

Table 3.2. Compiled ground-motion dataset.

Event Name	Station Name	Magnitude	Rjb (km)	Vs_{30} (m/sec)	H1 Record	PGA-H1 (g)	H2 Record	PGA-H2 (g)
Victoria_ Mexico	Chihuahua	6.33	18.53	242.05	RSN266_VICT_CHI102.AT2	0.151	RSN266_VICT_CHI192.AT2	0.097
Superstition Hills-02	Plaster City	6.54	22.25	316.64	RSN724_SUPER.B_B-PLS045.AT2	0.137	RSN724_SUPER.B_B-PLS135.AT2	0.200
Superstition Hills-02	Calipatria Fire Station	6.54	27.00	205.78	RSN720_SUPER.B_B-CAL225.AT2	0.190	RSN720_SUPER.B_B-CAL315.AT2	0.259
Superstition Hills-02	El Centro Imp. Co. Cent	6.54	18.20	192.05	RSN721_SUPER.B_B-ICC000.AT2	0.357	RSN721_SUPER.B_B-ICC090.AT2	0.259
Northern Calif-03	Ferndale City Hall	6.50	26.72	219.31	RSN20_NCALIF.FH_H-FRN044.AT2	0.163	RSN20_NCALIF.FH_H-FRN314.AT2	0.203
Kocaeli_ Turkey	Iznik	7.51	30.73	476.62	RSN1166_KOCAELI_IZN180.AT2	0.091	RSN1166_KOCAELI_IZN090.AT2	0.124
Kobe_ Japan	Abeno	6.90	24.85	256.00	RSN1100_KOBE_ABN000.AT2	0.221	RSN1100_KOBE_ABN090.AT2	0.231
Kobe_ Japan	Shin-Osaka	6.90	19.14	256.00	RSN1116_KOBE_SHI000.AT2	0.225	RSN1116_KOBE_SHI090.AT2	0.233
Kobe_ Japan	Yae	6.90	27.77	256.00	RSN1121_KOBE_YAE000.AT2	0.158	RSN1121_KOBE_YAE090.AT2	0.147
Joshua Tree_ CA	Thousand Palms Post Office	6.10	17.15	333.89	RSN6874_JOSHUA_5068045.AT2	0.205	RSN6874_JOSHUA_5068135.AT2	0.196
Imperial Valley-06	Cerro Prieto	6.53	15.19	471.53	RSN164_IMPVALL.H_H-CPE147.AT2	0.168	RSN164_IMPVALL.H_H-CPE237.AT2	0.157
Imperial Valley-06	Delta	6.53	22.03	242.05	RSN169_IMPVALL.H_H-DLT262.AT2	0.236	RSN169_IMPVALL.H_H-DLT352.AT2	0.350
Imperial Valley-06	El Centro Array #12	6.53	17.94	196.88	RSN175_IMPVALL.H_H-E12140.AT2	0.145	RSN175_IMPVALL.H_H-E12230.AT2	0.118
Hector Mine	Joshua Tree	7.13	31.06	379.32	RSN1794_HECTOR_JOS090.AT2	0.147	RSN1794_HECTOR_JOS360.AT2	0.191
El Mayor-Cucapah_ Mexico	Chihuahua	7.20	18.21	242.05	RSN5823_SIERRA.MEX_CHI000.AT2	0.248	RSN5823_SIERRA.MEX_CHI090.AT2	0.197
El Mayor-Cucapah_ Mexico	TAMAULIPAS	7.20	25.32	242.05	RSN5832_SIERRA.MEX_TAM000.AT2	0.207	RSN5832_SIERRA.MEX_TAM090.AT2	0.226
El Mayor-Cucapah_ Mexico	El Centro - Imperial & Ross	7.20	19.39	229.25	RSN5837_SIERRA.MEX_01711360.AT2	0.384	RSN5837_SIERRA.MEX_01711-90.AT2	0.370
Darfield_ New Zealand	Christchurch Cathedral College	7.00	19.89	198.00	RSN6888_DARFIELD_CCCCN26W.AT2	0.194	RSN6888_DARFIELD_CCCCN64E.AT2	0.233
Darfield_ New Zealand	Papanui High School	7.00	18.73	263.20	RSN6952_DARFIELD_PPHSS33W.AT2	0.211	RSN6952_DARFIELD_PPHSS57E.AT2	0.182
Darfield_ New Zealand	Pages Road Pumping Station	7.00	24.55	206.00	RSN6953_DARFIELD_PRPCW.AT2	0.198	RSN6953_DARFIELD_PRPCS.AT2	0.223
Chi-Chi_ Taiwan-04	CHY034	6.20	28.45	378.75	RSN2708_CHICHI.04_CHY034N.AT2	0.079	RSN2708_CHICHI.04_CHY034W.AT2	0.103
Chi-Chi_ Taiwan-04	CHY028	6.20	17.63	542.61	RSN2703_CHICHI.04_CHY028N.AT2	0.123	RSN2703_CHICHI.04_CHY028E.AT2	0.205
Chi-Chi_ Taiwan-04	CHY101	6.20	21.62	258.89	RSN2752_CHICHI.04_CHY101N.AT2	0.152	RSN2752_CHICHI.04_CHY101E.AT2	0.177
Big Bear-01	San Bernardino - E & Hospitality	6.46	34.98	296.97	RSN931_BIGBEAR_HOS090.AT2	0.092	RSN931_BIGBEAR_HOS180.AT2	0.101
Big Bear-01	Morongo Valley Fire Station	6.46	27.96	396.41	RSN6059_BIGBEAR_MVH045.AT2	0.148	RSN6059_BIGBEAR_MVH135.AT2	0.119

The geometrical mean (geomean) PGA of selected ground-motion records are scaled from 0.025 g to the PGA value, which causes dynamic instability in the model for IDA runs. The increment used for geomen PGA scaling is 0.025 g. Dynamic instability (collapse) is defined when a significant increase is observed in the EDP (e.g., interstory drift ratio) for small increments of the mean PGA. Dynamic instability is also assessed and when numeric instability is observed in the nonlinear response history analyses. A Tcl script is generated to stop running the IDA analysis for larger geomean PGA levels when dynamic instability problems is observed for that specific ground-motion record.

4. INCREMENTAL DYNAMIC ANALYSES RESULTS AND DEVELOPMENT OF FRAGILITY FUNCTIONS

4.1. Introduction

Incremental Dynamic Analysis (IDA) (Vamvatsikos and Cornell, 2002) is performed by running Nonlinear Response History Analysis (NRHA) with a scaled ground motion or a scaled suit of ground motions. The scaling of ground motions is based on a predefined Intensity Measure (IM) such as PGA or spectral acceleration at the fundamental period of the building ($SA(T_1)$). The predefined IM is scaled incrementally by setting scaling factors from small values (typically less than 1) to larger values (typically greater than 1) to inspect different modes of structural response (i.e., from elastic structural behavior until collapse). This way IDA yields information about the structural capacity against earthquake action at different levels of ground motion intensity that is mimicked by the chosen IM. The structural capacity is quantified by an Engineering Demand Parameter (EDP) that measures the seismic performance of the structure. The most frequently used EDPs are Maximum Interstory Drift Ratio (MIDR), roof displacement, plastic rotation etc.

There are many IDA algorithms available in the literature. The most easily implemented one is the stepping algorithm in which the IM is increased by a constant value at each step until the structure collapses. There are several alternative approaches in the stepping algorithm while determining the increments. For example, using larger increments at each step to increase the convergence speed for collapse, adding backward step-reducing procedure upon experiencing dynamic instability to improve the estimation of structure's collapse capacity, considering backward procedures to increase the demand resolution between steps having significant differences in demand gaps and combination of these algorithms to improve IDA results (Vamvatsikos and Cornell, 2002).

The visual aspect of IDA that describes the behavior of a given EDP as a function of IM yields important information about structural behavior for increasing levels of ground-motion intensity. Since IDA bears on NRHA, the information revealed also highlights the record-to-record variability and structural response to each specific record (interaction

between structure and ground motion). Such information cannot be observed in static pushover curves that are developed by scaling a static lateral force pattern that is representative of earthquake action. Besides, IDA curves exhibit complex and non-monotonic relation between IM and EDP since the structural response is dependent on the yielding pattern at different time steps of the ground motion record.

The most important use of the multi-record IDA is for Performance-Based Earthquake Engineering (PBEE) studies is to provide a probabilistic basis for EDP behavior conditioned on a given IM. For example, the probabilistic approach presented in FEMA-P58 report (FEMA, 2012) utilizes IDA for collapse fragility assessment. The PEER approach that makes use of total probability theorem to evaluate structural damage against earthquake action (Cornell 2004; Deierlein 2004; Krawinkler et al. 2004; Miranda et al. 2004) also relies on IDA studies the establish the conditional probabilities as described in Figure 4.1. This is because the multi-record IDA curves (as presented in Figure 2) would yield the probabilities of different damage states at each IM level (i.e., damage probabilities conditioned on IM; fragility functions). The conditional probabilities involved at each step help the analyst to consider the uncertainties resulting grom record-to-record variability and record-structure interaction pertaining to that step. Eq. 4.1 presents the triple integral used in PEER approach to estimate the annual exceedance rate of a given engineering EDP to assess the probabilistic seismic risk of the structural system under consideration.

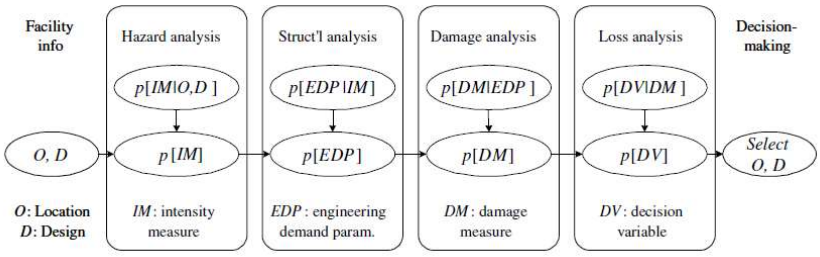

Figure 4.1. PEER probabilistic framework (Moehle et al., 2004).

$$\lambda(Dv > dv) = \int_{im}\int_{dm}\int_{edp} G(\,dv \mid dm\,)dG(\,dm \mid edp\,)dG(\,edp \mid im\,) \mid d\lambda(im) \mid \quad (4.1)$$

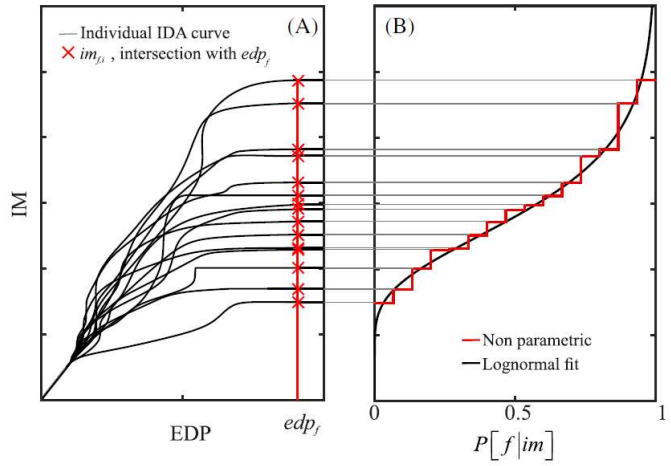

Figure 4.2. Schematic representation of the derivation of fragility functions using IDA. (Baltzopoulos et al., 2018).

There are other methods to develop analytical fragility curves similar to IDA, such as multiple stripe analyses that utilizes NRHA for fewer IM levels given a specific ground-motion set. Truncated IDA is also another method that performs the scaling up to a predefined IM level disregarding the collapse state of the structure (Baker, 2013). In other words, IDA is performed to a specific IM level without targeting the collapse state. These approaches have various advantages over conventional IDA such as computational efficiency and avoiding extreme scaling of recorded motions that has always been a debate among the seismological and engineering community. The conventional IDA is straightforward and does not require any prior knowledge about the capacity of the structure. The small increments in conventional IDA algorithm enable the detection of structural resurrection (extreme hardening case after a flat yielding plateau) at the intermediate IM levels and the better identification of actual collapse point.

For the objective of this thesis, the IDA is performed with step algorithm. Although this algorithm requires more analysis when compared to other strategies mentioned above, it is easily programmable and does not require any interpolation of the IM to fill the gaps and locate the collapse point. The considered building models in this study are representatives of either no-code or low-code buildings with little knowledge about their capacity and they exhibit distinctive differences among themselves. Thus, defining a maximum IM level for truncated IDA could lead to difficulties while fitting the fragility curves. Besides, although the number of NRHA is inflated, the selected ground-motion

records are scaled until collapse rather than limiting the number of analysis as in the case of truncated IDA. Since parallel processing algorithm is used in the analyses, the dense use of computers during the analysis stage did not jeopardize the completion time of the targeted runs.

A single set of ground motions, which are selected by considering the site-specific seismic hazard is used in the structural analysis. PGA is used as the ground-motion IM. It is a well-known fact that IMs such as pseudo-spectral acceleration at structure's fundamental period correlates better with the structural damage rather than PGA for first mode dominant structures. (Vamvatsikos and Cornell, 2002). This is because PGA is a high-frequency ground-motion IM and it is not an indicator of structural damage for long-period structures or when structural behavior is in the post-elastic range due to extreme softening (nonlinear behavior) in structural components. Since this study aims to provide fragility functions to assess the probabilistic risk of broad classes of building inventories, PGA, which is one of the structural period independent IMs is selected as the ground motion IM. PGA is also one of the most frequent IMs computed in Probabilistic Seismic Hazard Assessment (PSHA). Therefore, the fragility relations defined in terms of PGA can easily be implemented for seismic risk analysis along with available PSHA studies.

The IDA curves that are given in the following sections do not present consequential dispersion in terms of demand that can be a sign of good correlation with the damage states of the building models in this study. Note that the geomean PGA values of the compiled ground motion set (Table 3.2), do not lead to large scale factors to reach to collapse state for each model building that led to confidence in the scaling procedure applied for the present study.

4.2. Evaluation of the IDA Curves

Response parameters, including interstory drift ratios in both direction, strains, chord rotations, and plastic rotations, are recorded during the NRHA. The graphical illustrations of maximum interstory drift ratio vs. PGA IDA curves are presented to evaluate the seismic performance of building models considered in the thesis. This section also presents the outcomes of the IDA studies.

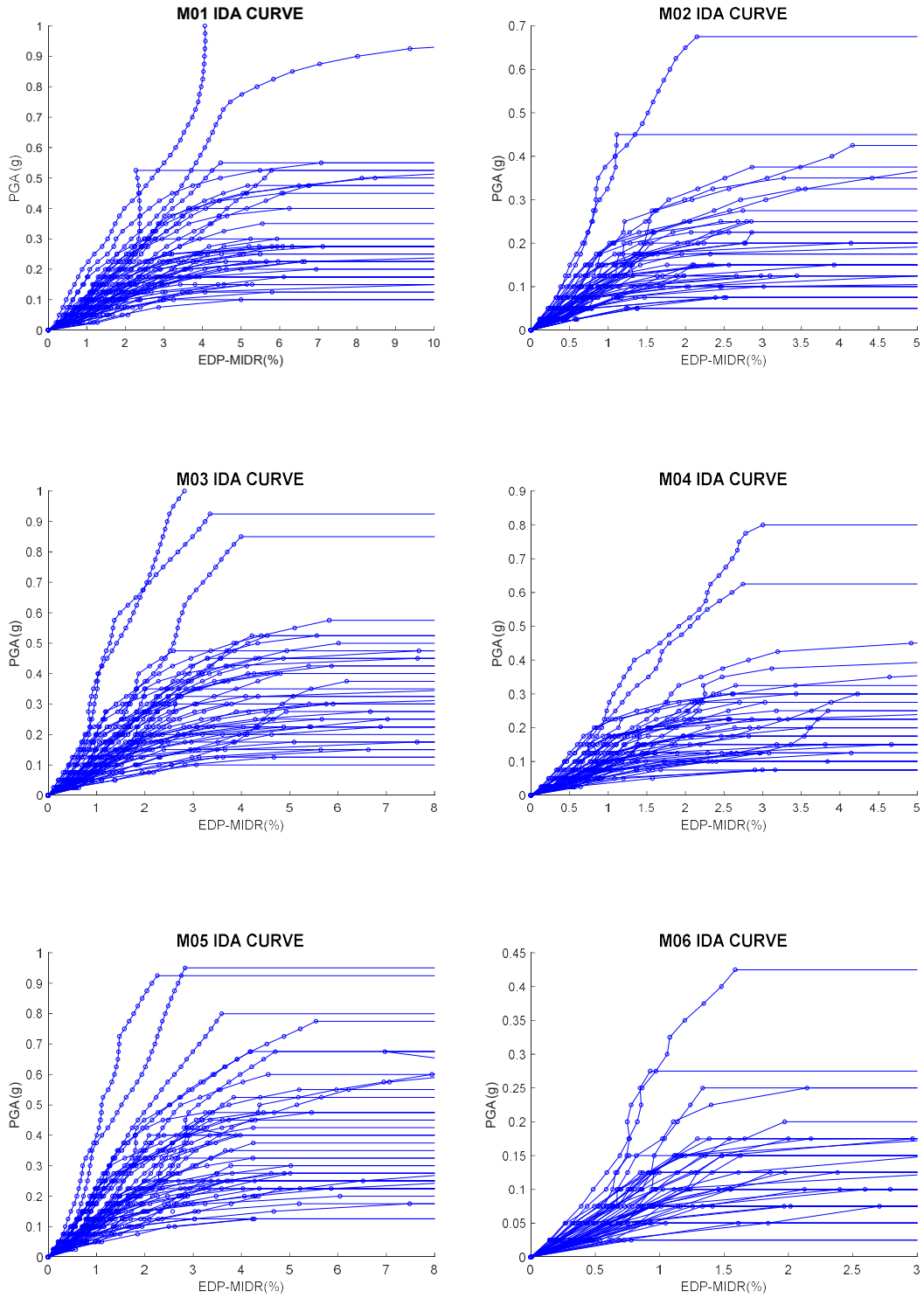

Figure 4.3. Maximum interstory drift ratio IDA curves of the model buildings. (16 model buildings representing different features of Mid-rise No Code / Low Code RC frame buildings in Istanbul). cont.

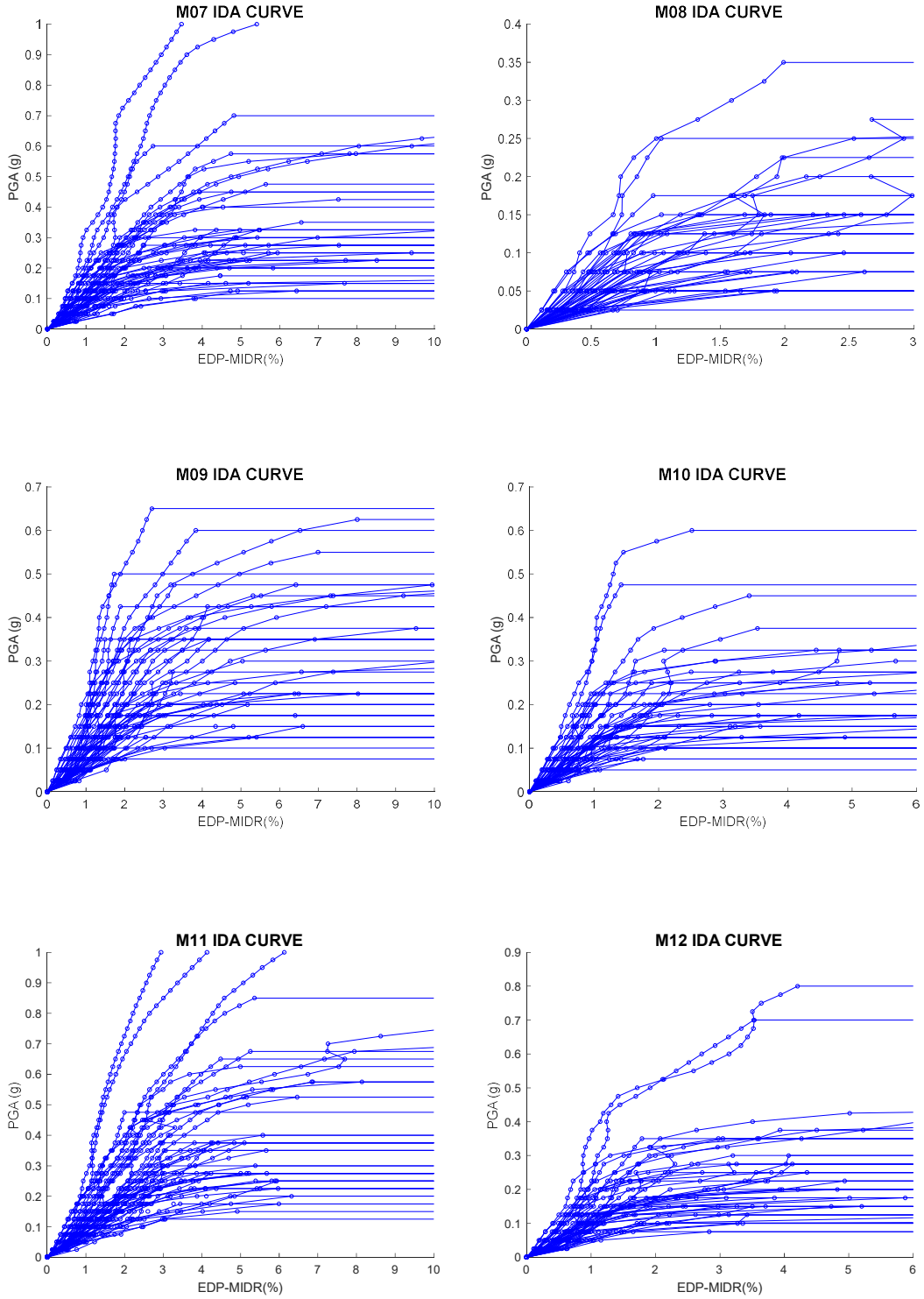

Figure 4.4. Maximum interstory drift ratio IDA curves of the model buildings. (16 model buildings representing different features of Mid-rise No Code / Low Code RC frame buildings in Istanbul). cont.

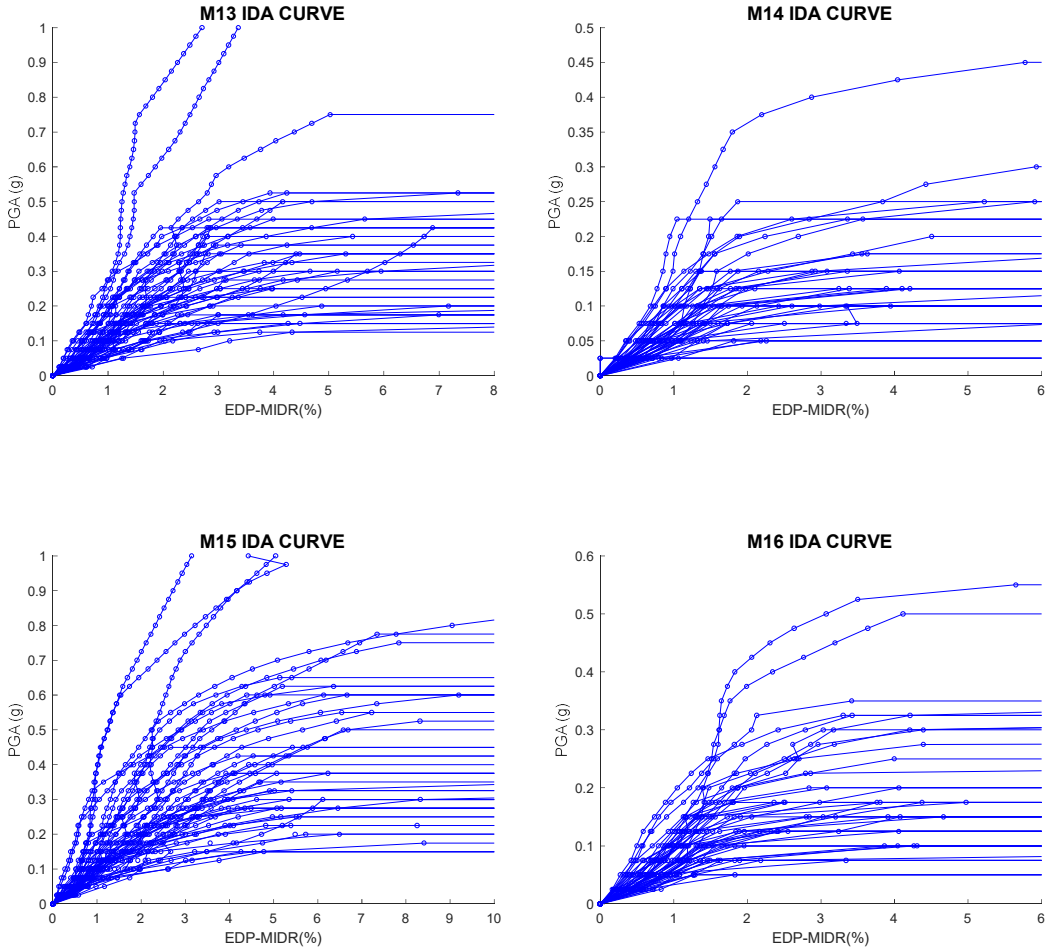

Figure 4.5. Maximum interstory drift ratio IDA curves of the model buildings. (16 model buildings representing different features of Mid-rise No Code / Low Code RC frame buildings in Istanbul).

The IDA curves presented in Figure 4.3, Figure 4.4 and Figure 4.5 include information about the linear elastic region, nonlinear region, and the collapse state of the structure. The building models respond to each record in a different way in the elastic range because PGA-based scaling disregards the modal effects in the structure. The record-to-record based variability observed in the linear elastic region is more apparent in the nonlinear region because structural yielding patterns are different at different time steps for each record that result in such differences in structural response. As it is seen from the IDA curves, record-to-record variability as well as the chosen IM and EDP play important roles while evaluating and using the results of multi-record IDA.

The trial and error methods were evaluated during the preparatory phases of analytical building model development. Numerical problems related to numerical solution algorithms,

iterative procedures for fiber models and etc. were treated substantially. These preliminary studies indicated that the dynamic instability in the building models is strictly associated with numerical instability. In almost all cases, flat-lining of the IDA curve, which is the indication of abnormal increase in the EDP within a small IM increment is observed at the onset of dynamic instability. Hence, the onset of the flat-line in the IDA curve is considered as the start of dynamic instability while evaluating the analysis results.

It should be noted that the EDP (maximum interstory drift ratio in this case) does not always increase with increasing IM in IDA curves. During the scaling procedure, weak response cycles in the early parts of the response time history may trigger the yielding and change the structural parameters for stronger response cycles (Vamvatsikos and Cornell, 2002). This situation may end up with the same or lower EDP for higher IM levels since the structure becomes less responsive (hardening behavior in IDA curves). Most of the IDA curves exhibit wavy behavior due to structural softening followed by structural hardening case as explained in the above lines (Figure 4.6).

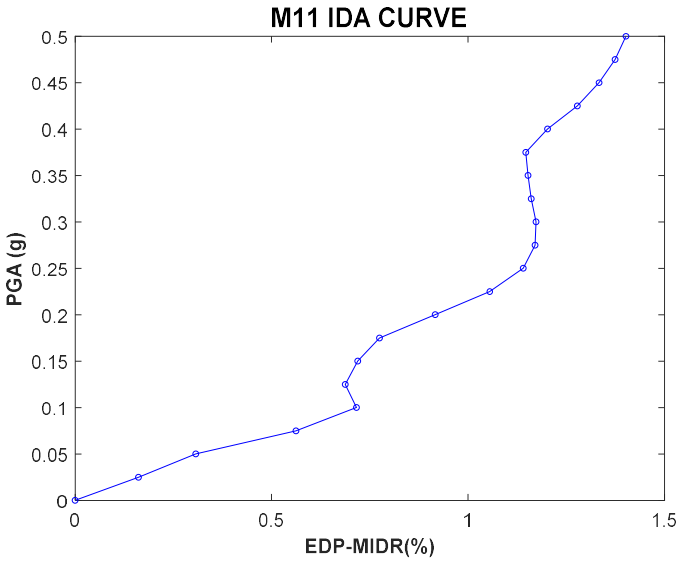

Figure 4.6. Example IDA curve exhibiting wavy behavior.

In some cases, after the flat-lining of IDA, which is considered as collapse, extreme hardening occurs, and the EDP results in a non-collapsing value (Figure 4.7). This situation is called as structural resurrection (Vamvatsikos and Cornell, 2002). There are other IDA cases, where the structure softens by increased IM and reaches the collapse point without

exposing any hardening behavior (Figure 4.8). For such cases no additional analyses were conducted to pinpoint the collapse EDP level.

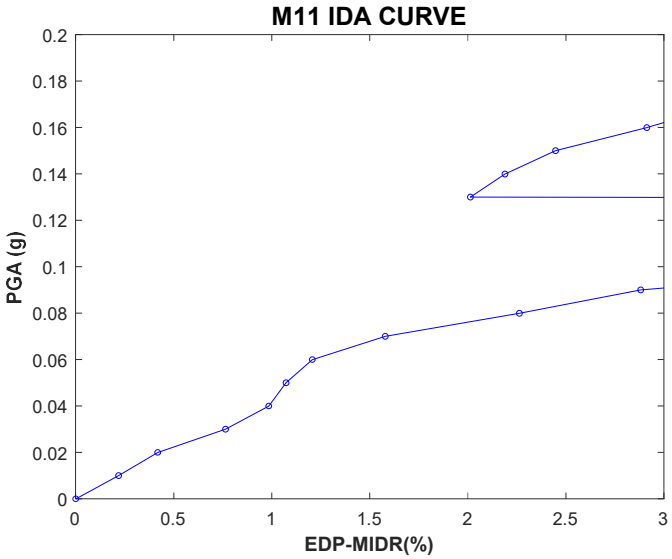

Figure 4.7. Example IDA curve exhibiting structural resurrection.

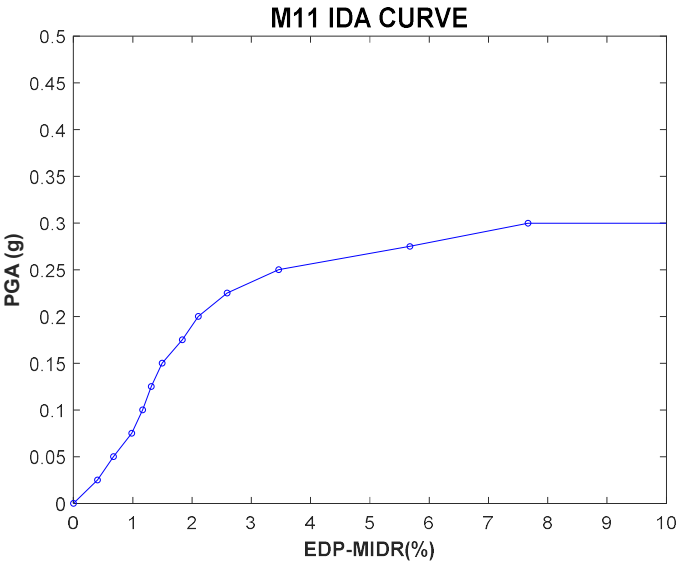

Figure 4.8. Example IDA curve exhibiting softening behavior.

4.3. Development of Analytical Fragility Curves

The damage states for developing fragility functions are based on the local performances of individual members. Strains are used to assess the damage states of individual structural members. The threshold strain values to represent Immediate

Occupancy (IO), Life Safety (LS) and Collapse Prevention (CP) damage states are taken from TEC-2019 (Disaster and Emergency Management Authority, 2018). The CP and LS damage limit states depend on the material properties, volumetric amount of the transverse reinforcement, section dimensions, stirrup spacing and longitudinal reinforcement spacing. To this end, different damage threshold values are used for confined and unconfined concrete models (see Table 4.1 for strain limits for each damage state). A damage state is defined for each element based on the exceedance of the predefined limit states as illustrated in Figure 4.9.

Table 4.1 Threshold component-based strain limits for different damage states.

	Confined Concrete Model		Unconfined Concrete Model		Reinforcement Steel
	Column	Beam	Column	Beam	
CP	0.0130	0.0048	0.0035	0.0035	0.0480
LS	0.0097	0.0036	0.0026	0.0026	0.0360
IO	0.0025	0.0025	0.0025	0.0025	0.0075

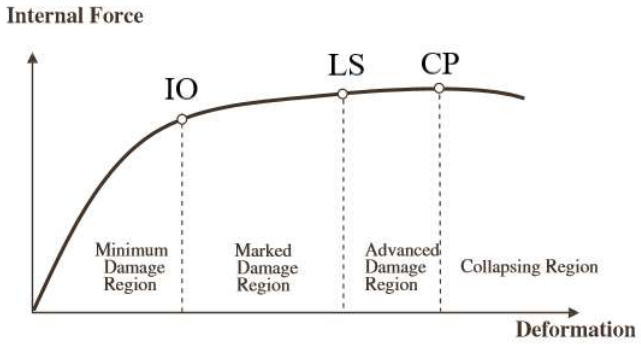

Figure 4.9. Damage States of the Structural Members (TEC-2019).

The percentage of structural elements falling into each damage state (in accordance with stain limits given in Table 4.1) is examined to obtain the overall damage state of the building. The following criteria, are used while assessing the overall building damage states (or overall building seismic performance):

1. IO performance level is assigned if less than 20% of beams reach the “marked damage region” (see Figure 4.9) and all the columns remain in the “minimum damage region” (see Figure 4.9) in all stories.
2. LS performance level is assigned if less than 35% of beams reach the “advanced damage region” (see Figure 4.9) and if all columns remain either in the “minimum

damage region" (see Figure 4.9) or in the "marked damage region" (see Figure 4.9) in all stories.

3. CP performance level is assigned if less than 20% of beams exceed to the "collapsing region" (see Figure 4.9) and if no column reaches the "collapsing region" (see Figure 4.9) in any stories.
4. It is not allowed to have a shear failure in any structural member for IO and LS performance levels. However, for CP performance level, shear failure is allowed only in the beams that are in the collapsing region.

Apart from above listed seismic performance (damage state) metrics, no global damage state is assigned if all the structural members remain in the "minimum damage region". One of the above seismic performance levels are assigned to the building model at every increment of PGA for a given IDA curve. After computing the entire suit of IDA curves for a specific building model, count statistics are employed at every PGA level in order to compute the exceedance probability of each performance level (or damage state). Given a PGA level, count statistics normalize the total number of cases falling into a specific performance level (e.g., IO) with the total number of analysis at that PGA level. This fraction would correspond to exceedance probability of the given performance level at that PGA level for the considered building model. This process is repeated for the entire PGA interval considered in the IDA runs.

Lognormal cumulative distribution is assumed for a continuous estimate of exceedance probability for each damage state (performance level) (Eq. 4.2) after completing the count statistics for each performance level given a specific building model. The term on the left side of Eq. 4.2 is the probability of reaching or exceeding the performance level of interest conditioned on a specific PGA value. The symbol Φ $(\cdot)$ is the normal cumulative distribution and μ and β are the logarithmic mean and standard deviation of PGA. Provided that lognormal assumption holds, e^{μ} and β represent the median and dispersion of PGA for the damage state of interest.

$$P(C|PGA = x) = \Phi\left(\frac{lnx - \mu}{\beta}\right) \tag{4.2}$$

Generalized linear regression is utilized in Matlab® software for the estimation of the fragility parameters (μ and β). This method provides optimum fragility parameters and the fitted distribution curve gives the closest probability values to those obtained from count statistics (Baker, 2011). The fitted fragility curves and the computed probabilities from count statistics of IDA curves are presented in Figure 4.10, Figure 4.11 and Figure 4.12 for each model building. Note that fragility functions could not be fitted for Model 14 since this building reaches the dynamic instability at very low seismic intensities. This building fails in the early stages of the IDA due to long span dimensions. Thus, it is not possible to fit a smooth log-normal cumulative function on this model. Estimated fragility parameters are given in Table 4.2.

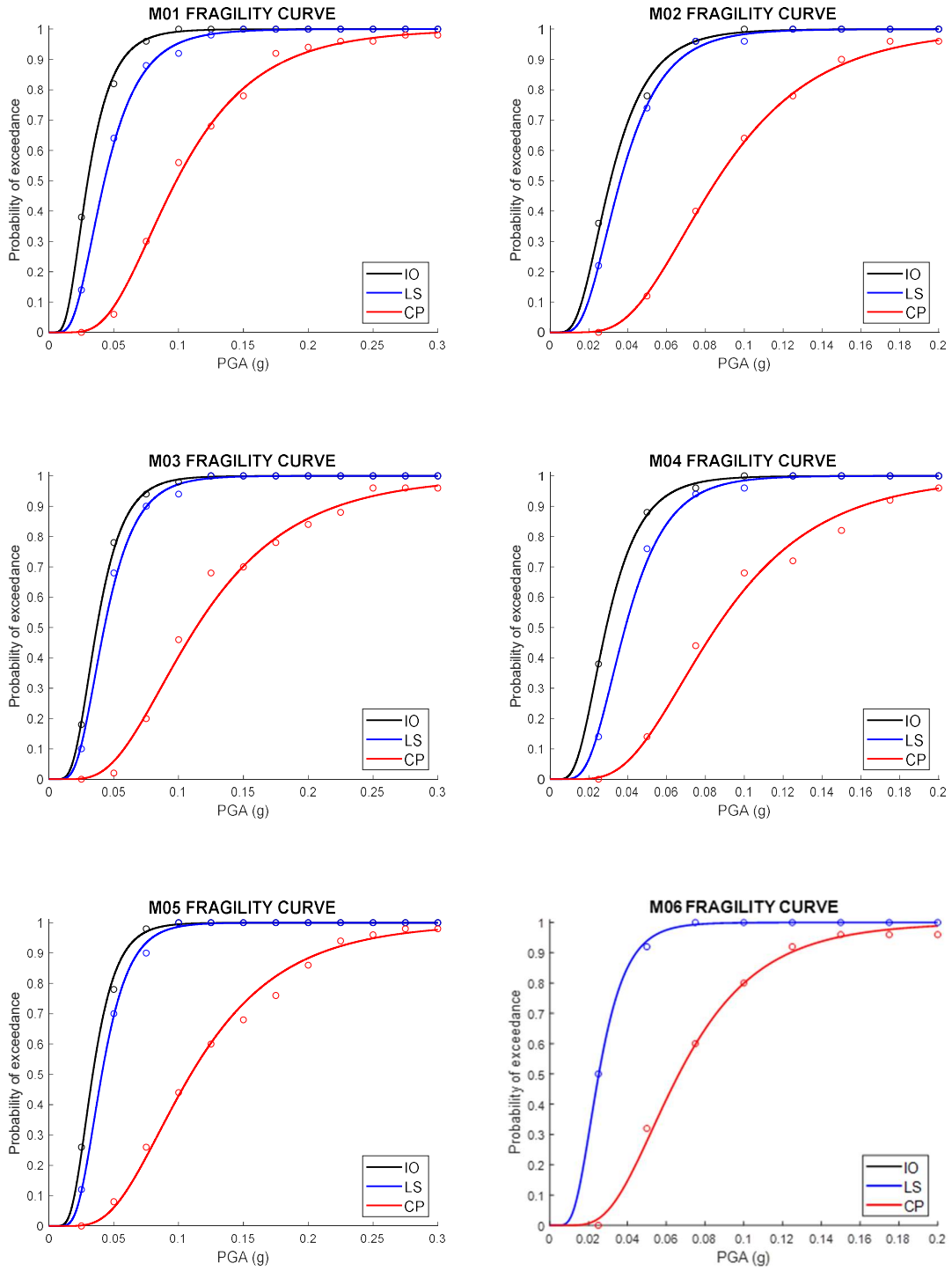

Figure 4.10. Fragility curves of the model buildings considered in this study.cont.

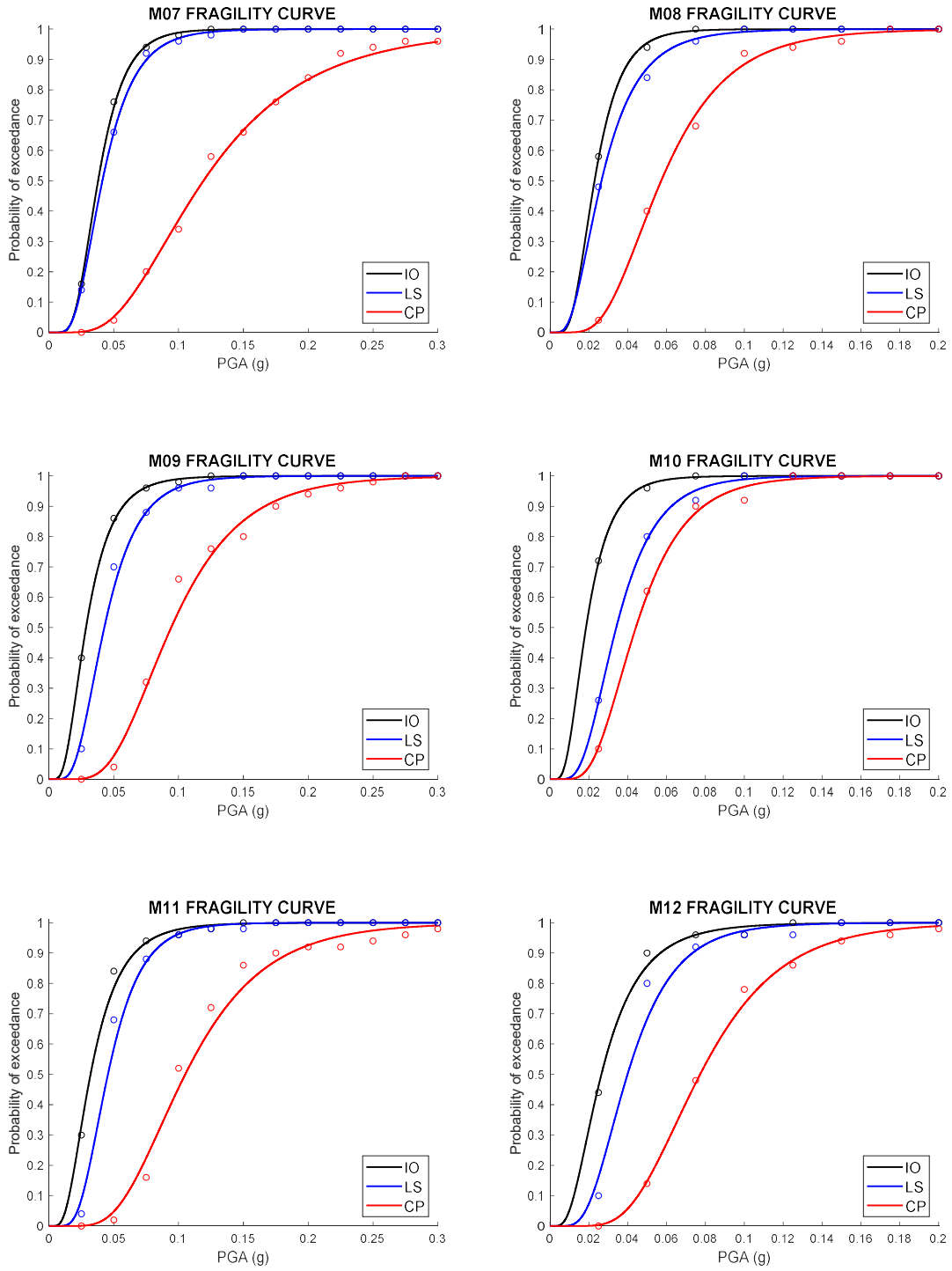

Figure 4.11. Fragility curves of the model buildings considered in this study. cont.

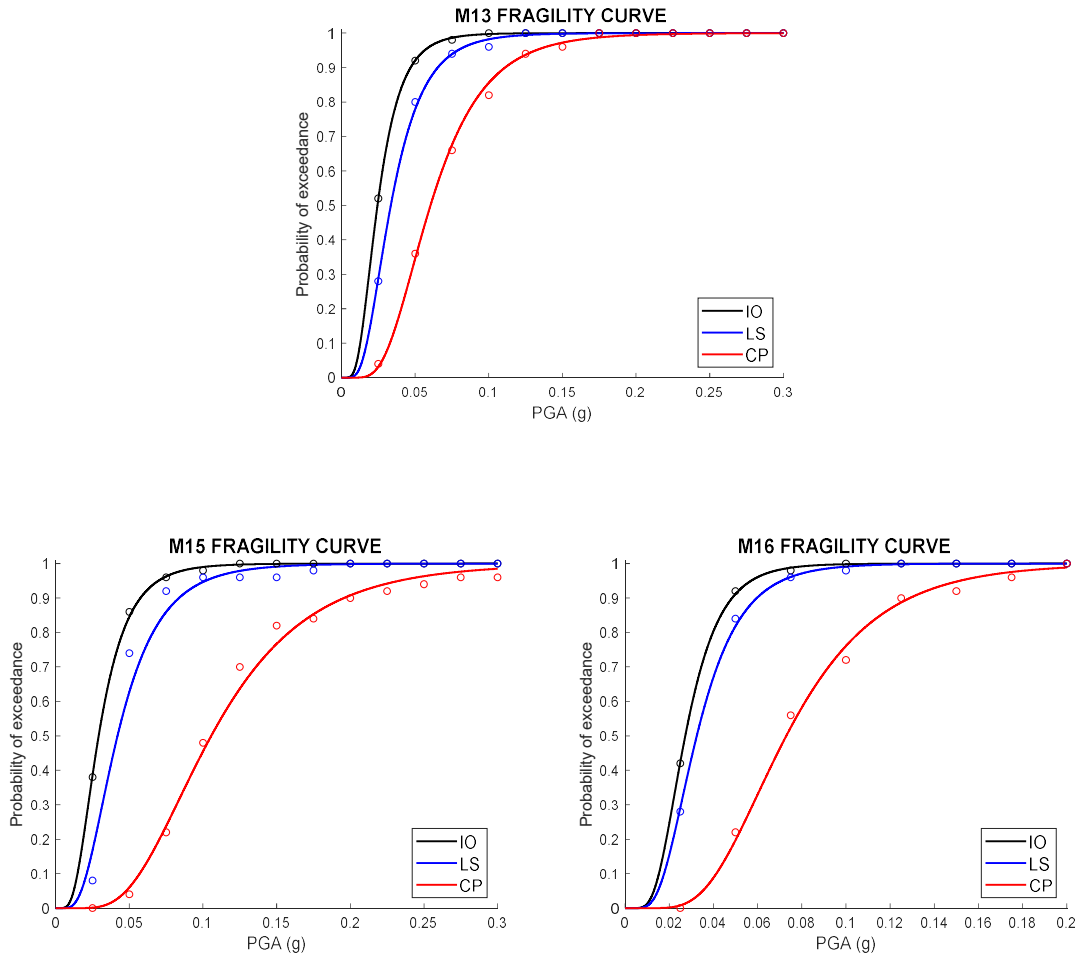

Figure 4.12. Fragility curves of the model buildings considered in this study.

Table 4.2 Estimated fragility parameters of the model buildings.

MODEL ID	IO		LS		CP	
	μ	β	μ	β	μ	β
M01	-3.5106	0.5034	-3.1523	0.5060	-2.3197	0.4926
M02	-3.4706	0.5020	-3.3174	0.4779	-2.4570	0.4722
M03	-3.3005	0.4390	-3.1537	0.4438	-2.1758	0.5252
M04	-3.5410	0.4818	-3.2501	0.4378	-2.4574	0.4878
M05	-3.3890	0.4239	-3.2002	0.4057	-2.2123	0.5062
M06	-3.8262	0.0883	-3.6780	0.4423	-2.7090	0.4850
M07	-3.2735	0.4285	-3.1890	0.4719	-2.1268	0.5331
M08	-3.7731	0.4618	-3.6290	0.5611	-2.8600	0.4669
M09	-3.5557	0.5423	-3.1540	0.4798	-2.3616	0.4443
M10	-3.9847	0.5236	-3.3771	0.4723	-3.1187	0.4533
M11	-3.4403	0.5643	-3.0906	0.4418	-2.2527	0.4457
M12	-3.6304	0.5951	-3.2202	0.4743	-2.5603	0.4161
M13	-3.7111	0.5089	-3.3961	0.5216	-2.8061	0.4749
M15	-3.5344	0.5296	-3.1707	0.5384	-2.2479	0.4814
M16	-3.6011	0.4484	-3.4264	0.4742	-2.6172	0.4439

4.4. Classification and Evaluation of the Fragility Curves

Details of IDA results indicate that the damage states of beams are dominated by the yielding of reinforcement steel, and IO and LS limits of reinforcement are exceeded at very low PGA levels due to poor construction quality (typical of low-code and no-code RC buildings in Turkey). For columns, the concrete strain level dominate the performance of these structural members for the investigated building models. As inferred from Table 4.1, the differences between IO, LS, and CP limit strains are not significant both for confined and unconfined cases. It should be noted that poor construction quality results in relatively small strain limits for the confined models when compared to the adequately designed structural members. Due to small differences in the concrete strain thresholds and deficiencies in the seismic design, the transitions between slight, marked and advanced damage regions (Figure 4.9) are rapid for the column members. This fact results in very close (in some cases almost indifferent) IO and LS fragility curves. The dynamic response of model buildings change significantly when the columns reach to the advanced damage region due to the excessive nonlinearity. Therefore, CP performance level does not present a similar trend with those of IO and LS performance levels.

The rapid increase of exceedance probabilities at all damage states within small increments of PGA is the common situation for all the model buildings in this study. The current building code (TEC, 2019) requires CP performance level for RC frame-type residential buildings for an earthquake producing ground-motion spectral amplitudes having a 475-year return period. The hazard curves that are introduced in Chapter 3 describe 475-year return period PGA values of 0.29g (Kale et al., 2015), 0.42g (Akkar et al., 2014) and 0.37g (Chiou and Youngs, 2014). Given fragility curves developed in this chapter for the model buildings, under the above PGA values none of the low-code and high-code mid-rise RC frame buildings could survive in Istanbul.

Figure 4.13 compares the fragility curves of the model buildings having confined and unconfined structural members. The likelihood of probability exceedance for any damage state reduces for confined building models. Figure 4.14 and Figure 4.15 compare the fragility curves to highlight the influence of mezzanine floor on the structural performance of the model buildings. Figure 4.14 compares the fragilities of confined building models at three

performance levels for with and without mezzanine floor effect. Figure 4.15 does the same comparison for unconfined model buildings. The fragility trends in these figures do not suggest an apparent influence of mezzanine floor on the structural capacity of model buildings. Note that each model building in this study has a unique plan configuration having different span lengths, and floor plan asymmetry. To this end, the actual effect of mezzanine floor on structural capacity seems to be masked behind these other dominating factors.

Similarly, the existence of added floor (Figure 4.16 and Figure 4.17) and the percentage of unrestrained column (Figure 4.18 and Figure 4.19) effects on confined and unconfined building fragilities could not be captured with the current configurations of the model buildings. Therefore, the fragilities of model buildings are grouped to bring forward the confinement effects (i.e., confined and unconfined buildings). The rest of the structural properties are considered as additional uncertainties inflating the variations in the confined and unconfined mid-rise no-code RC frame buildings in Istanbul. The proposed mean fragility curves for confined and unconfined buildings are presented in Figure 4.20 and Figure 4.21, respectively.

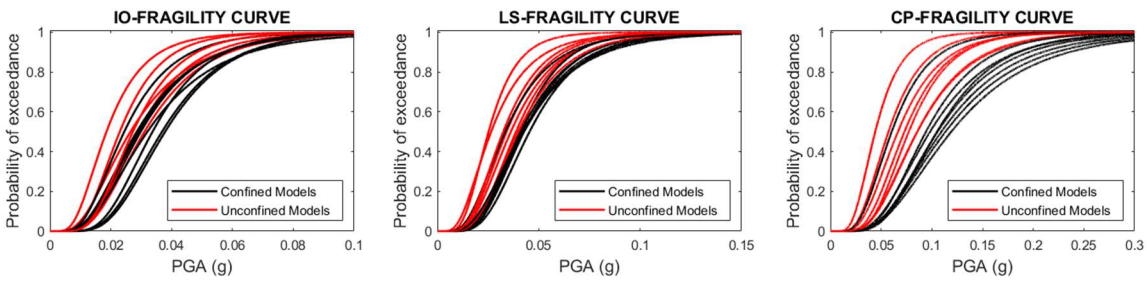

Figure 4.13. Fragility curves of the model buildings grouped for confinement effect.

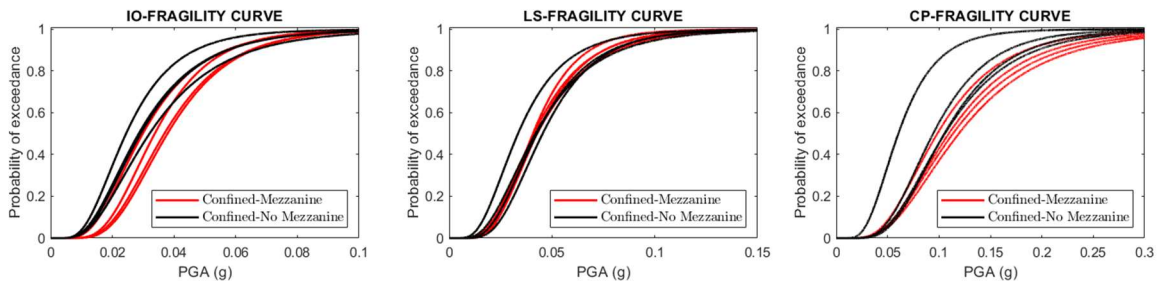

Figure 4.14. Fragility curves of the confined building models binned for with and without mezzanine floor.

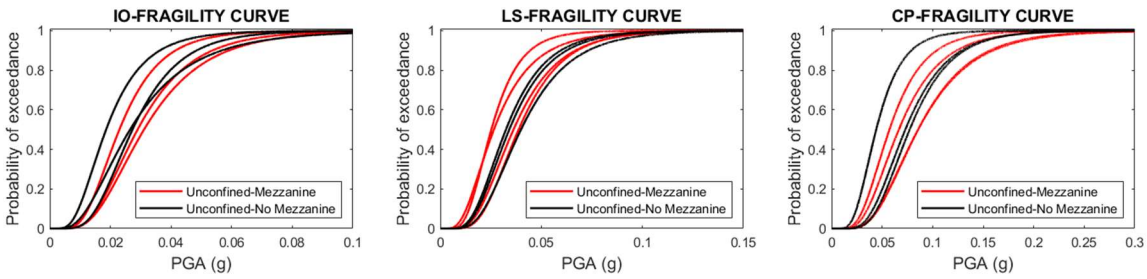

Figure 4.15. Fragility curves of the unconfined building models binned for with and without mezzanine floor.

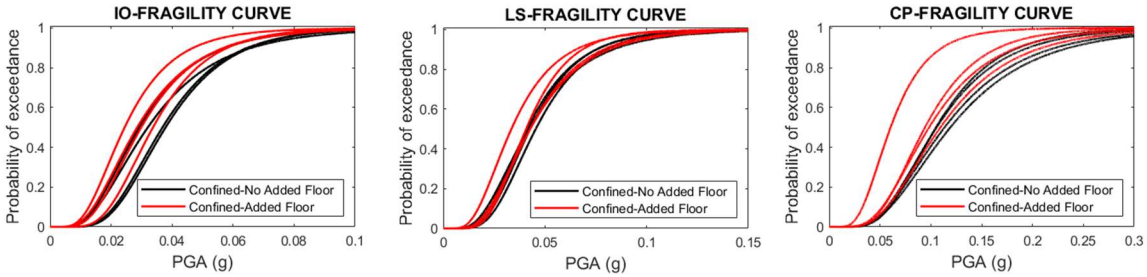

Figure 4.16. Fragility curves of confined building models binned for with and without added floor.

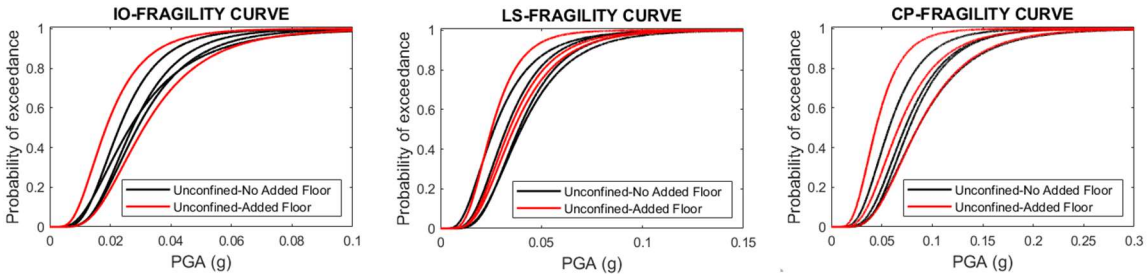

Figure 4.17. Fragility curves of unconfined building models binned for with and without added floor.

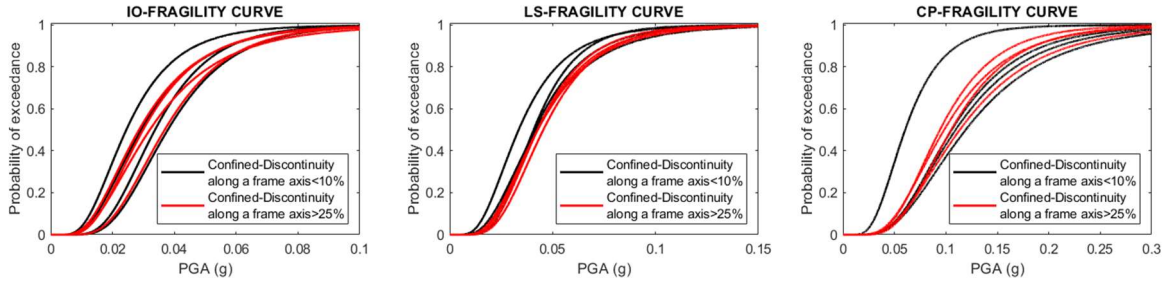

Figure 4.18. Fragility curves of confined models binned for the degree of discontinuity along a given frame axis.

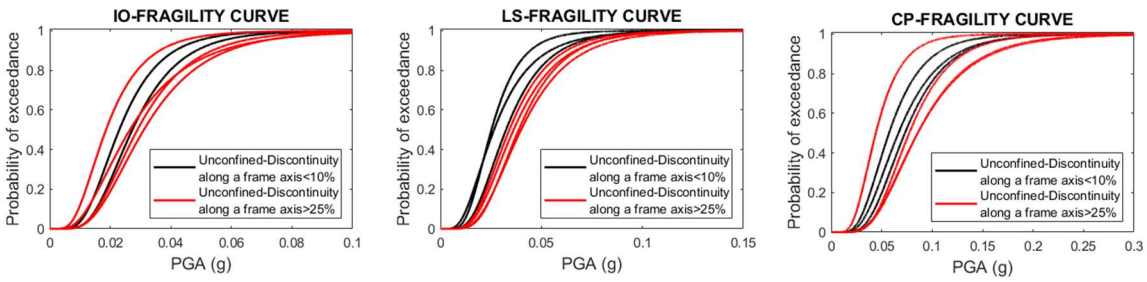

Figure 4.19. Fragility curves of unconfined models binned for the degree of discontinuity along a given frame axis.

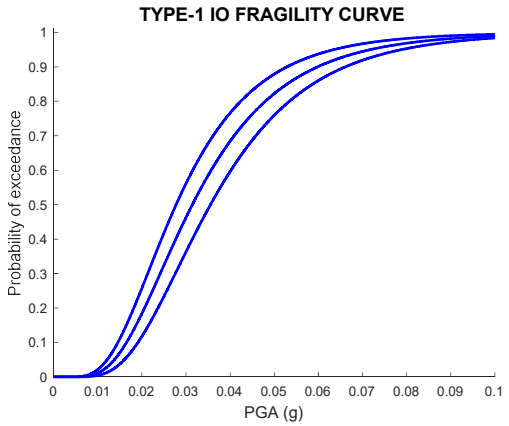

Figure 4.20. IO Fragility curve for confined mid rise RC frame buildings in Istanbul with 95 % confidence intervals.

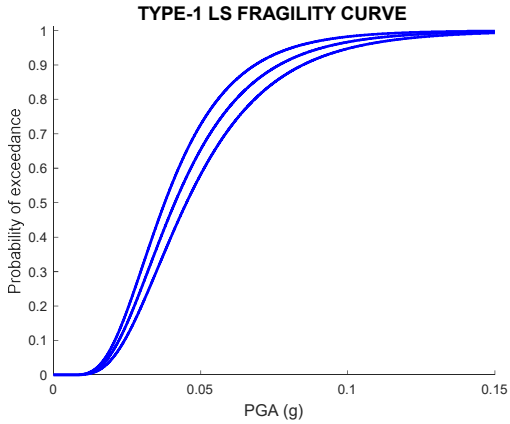

Figure 4.21. LS Fragility curve for confined mid rise RC frame buildings in Istanbul with 95 % confidence intervals.

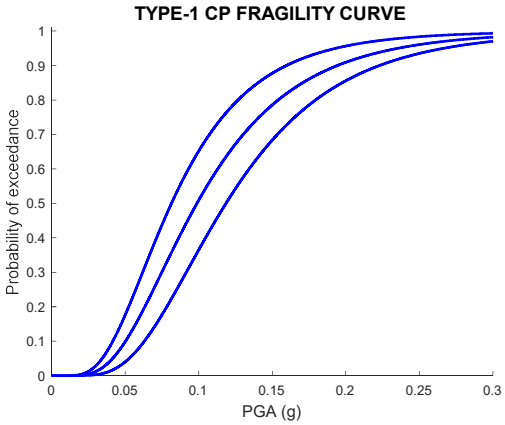

Figure 4.22. CP Fragility curve for confined mid rise RC frame buildings in Istanbul with 95 % confidence intervals.

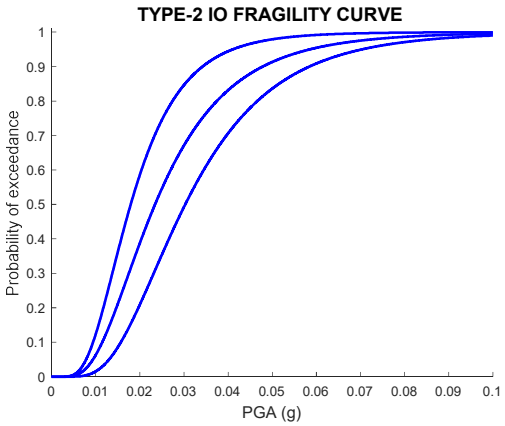

Figure 4.23. IO Fragility curve for unconfined mid rise RC frame buildings in Istanbul with 95 % confidence intervals.

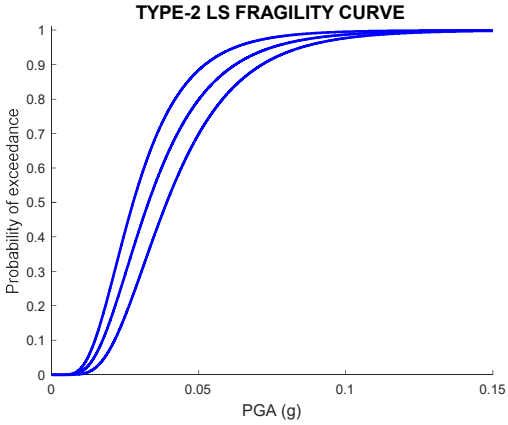

Figure 4.24. LS Fragility curve for unconfined mid rise RC frame buildings in Istanbul with 95 % confidence intervals.

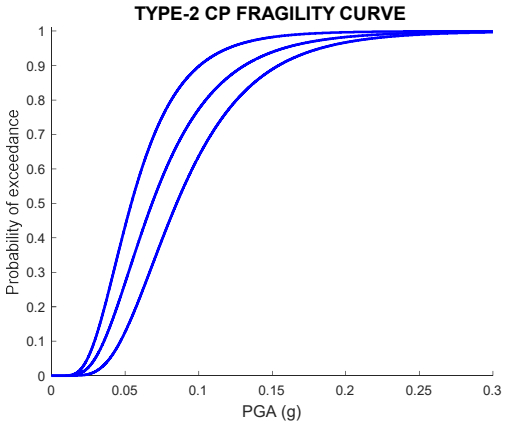

Figure 4.25. CP Fragility curve for unconfined mid rise RC frame buildings in Istanbul with 95 % confidence intervals.

Table 4.3. Estimated fragility parameters for confined and unconfined mid-rise RC frame buildings in Istanbul.

	TYPE ID	IO		LS		CP	
		μ	β	μ	β	μ	β
MEAN	CONFINED	-3.4595	0.5019	-3.1883	0.4842	-2.3145	0.5274
	UNCONFINED	-3.7530	0.5564	-3.4134	0.4996	-2.6834	0.5082
LOWER BAND	CONFINED	-3.3368	0.4843	-3.0971	0.4909	-2.1323	0.4924
	UNCONFINED	-3.4971	0.5126	-3.2407	0.4706	-2.4650	0.4648
UPPER BAND	CONFINED	-3.5841	0.5031	-3.2761	0.4648	-2.5070	0.5244
	UNCONFINED	-4.0210	0.5038	-3.5851	0.4928	-2.9150	0.4828

5. CONCLUSION

5.1. Major Outcomes and Observations

The inventory survey reveals that the subject building stock has poor geometrical configuration and low material quality, which are the general characteristics of pre-1975 construction practice in Istanbul. The most notable geometrical layout characteristics are the unsymmetrical plan configuration, discontinuities in columns and beams along a frame axis, the existence of added floor and mezzanine floor. It is believed that neither of these geometrical characteristics are considered during the design stage at that time. For instance, it is observed that the column dimensions are invariant even though the buildings with mezzanine floor have taller ground stories in height. Similarly, no correlation is detected between the section dimensions and span dimensions or discontinuities along the frame axis.

The consequences of the badly configured characteristics of the model buildings are clear in the results of NRHA. Due to inadequate section dimensions, the model buildings are weak against the lateral forces resulting from earthquake action, which lead structural components to behave in nonlinear range at the early stages of IDA. Besides flat-lining of the IDA curves are observed at low ground motion intensity levels because the structural components are not ductile enough to meet the excessive deformation demands and failure.

The lognormal cumulative distribution successfully fits to the results of IDA for all performance levels defined in this study except for one model building (M14). This model building fails in the early stages of IDA due to long-span dimensions. Thus, it is not possible to fit a smooth lognormal cumulative function on this model.

For all damage states, there is a rapid increase in the damage exceedance probabilities within small PGA increments. Especially, high damage exceedance probabilities of immediate occupancy (IO) and life safety (LS) performance levels at low seismic intensities are common for all building models. There are mainly two reasons for this observation: firstly, since the model buildings are weak against the lateral load capacity as mentioned before, buildings tend to behave in the nonlinear range at low seismic intensities; secondly, the structural components do not have detailing providing ductile behavior and threshold

values to quantify damage states (strain in this study) are low, and hence there are no distinct differences between them. Therefore, the transition from IO to LS performance levels is fast. Since only restricted nonlinear behavior is permitted for IO and LS limit states, reasons described above cause high exceedance probabilities for these damage states.

For Collapse Prevention (CP) performance state, fragility curves are not as steep as IO and LS damage states. Analysis results show that this is due to the changes in the dynamic response of the model buildings within the allowed nonlinearity. However, it should be noted that the exceedance probabilities for CP performance level are still high, which indicates that the subject building stock is highly vulnerable to seismic action.

5.2. Recommendations for Future Studies

The building database is compiled from Zeytinburnu district in Istanbul, which has similar construction practice with most of the existing no-code buildings in Istanbul. Although approximately 800 mid-rise RC-MRF buildings are examined in the inventory study, the subject buildings do not have a large coverage in terms of story number. On the other hand, the variability in the number of stories for such no-code RC-MRF buildings can be important in the other districts of Istanbul. It is recommended to broaden the building inventory in this aspect since the story number has a critical effect on the seismic performance of no-code buildings.

For the scope of this study, each representative building (a total of 16 models) has a unique plan configuration. Although the model buildings have distinct behavioral characteristics in terms of existence of mezzanine and added floors, the effects of such deficiencies (because such floors are generally not considered in the design stage in most pre-1975 construction practice) could not be captured properly. It is believed that the actual effect of mezzanine and added floors can be examined more systematically through establishing models having identical floor plans and by modifying the other important model features of these buildings such as mezzanine and added floors as well as the weaknesses in section dimensions and material quality.

As a final remark, the results of this study are believed to be useful for the no-code mid-rise RC-MRF building stock in the typical big cities of Turkey as Istanbul. However,

additional studies should be conducted by collecting similar building databases from other cities of similar size (e.g., Ankara, Istanbul, Antalya, Adana, etc.) to warrant the similarities (or to pinpoint the differences) about their seismic vulnerability.

REFERENCES

Al Mamun, A., and Saatcioğlu, M., "Seismic Fragility Analysis of Pre-1975 Conventional Concrete Frame Buildings in Canada", *Canadian Journal of Civil Engineering*, 45(9): 728-738, 2018.

Akkar, S., Sucuoğlu, H., and Yakut, A., "Displacement-Based Fragility Functions for Low and Mid-Rise Ordinary Concrete Buildings" *Earthquake Spectra*, 21(4):901–927, 2005.

Ay, B.Ö., and Erberik, M.A., "Vulnerability of Turkish Low-Rise and Mid-Rise Reinforced Concrete Frame Structures", *Earthquake Engineering*, 12(S2):2-11, 2008.

Ay, B.Ö., "Fragility Based Assessment of Low–Rise and Mid–Rise Reinforced Concrete Frame Buildings in Turkey", *M.Sc. Thesis, Department of Civil Engneering, Middle East Technical University*, Ankara, Turkey, 2006.

Baker, JW., "Efficient Analytical Fragility Function Fitting Using Dynamic Structural Analysis" *Earthquake Spectra*, 31:579–99, 2015.

Baker, J.W., "Fitting Fragility Functions to Structural Analysis Data Using Maximum Likelihood Estimation" *Earthquake Spectra*, Vol.2 No.12, 2014.

Baltzopoulos, G., Baraschino, R., and Iervolino, I., "On the Number of Records for Structural Risk Estimation in PBEE", *Earthquake Engineering and Structural Dynamics,* Vol. 48, Issue 525, Pages 489-506, April 2019.

Bazzurro, P., and Cornell, C.A., "Disaggregation of Seismic Hazard", *Bulletin of the Seismological Society of America*, 89:501–520, 1999.

Bilgin, H., "Fragility-based assessment of public buildings in Turkey", *Engineering Structures*, 56:1283-1294, 2013.

Bilgin, H., "Generation of fragility curves for typical RC health care facilities", *Performance of Constructed Facilities*, Emphasis on hospitals in Turkey, 30(3), 2016.

Bogazici University, "Earthquake Risk Assessment for Istanbul Metropolitan Area", *Kandilli Observatory and Earthquake Research Institute*, Istanbul, 2003.

Chopra, A.L., and McKenna, F., "Modeling Viscous Damping in Nonlinear Response History Analysis of Buildings for Earthquake Excitation", *Earthquake Engineering and Structural Dynamics*, 45:193–211, 2016.

Correia, A.A., Almeida, J.P., and Pinho, R., "Force-Based Versus Displacement-Based Formulations in the Cyclic Nonlinear Analysis of RC Frames" *The 14th World Conference on Earthquake Engineering*, Beijing, China, October 12-17, 2008.

Du, K., Sun, J., and Xu, W., "Evaluation of Section and Fiber Integration Points in Fiber Model", *Proceedings of the 15th World Conference on Earthquake Engineering*, Lisbon, Portugal, 2012.

Erberik, M.A., "Fragility-Based Assessment of Typical Mid-Rise and Low-Rise RC Buildings in Turkey", *Engineering Structures*, 30:1360-1374, 2007.

Erberik, M.A., and Elnashai, A.S., "Fragility Analysis of Flat-Slab Structures" *Engineering Structures*, 26:937-948, 2004.

Erberik, M.A., "Generation of Fragility Curves for Turkish Masonry Buildings Considering In-Plane Failure Modes", *Earthquake Engineering and Structural Dynamics*, 37:387-405, 2007.

Erdik, M., Şeşetyan, K., Demircioğlu, M.B., Zülfikar, C., Hancılar, U., Tüzün, C., and Harmandar, E., "Rapid Earthquake Loss Assessment After Damaging Earthquakes" *Soil Dynamics and Earthquake Engineering*, Vol. 31, Issue 2, Pages 247-266, February 2011.

FEMA-356, "NEHRP Prestandard and Commentary for the Seismic Rehabilitation of Buildings", *Federal Emergency Management Agency*, Washington, DC., 2000.

FEMA-440, “Improvement of Nonlinear Static Seismic Analysis Procedures”, *ATC-55 Draft,* Washington D.C., 2005.

FEMA-P-58-1, “Seismic Performance Assessment of Buildings”, *Federal Emergency Management Agency*, Washington, DC., 2012.

FEMA-P695, “Quantification of Building System Performance and Response Parameters”, *Federal Emergency Management Agency*, Washington, DC., 2009.

Feng, D., and Li, J., “Stochastic Nonlinear Behavior of Reinforced Concrete Frames. II: Numerical Simulation”, *Structural Engineering*, Vol. 142, Issue 3, March 2016.

Filippou, F.C., and Taucer, F.F., “Fibre Beam-Column Model for Non-Linear Analysis of R/C Frames: Part I. Formulation”, *Earthquake Engineering and Structural Dynamics*, Vol. 25, Pages 711-725, 1996.

Ghobarah, A., “On Drift Limits Associated with Different Damage Levels”, *Proceedings of International Workshop on Performance-Based Seismic Design, Department of Civil Engineering, McMaster University*, Bled, 28 June-1 July 2004.

Ghobarah, A., “Performance-Based Design in Earthquake Engineering: State of Development”, *Engineering Structures*, Pages 878–884, 2001.

Hancılar, U., Çaktı, E., Erdik, M., Franco, G. E., and Deodatis, G., “Earthquake Vulnerability of School Buildings Probabilistic Structural Fragility Analyses” *Soil Dynamics and Earthquake Engineering*, 67:169–178, 2014.

Hancılar, U., and Çaktı, E., “Fragility Functions for Code Complying RC Frames via Best Correlated IM–EDP Pairs” *Bulletin of Earthquake Engineering*, 13:3381–3400, 2015.

Hancılar, U., “Correlation Between Ground Motion Intensity Measures and Structural Response Parameters Through Nonlinear Dynamic Analyses”, *Ph.D. Thesis, Department of Earthquake Engneering, Bogazici University*, Istanbul, Turkey, 2009.

Haselton, C.B., and Deierlein, G.G., "Assessing Seismic Collapse Safety of Modern Reinforced Concrete Moment Frame Buildings", *Earthquake Engineering Center, Civil and Environmental Engineering Department*, *Stanford University*, California, Report No. 156, February 2007.

Huang, H., "Applicability Criteria of Fiber-Section Elements for The Modelling of RC Columns Subjected to Cyclic Loading", *M.Sc. Thesis, Department of Civil Engneering, University of Toronto*, Toronto, Canada, 2012.

Ibarra, L.F., and Krawinkler, H., "Global Collapse of Frame Structures Under Seismic Excitations", *Earthquake Engineering Center, Civil and Environmental Engineering Department*, *Stanford University*, California, Report No. 152, August 2005.

İstatistik Konseyi ve Türkiye İstatistik Kurumu Başkanlığı, "Türkiye İstatistik Kurumu", Ankara, 2005.

Kırçıl, M.S., and Polat, Z., "Fragility Analysis of Mid-Rise RC Frame Buildings" *Engineering Structures*, 28(9):1335–1345, 2006.

Liel, A.B., Haselton, C.B., Deierlein, G.G., and Baker, J.W., "Incorporating Modeling Uncertainties in the Assessment of Seismic Collapse Risk of Buildings", *Structural Safety*, 31, 197–211, 2009.

Mander, J. B., Priestley, M.J.N., and Park, R., "Theoretical Stress-Strain Model for Confined Concrete", *Structural Engineering*, Vol. 114, Issue 8, 1988.

Mathworks., "MATLAB-The Language of Technical Computing", *The Math Works, Natick*, USA, 2013.

Moehle, J., and Deierlein, G., "A Framework Methodology for Performance-Based Earthquake Engineering," *The 13th World Conference on Earthquake Engineering*, Vancouver, British Columbia, 2004.

Mwafy, A.M., Elnashai, A.S., "Static Pushover versus Dynamic Collapse Analysis of RC Buildings", *Engineering Structures*, Vol. 23, Pages 407–424, 2001.

Neuenhofer A., Filippou, F.C., "Evaluation of Nonlinear Frame Finite-Element Models", *Journal of Structural Engineering ASCE*, Vol. 123, Pages 704-711, 1997.

Odabaşı, Ö., "Characteristics Structural Features of Tall Buildings in Turkey and Their Dynamic Behavior", *M.Sc. Thesis, Department of Earthquake Engneering, Bogazici University*, Istanbul, Turkey, 2016.

Özmen, H.B., İnel, M., Meral, E., and Bucaklı, M., "Vulnerability of Low and Mid-Rise Reinforced Concrete Buildings in Turkey", *The 14th European Conference on Earthquake Engineering*, Ohrid, 2010.

Pinho, R., Bhatt, C., Antoniou, S., and Bento, R., "Modelling of the Horizontal Slab of a 3D Irregular Building for Nonlinear Static Assessment", *The 14th World Conference on Earthquake Engineering*, Beijing, China, October 12-17, 2008.

Priestley, M.J.N., "Performance Based Seismic Design", *12th World Conference on Earthquake Engineering*, Auckland, New Zeland, Sunday 30 January - 4 February 2000.

Rossetto, T., and Elnashai, A., "Derivation of Vulnerability Functions for European-Type RC Structures Based on Observational Data", *Engineering Structures*, Vol. 25, Issue 10, 2003.

Scott, M.H., Fenves, G.L., McKenna, F., and Filippou, F.C., "Software Patterns for Nonlinear Beam-Column Models", *Structural Engineering*, Vol. 134, Issue 4, 2008.

Scott, M.H., Franchin, P., Fenves, G.L., and Filippou, F.C., "Response Sensitivity for Nonlinear Beam–Column Elements" *Structural Engineering*, Vol. 130, Issue 9, 2004.

Spacone, E., Ciampi, V., and Filippou, F.C., "Mixed Formulation of Nonlinear Beam Finite Element", *Computers and Structures*, Vol. 58, Issue 1, Pages 71-83, 3 January 1996.

Spacone, E., Filippou, F.C., and Taucer, F.F., "Fibre Beam-Column Model for Non-Linear Analysis of R/C Frames: Part II. Applications", *Earthquake Engineering and Structural Dynamics*, Vol. 25, Pages 727-742, 1996.

Taucer, F.F., Spacone, E., and Filippou, F.C., "A Fiber Beam-Column Element for Seismic Response Analysis of Reinforced Concrete Structures" *Earthquake Engineering Research Center College of Engineering University of California,* Berkeley, December 1991.

Turkish Earthquake Code, "Specification for Structures to be Built in Disaster Areas", *Ministry of Public Works and Settlement*, Government of Republic of Turkey, 1968.

Turkish Earthquake Code, "Specification for Structures to be Built in Disaster Areas", *Ministry of Public Works and Settlement*, Government of Republic of Turkey, 1975.

Turkish Earthquake Code, "Specification for Structures to be Built in Disaster Areas", *Ministry of Public Works and Settlement*, Government of Republic of Turkey, 2007.

Tüzün, C., and Aydınoglu, M.N., "Development of Fragility Relationships from Nonlinear Analysis of Real Buildings", *The 6th National Conference on Earthquake Engineering, İTÜ*, İstanbul, 2007.

Tüzün, C., "A Seismic Vulnerability Analysis Procedure for Urban Loss Assessment", *Ph.D. Thesis, Department of Earthquake Engneering, Bogazici University*, Istanbul, Turkey, 2008.

Uçar, T., and Düzgün, M., "Betonarme Binalar için Artımsal İtme Analizi Esaslı Analitik Hasargörebilirlik Eğrilerinin Oluşturulması", *İMO Teknik Dergi,* 24(3):6421-6446, 2013.

Vamvatsikos, D., and Cornell, C.A., "Applied Incremental Dynamic Analysis", *Earthquake Spectra*, Vol. 20, No. 2, pp. 523-553, May 2004.

Vamvatsikos, D., and Cornell, C.A., "Incremental Dynamic Analysis", *Earthquake Engineering and Structural Dynamics*, 31:491–514, 2002.

Vamvatsikos, D., and Cornell, C.A., "The Incremental Dynamic Analysis and Its Application to Performance-Based Earthquake Engineering", *12th European Conference on Earthquake Engineering*, Paper Reference 479, January 2002.

Vamvatsikos, D., "Performing Incremental Dynamic Analysis in Parallel", *Computers and Structures*, Vol. 89(1), Pages 170-180, January 2011.

Zhou, J., and Kunnath, S.K., "Effect of Reinforcing Steel Modeling in Seismic Collapse Assessment of Reinforced Concrete Buildings", *The 2018 Structures Congress (Structures18) Songdo Convensia*, Incheon, Korea, August 27 - 31, 2018.

APPENDIX A: MODEL BUILDINGS

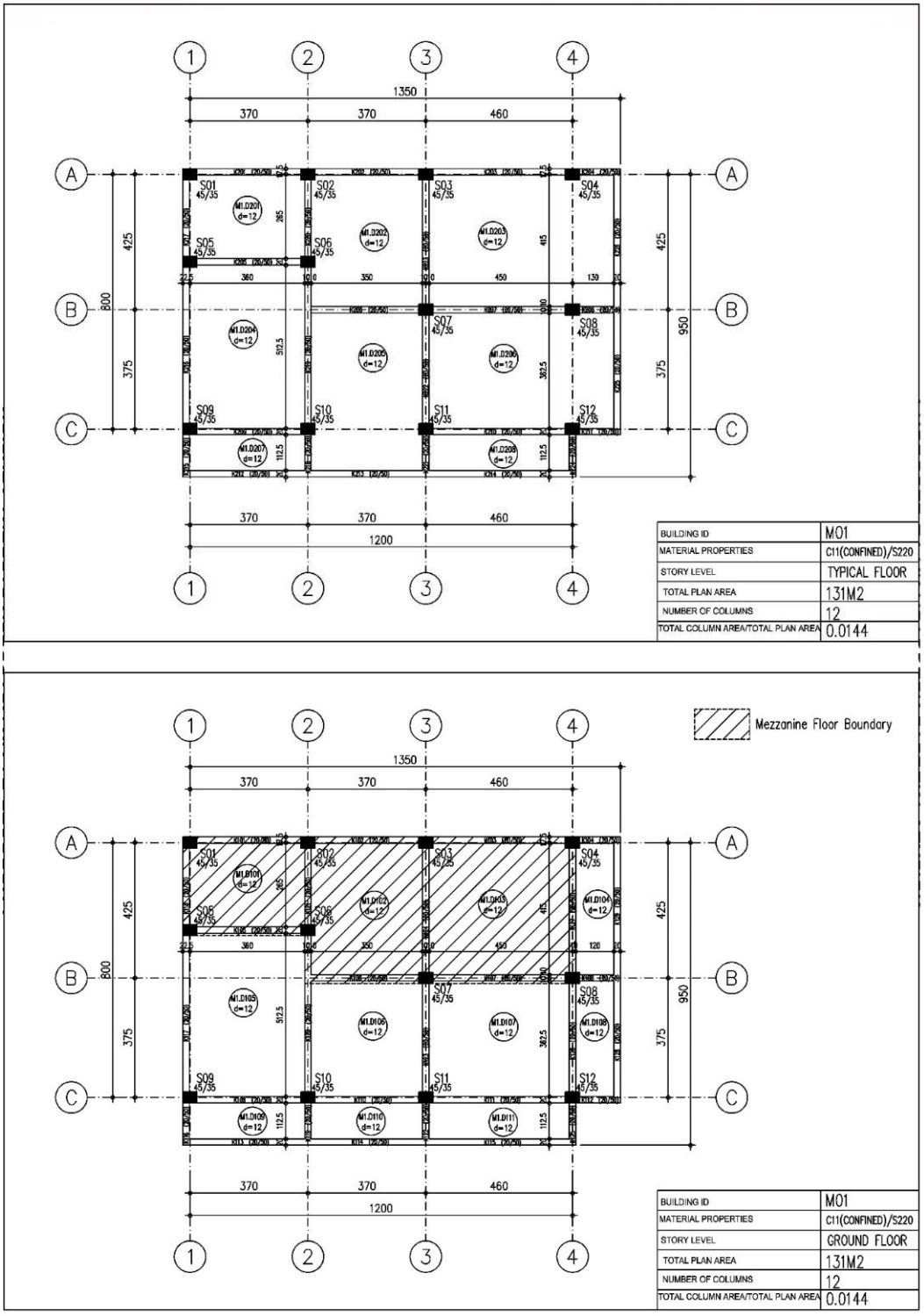

Figure A.1. Ground floor and typical floor plan of Model01.

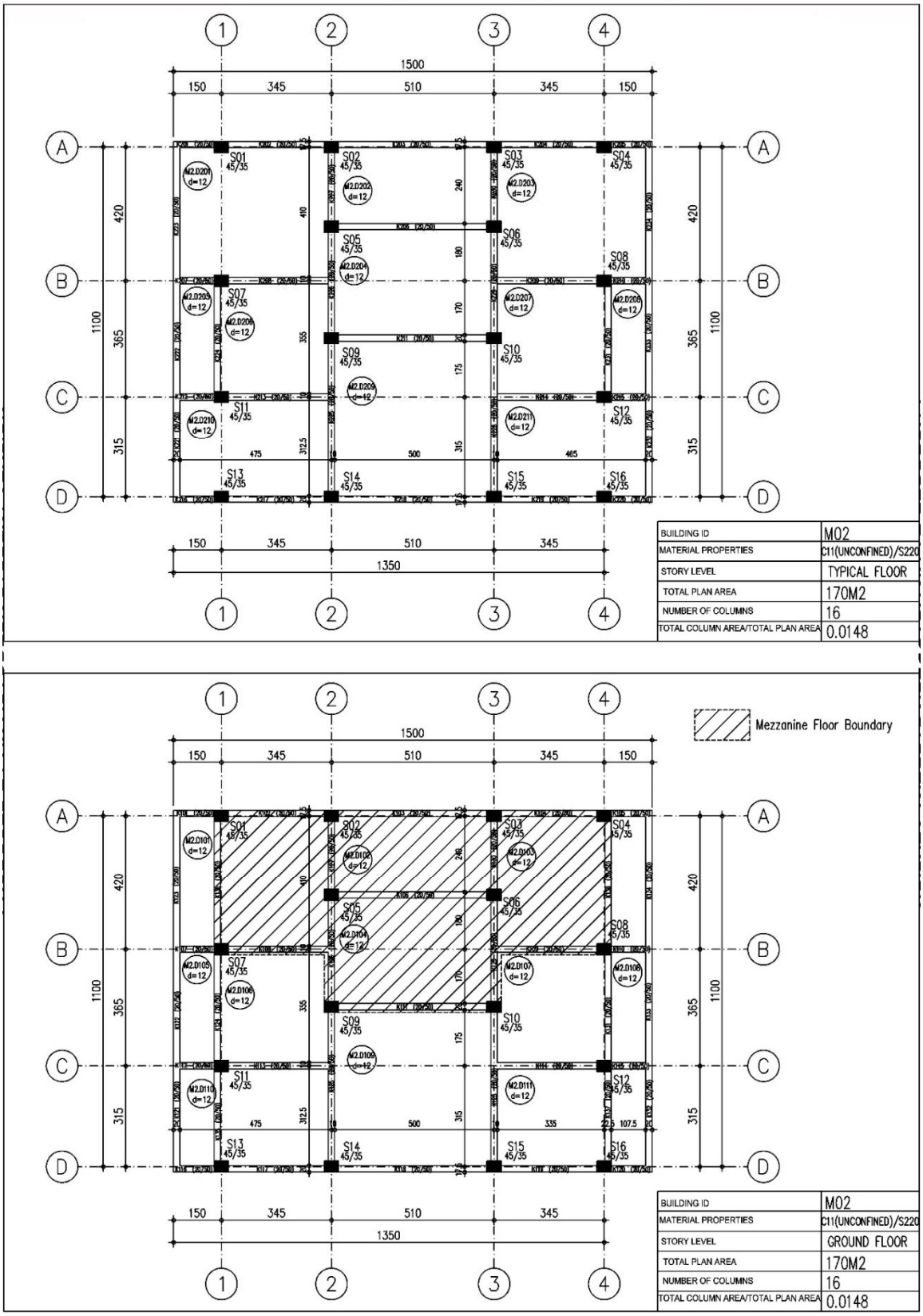

Figure A.2. Ground floor and typical floor plan of Model02.

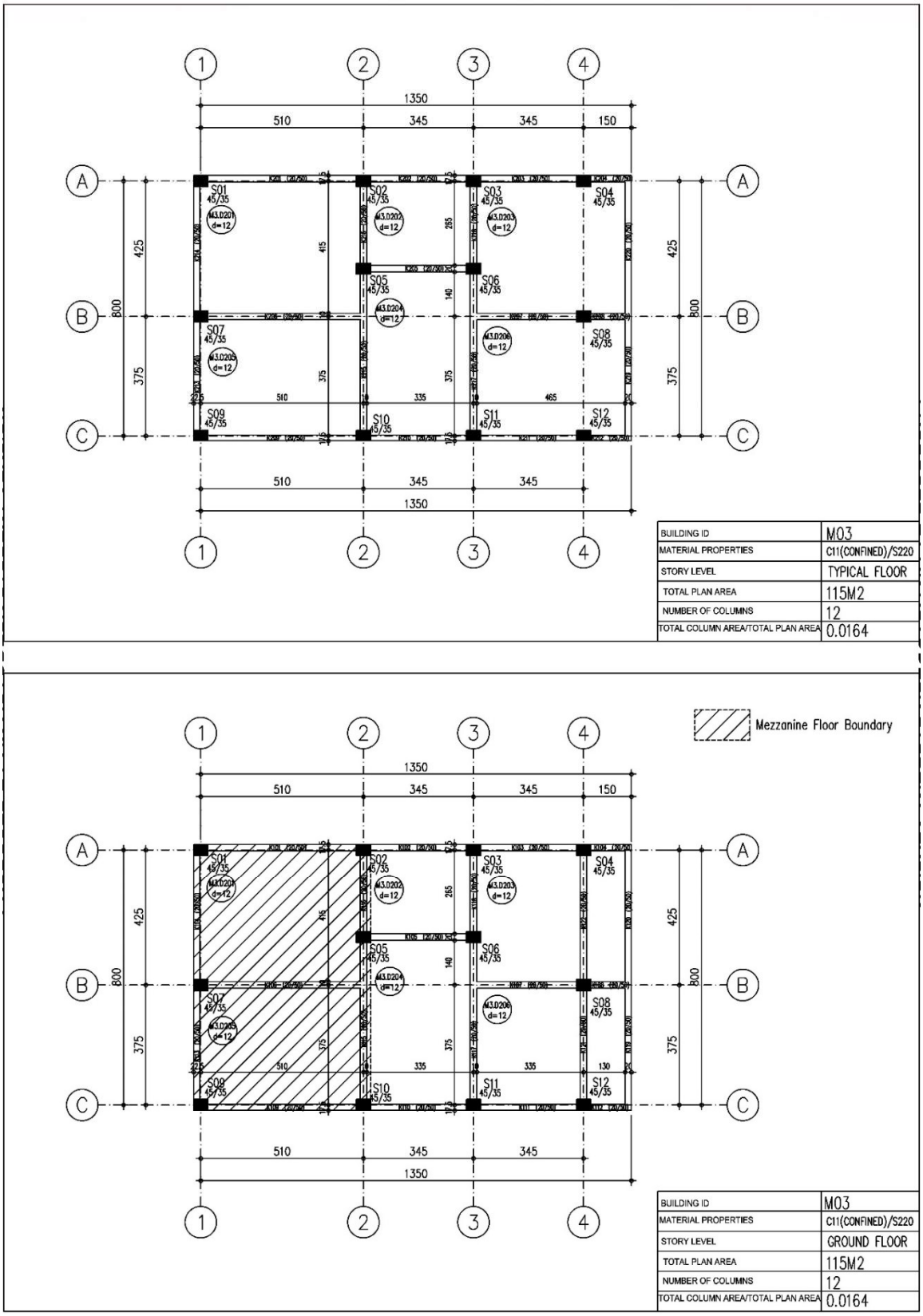

Figure A.3. Ground floor and typical floor plan of Model03.

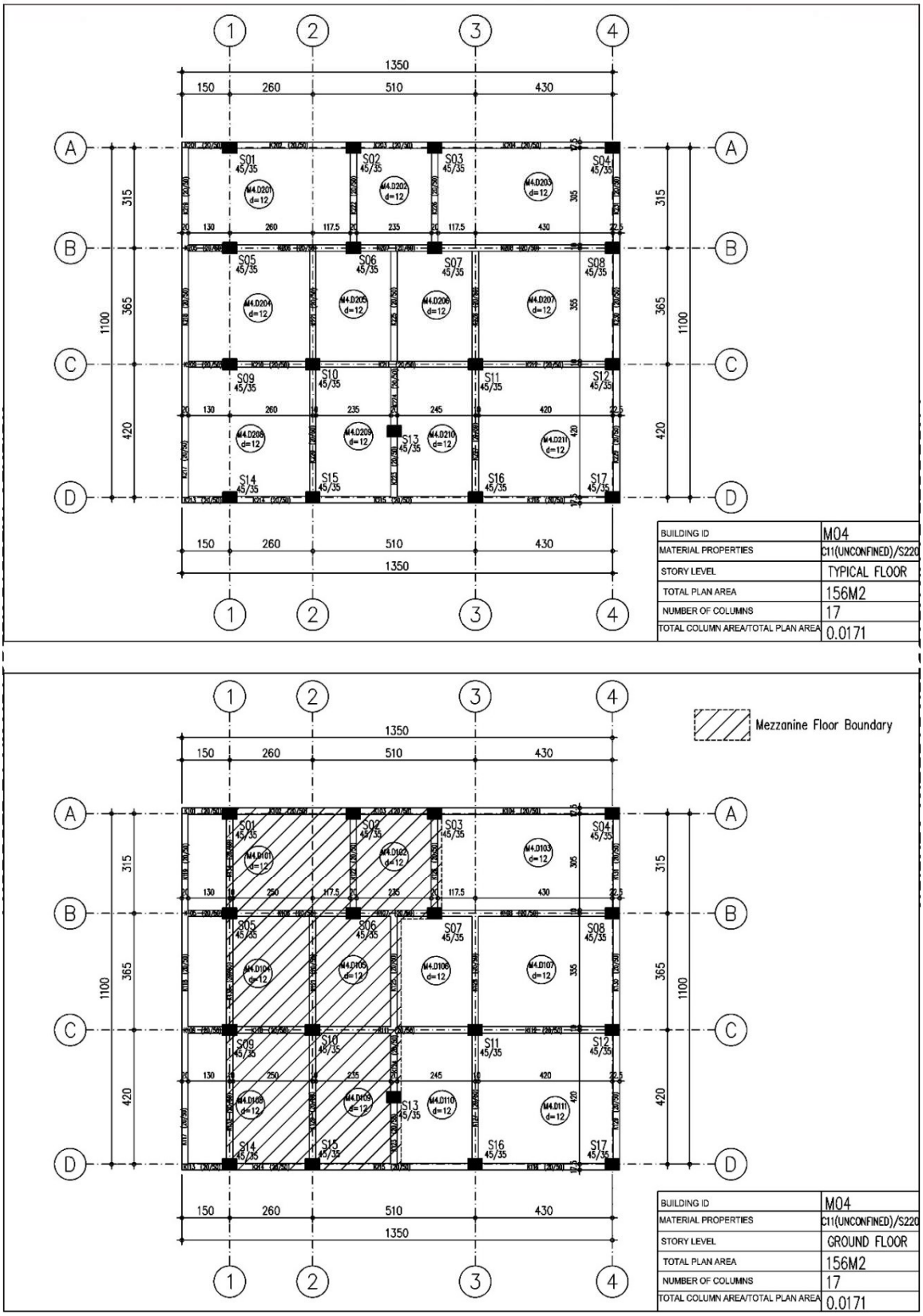

Figure A.4. Ground floor and typical floor plan of Model04.

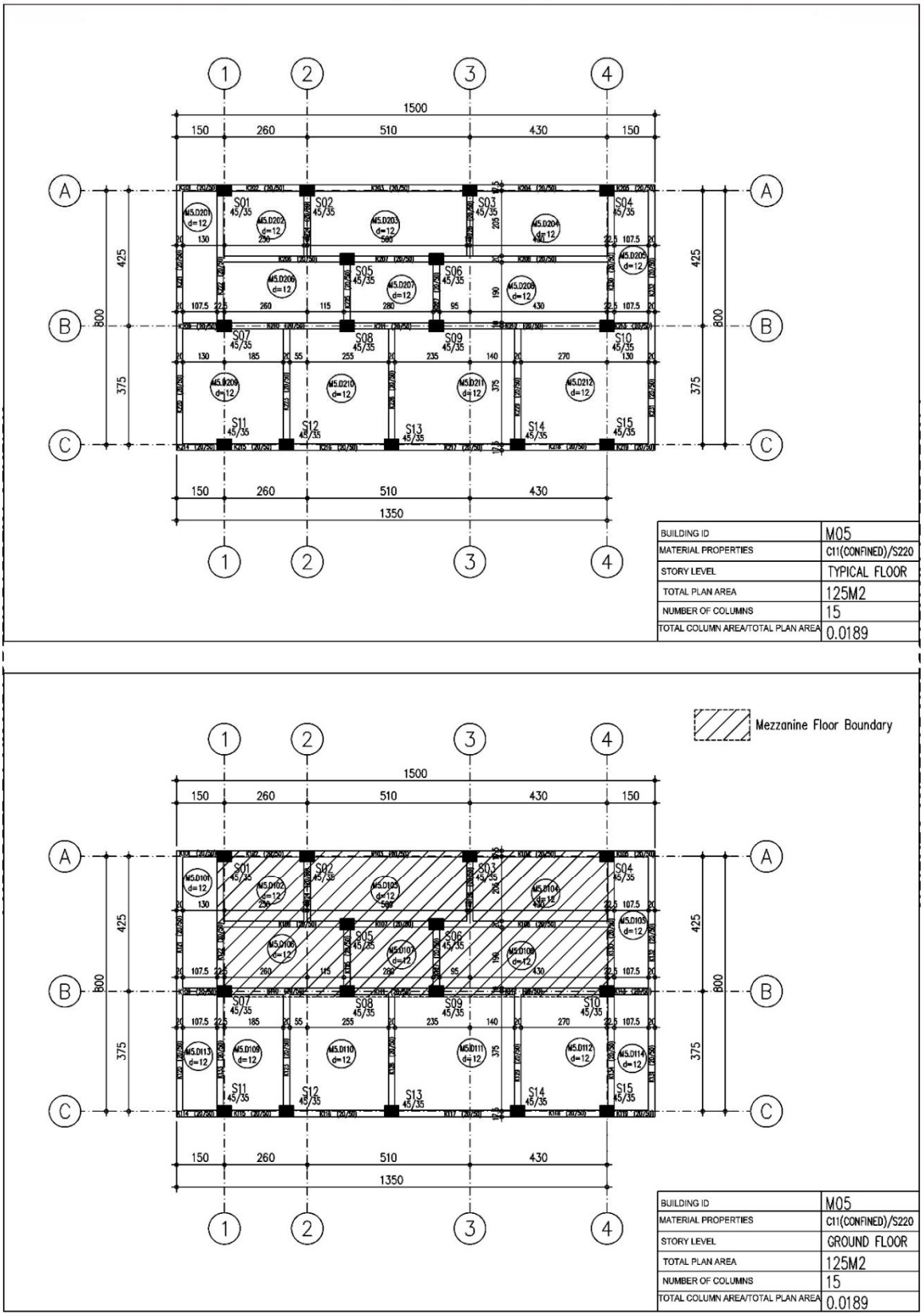

Figure A.5. Ground floor and typical floor plan of Model05.

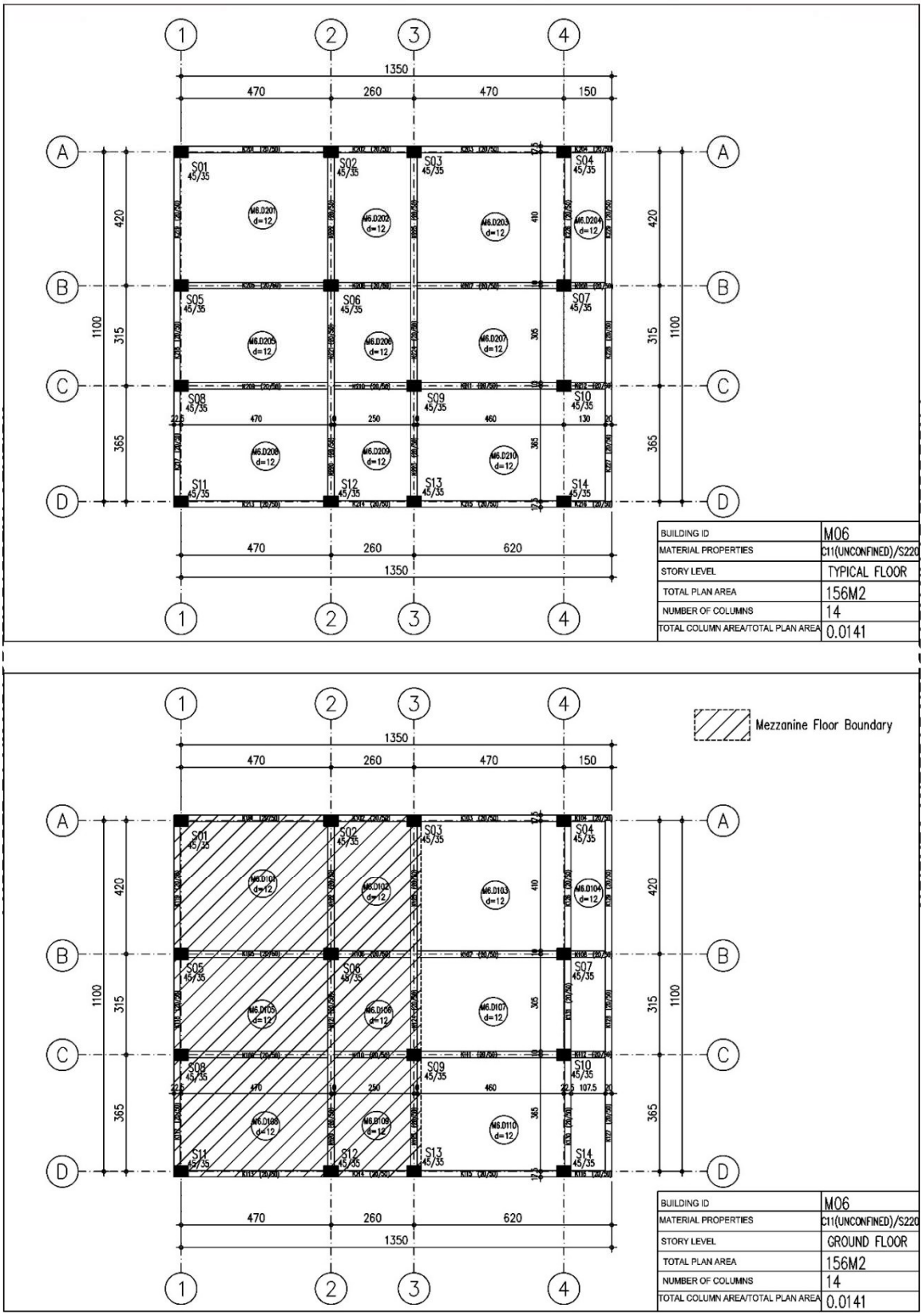

Figure A.6. Ground floor and typical floor plan of Model06.

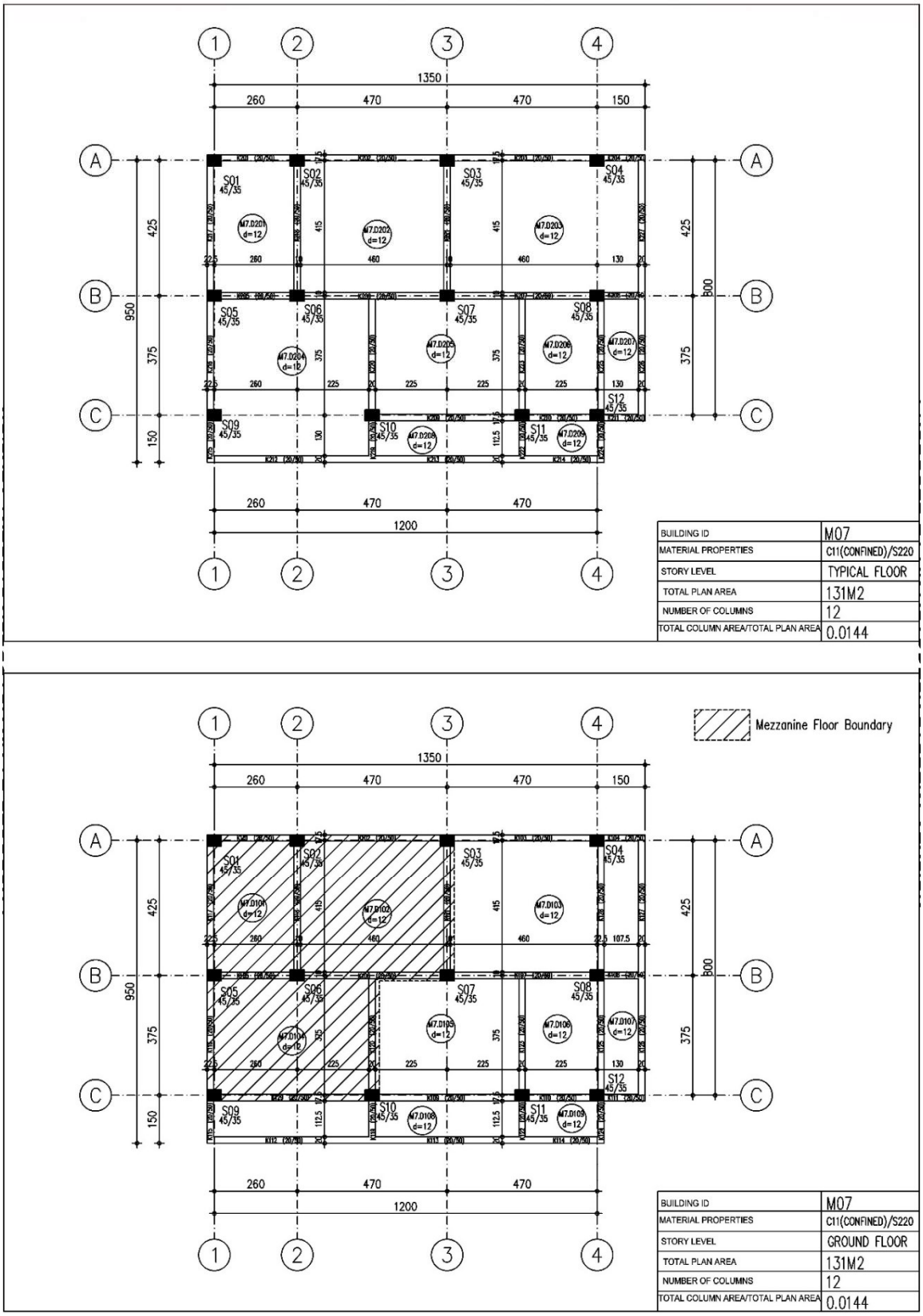

Figure A.7. Ground floor and typical floor plan of Model07.

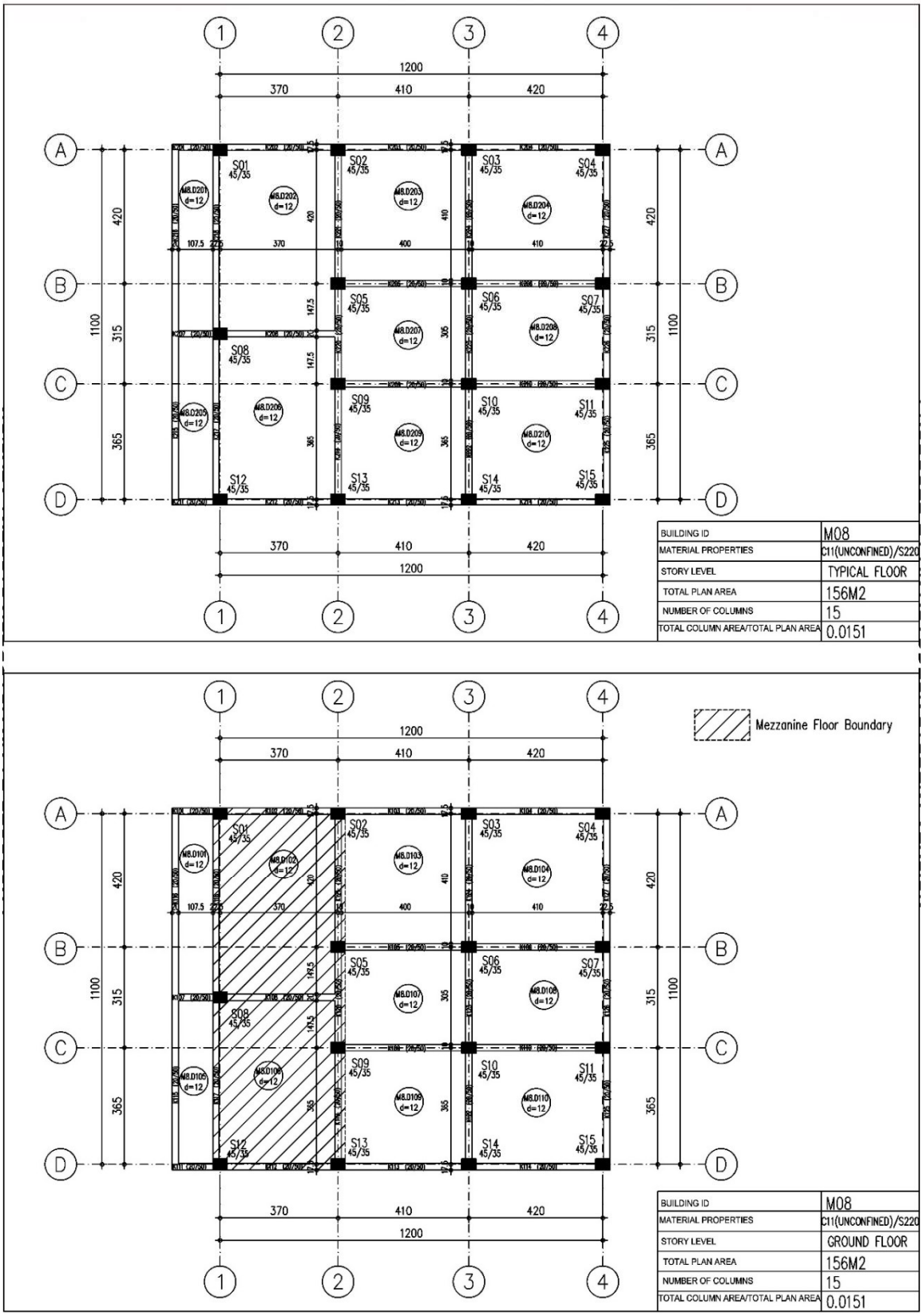

Figure A.8. Ground floor and typical floor plan of Model08.

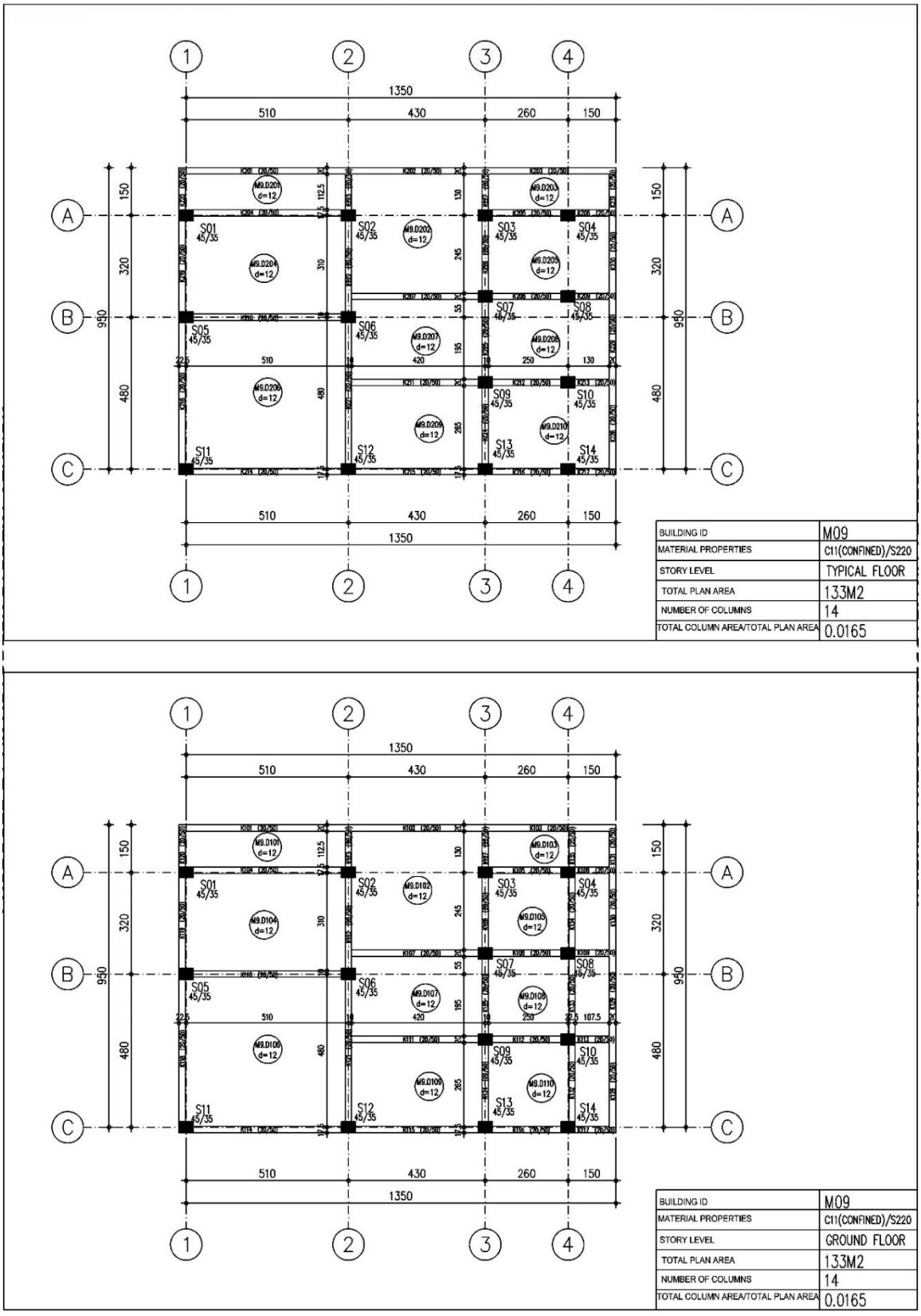

Figure A.9. Ground floor and typical floor plan of Model09.

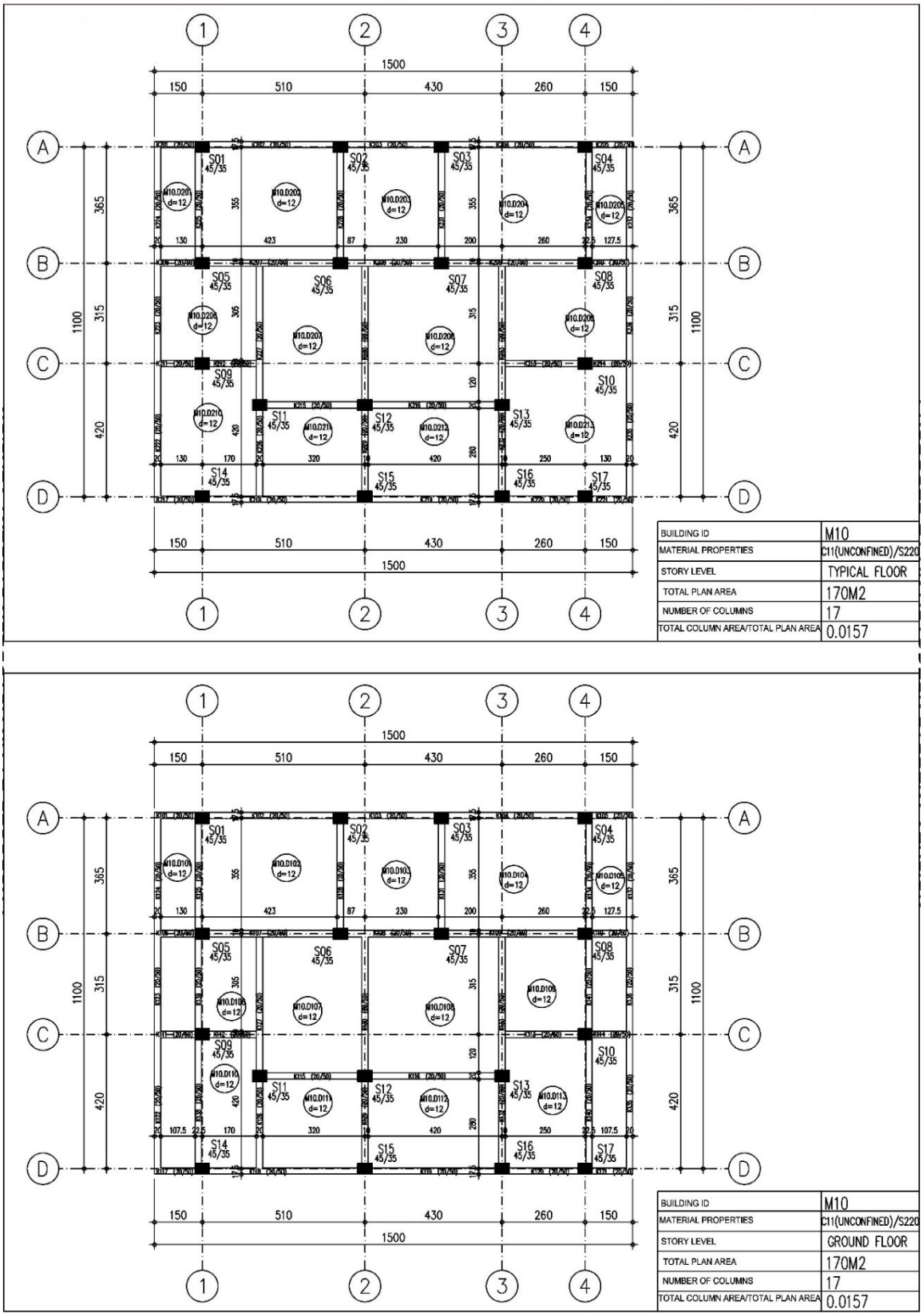

Figure A.10. Ground floor and typical floor plan of Model10.

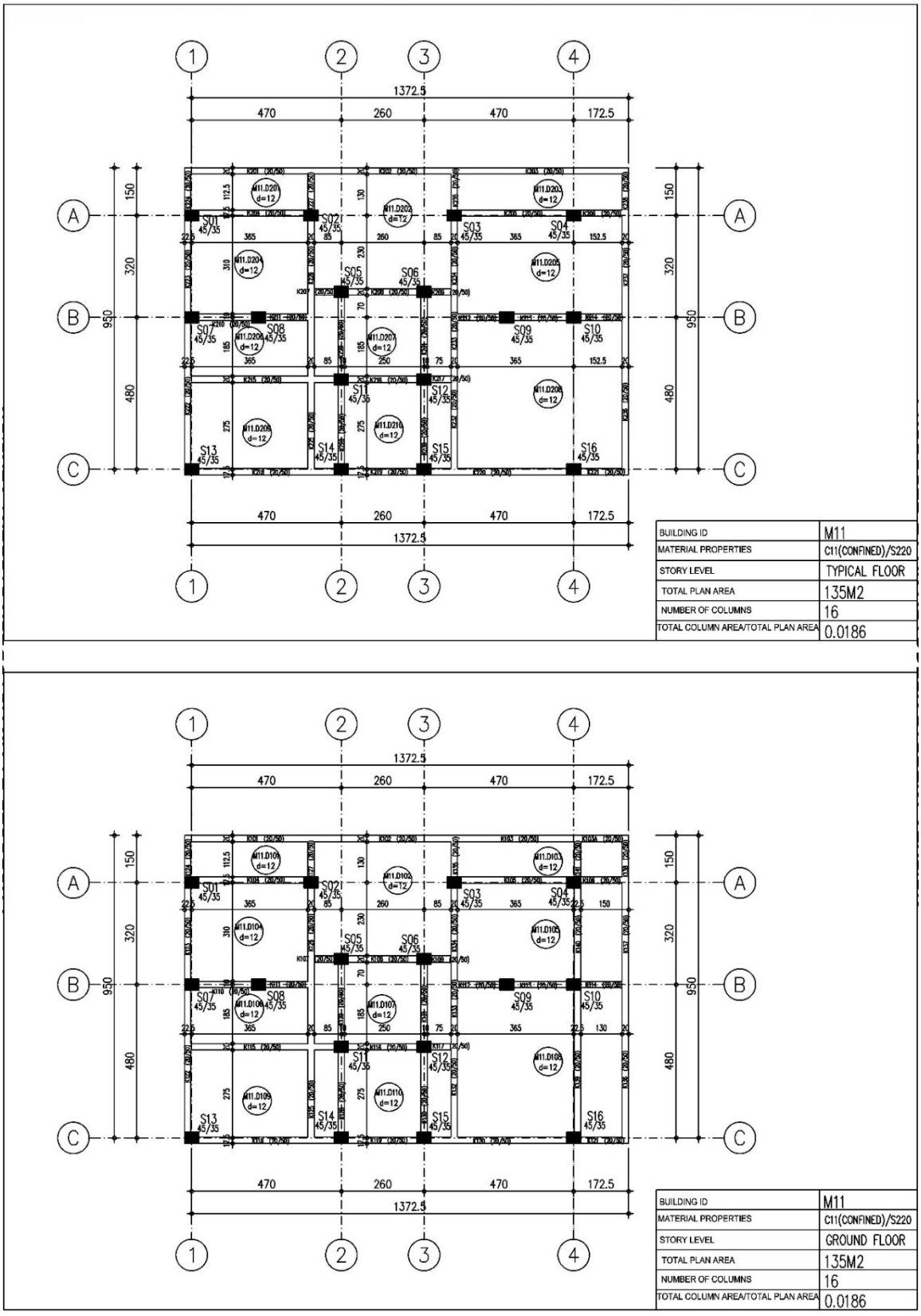

Figure A.11. Ground floor and typical floor plan of Model11.

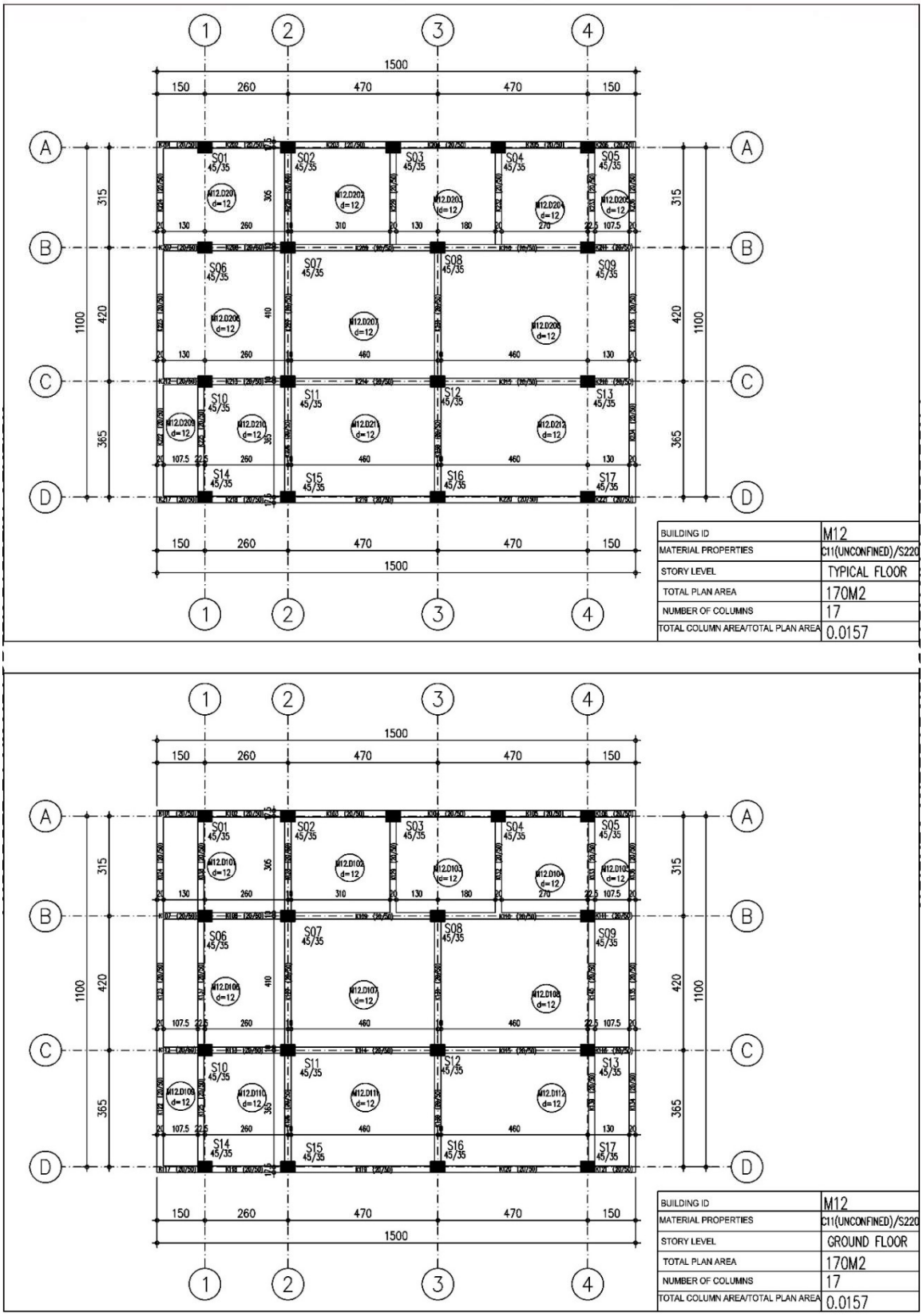

Figure A.12. Ground floor and typical floor plan of Model12.

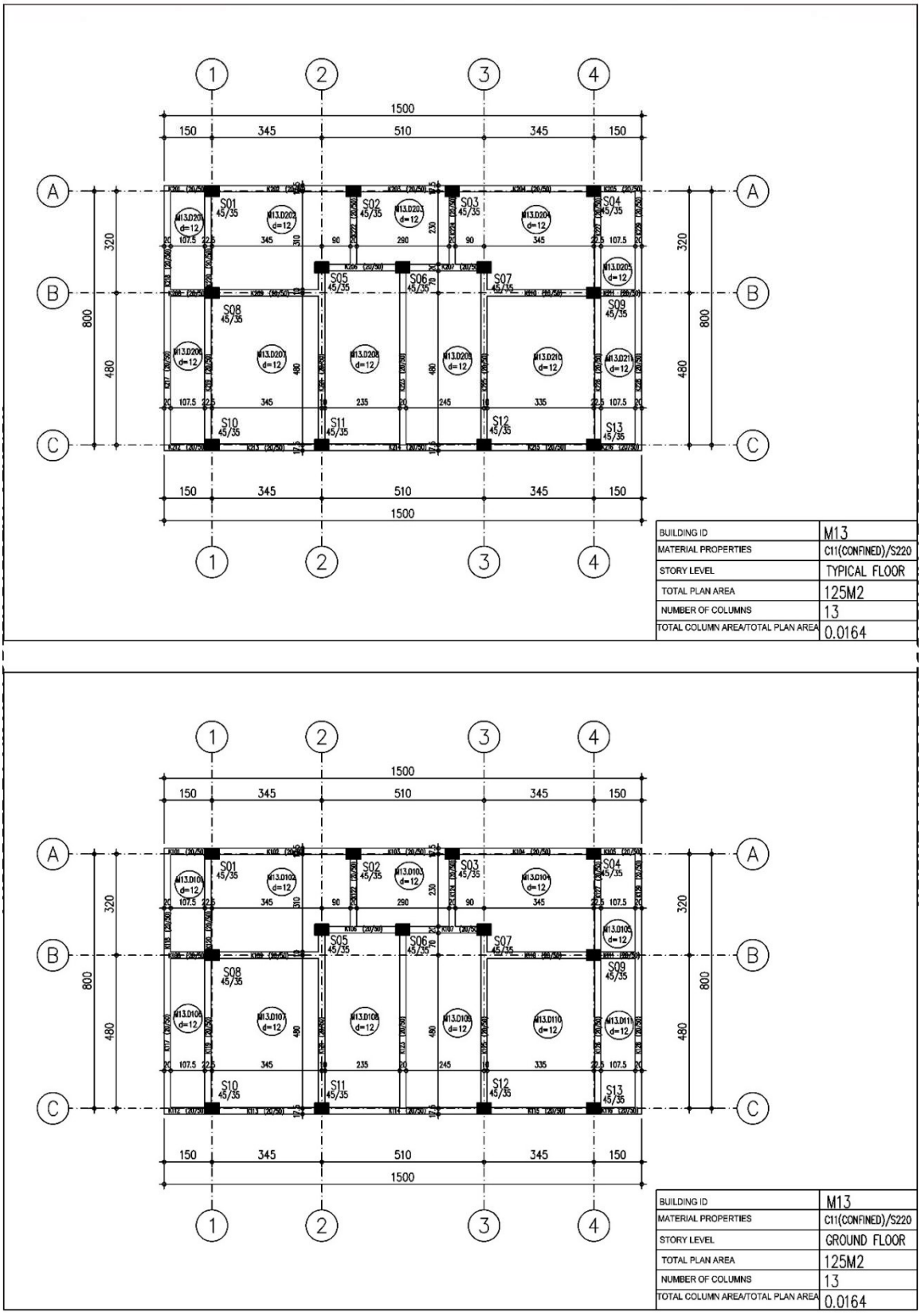

Figure A.13. Ground floor and typical floor plan of Model13.

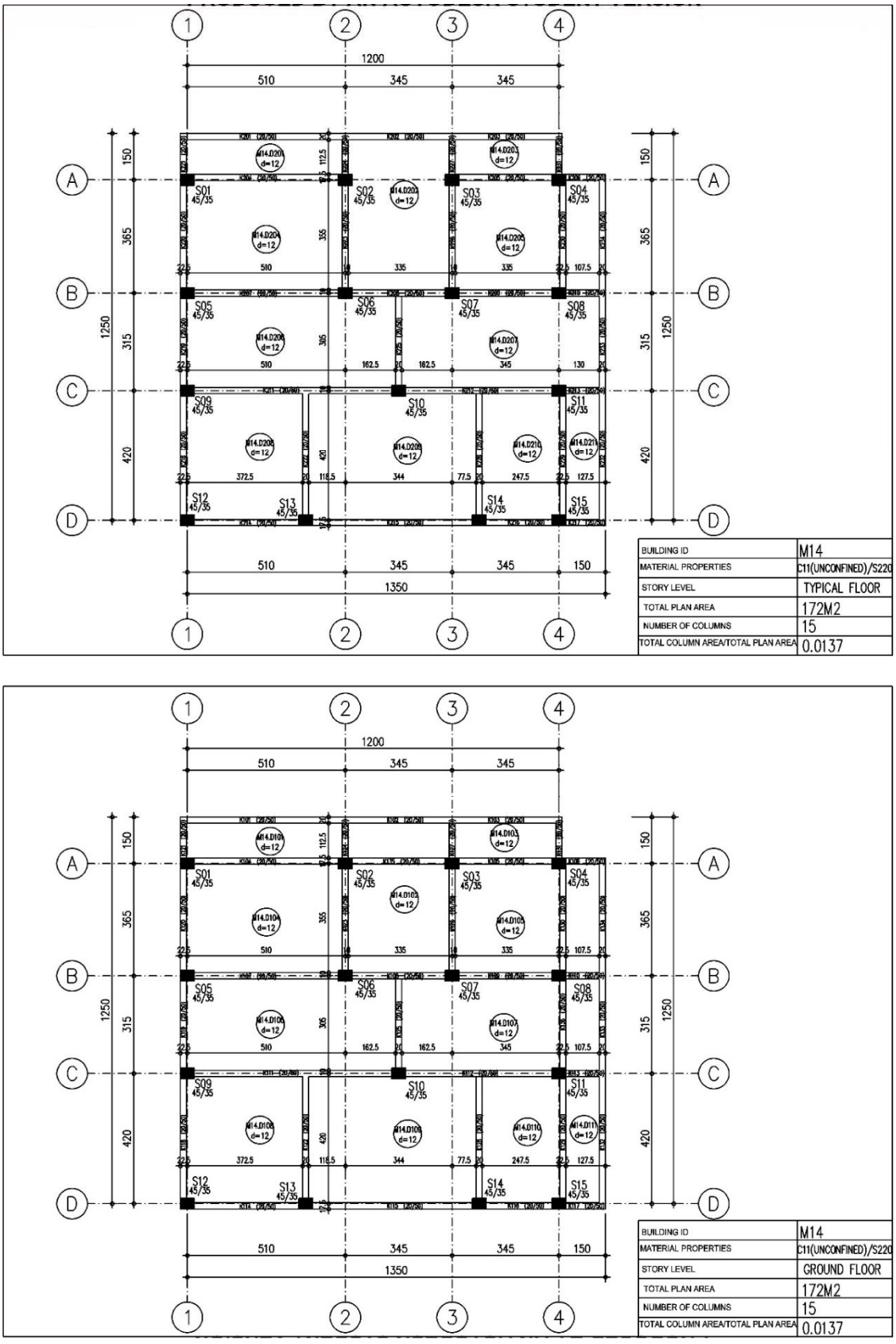

Figure A.14. Ground floor and typical floor plan of Model14.

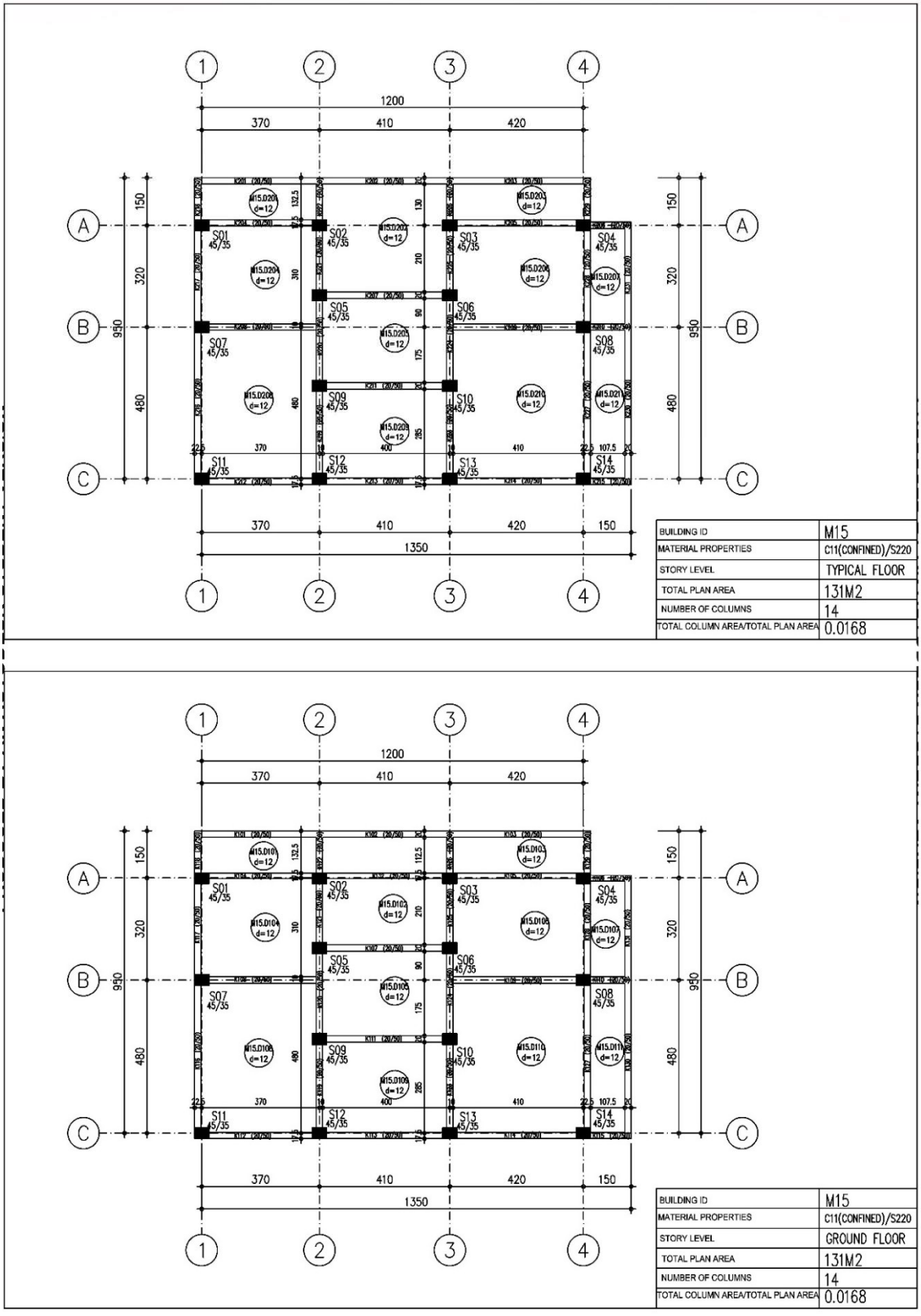

Figure A.15. Ground floor and typical floor plan of Model15.

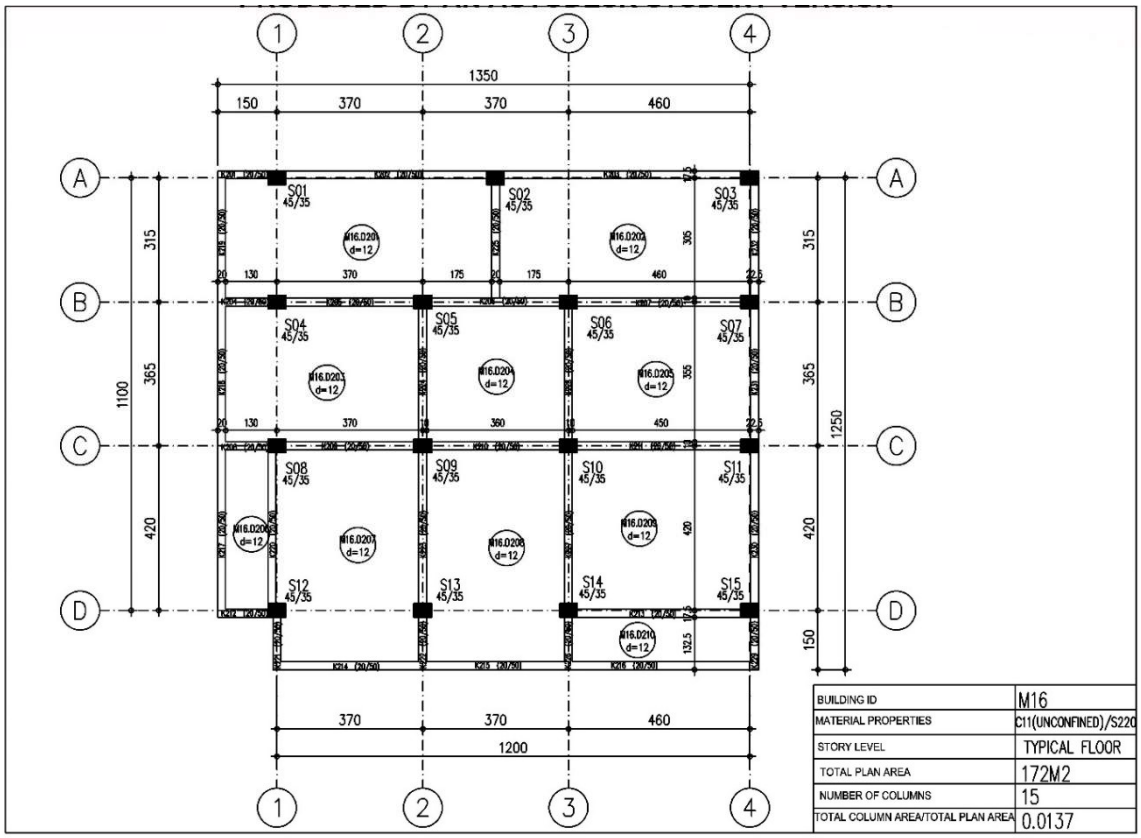

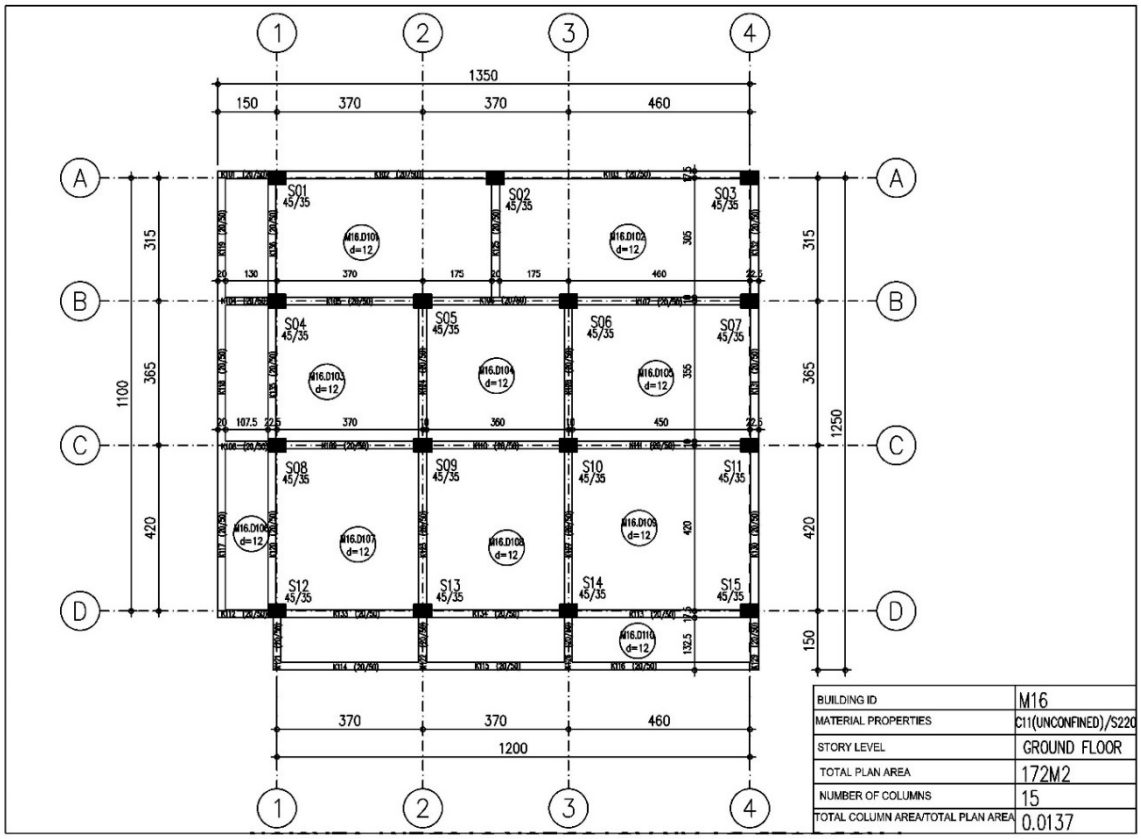

Figure A.16. Ground floor and typical floor plan of Model16.

APPENDIX B: HISTOGRAMS COLLECTED FROM BUILDING INVENTORY

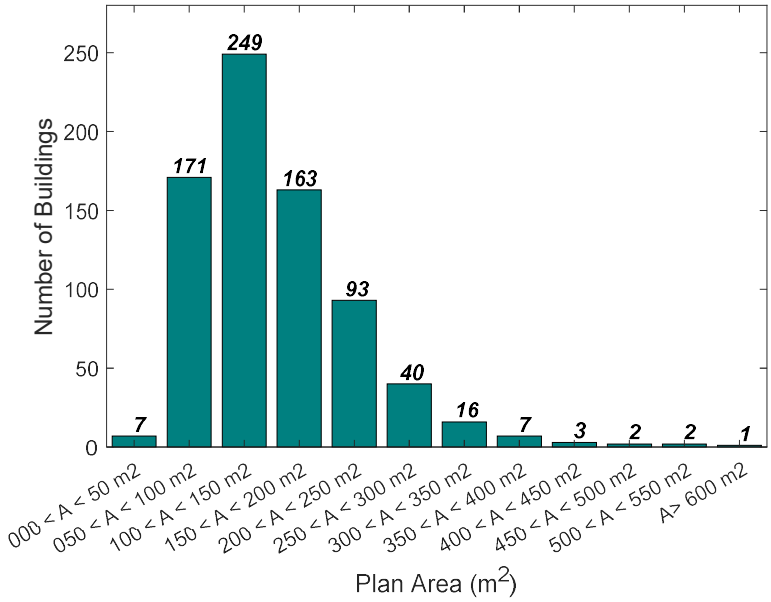

Figure B.1. Distribution of the building inventory in terms of the plan area.

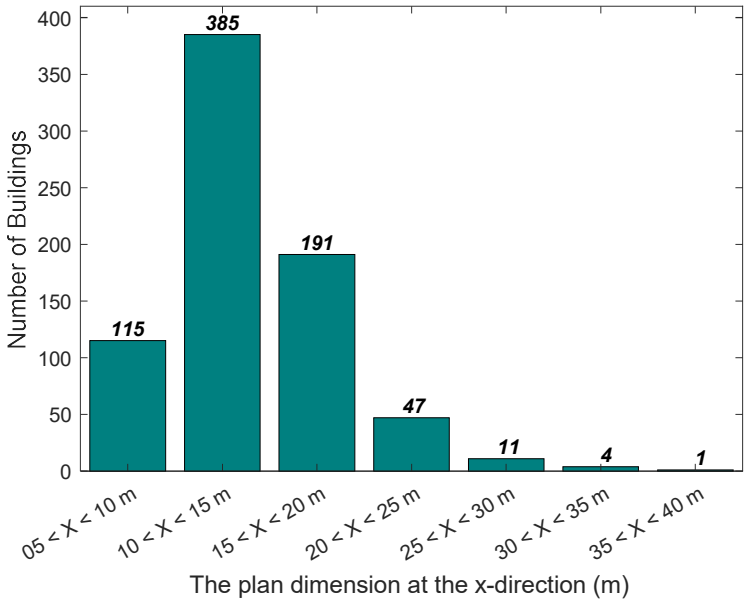

Figure B.2. Distribution of the building inventory in terms of the plan dimensions at the x-direction.

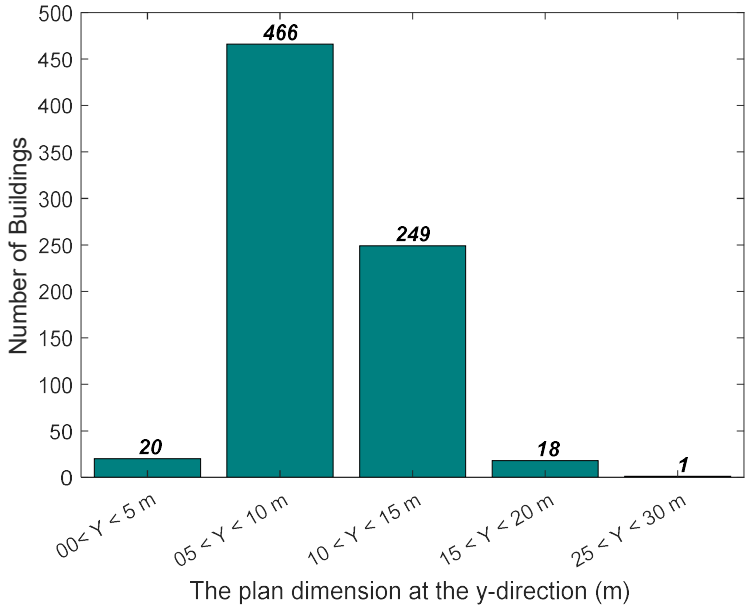

Figure B.3. Distribution of the building inventory in terms of the plan dimensions at the y-direction.

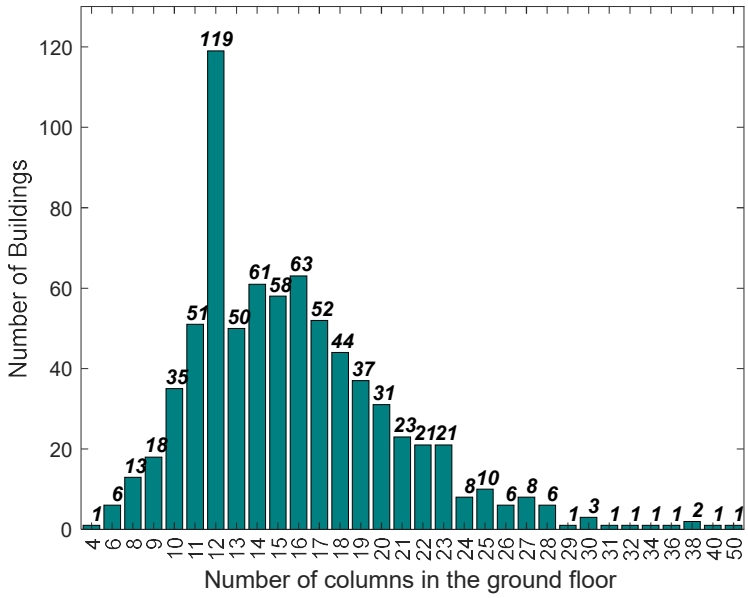

Figure B.4. Distribution of the building inventory in terms of the number of columns.

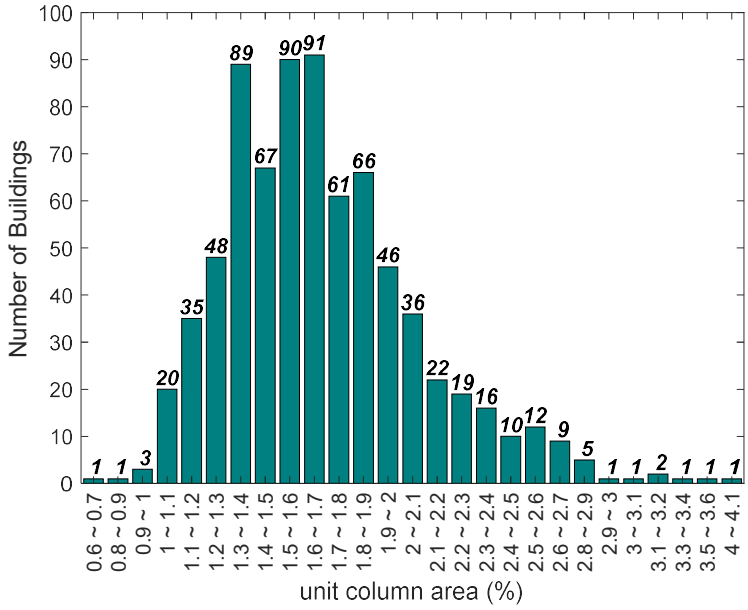

Figure B.5. Distribution of the building inventory in terms of column density.